Theoretical Notes
Note 55

U. S. DEPARTMENT OF COMMERCE
John T. Connor, Secretary
ENVIRONMENTAL SCIENCE SERVICES ADMINISTRATION
Robert M. White, Administrator
INSTITUTES FOR ENVIRONMENTAL RESEARCH
George S. Benton, Director

ESSA TECHNICAL REPORT IER 22-ITSA 22

Electromagnetic Pulse Propagation in a Disturbed Terrestrial Waveguide

J. RALPH JOHLER

INSTITUTE FOR TELECOMMUNICATION SCIENCES AND AERONOMY
BOULDER, COLORADO
December, 1966

Contents

	Page
Foreword	iv
Abstract	1
1. Introduction	1
2. The Gas Mixture as a Model Ionosphere	2
3. Transforms for the Nuclear Model Propagation Medium	5
4. Propagation of the Pulse to Great Distances	6
5. Conclusions	8
6. References	9
Figures 1 through 57	11

Foreword

This work was sponsored by the Air Force Systems Command, Electronic Systems Division, Directorate of Planning and Technology, Strategic Planning Division, L. G. Hanscom Field, Bedford, Massachusetts 01730. Other pertinent information may be found in the following documentation already published or soon to be published:

a. "Propagation of an Electromagnetic Pulse from a Nuclear Burst", J. R. Johler, IEEE Transactions on Antennas and Propagation, (to be published).

b. "Electromagnetic Pulse Propagation in the Normal Terrestrial Waveguide Environment," J. R. Johler, U. S. Dept. of Commerce, ESSA Technical Report, IER-21 ITSA-21, December 1966. EMP Theoretical Note 54.

c. "Propagation of the Ground Wave Electromagnetic Signal, with Particular Reference to a Pulse of Nuclear Origin," J. R. Johler and J. C. Morgenstern, Proc. IEEE 53, No. 12 (December, 1965).

ABSTRACT

Previous papers which treat pulse propagation (with special reference to the nuclear pulse) assume the ionosphere to be "normal." Thus, a theoretical model of the ionosphere has been employed which represents undisturbed conditions. This paper extends this propagation analysis to a disturbed condition resulting from the ionizing radiation of nuclear debris spread over a large area. The effect of the debris on the transforms for the propagation medium together with the detailed dispersion of a particular pulse are considered. The lowering of the ionosphere reflection height at low frequencies causes shorter propagation times for the pulses reflected from the ionosphere. This effect causes considerable change in the form or shape of the observed composite pulse at great distance from the source.

Key Words: EM-pulse, EM-pulse of nuclear origin, LF, VLF, ELF transient propagation, pulse propagation, transient propagation, and transient response of terrestrial waveguide.

1. Introduction

In a companion paper [Johler, 1966c] and in previous papers [Johler, 1967; Johler and Morgenstern, 1965] the propagation of a low frequency pulse of nuclear origin was described in the normal daytime terrestrial waveguide environment. Particular emphasis was placed on the construction of transforms to propagate theoretically almost any shape pulse with energy at low frequencies (< 1000 kc/s).

The electrical properties of the ionosphere are altered markedly under natural or man-made disturbance. The particular case of a nuclear disturbance in which the nuclear debris is spread over large areas of the terrestrial sphere has been described by Crain [1961, 1964], and Crain and Booker [1963, 1964]. Employing profiles of electrification of the atmosphere and lower ionosphere, Johler and Berry [1965] detailed the theory of propagation which took account of ions produced by the nuclear environment.

In this paper various models of a nuclear debris disturbance are employed to construct theoretical propagation transforms of the terrestrial radio waveguide for low frequencies. The propagation of a pulse from a nuclear burst is simulated with the aid of these transforms.

2. The Gas Mixture as a Model Ionosphere

Almost universally, the ionosphere or upper boundary of the terrestrial waveguide is treated as an electron gas (taking account of electron-neutral collisions). This is not always a valid theoretical assumption. Thus, not withstanding the great mass and hence low gyro resonance frequency of the ions, cases can be cited in which the ions play an important, even dominant role in the propagation. Examples are propagation at ELF and the propagation in the nuclear environment for LF, VLF, ELF.

A gas mixture with number densities, N_i, for each species, i = e, +, -, o corresponding to electrons, positive ions, negative ions, and neutrals, respectively, can be described theoretically as a plasma in which electromagnetic wave propagation is determined by Maxwell's equations and a set of hydrodynamic equations,

$$\nabla \times \vec{E} + \mu_0 i\omega \vec{H} = 0$$

$$\nabla \times \vec{H} - \epsilon_0 i\omega \vec{E} = \sum_i q_i N_i \vec{V}_i \tag{2.1}$$

and,

$$i\omega \vec{V}_i + \frac{q_i}{m_i} \vec{E} + \frac{\mu_0 q_i}{m_i} (\vec{V}_i \times \vec{H}) + \sum_j \nu_{ij} \frac{m_i}{m_i + m_j} (\vec{V}_i - \vec{V}_j) \tag{2.2}$$

where,

$$q_i = \begin{bmatrix} -e \\ e \\ e \\ 0 \end{bmatrix} \quad \text{if} \quad i = \begin{bmatrix} + \\ e \\ - \\ o \end{bmatrix} \tag{2.3}$$

and

$$j = \begin{bmatrix} o - e \\ o - + \\ o + e \\ - + e \end{bmatrix} \quad \text{if} \quad i = \begin{bmatrix} + \\ e \\ - \\ o \end{bmatrix} \tag{2.4}$$

Here m is the ion or electron mass, e is the electronic charge, $\vec{V}$ is the velocity, $f = \omega/2\pi$ is the frequency, $\vec{H}$ is the terrestrial magnetic field, $\vec{E}$ and $\vec{H}$ are the electric and magnetic solutions of Maxwell's equation, μ_0 is the permeability of space, ϵ_0 is the permittivity of space, and ν_{ij} is the collision frequency between the i-th and j-th species.

Equations (2.1), (2.2), (2.3), and (2.4) define a gas mixture of four species. The mathematical details for solving this set of equations and inserting the results into the terrestrial waveguide propagation theory is given in the Johler and Berry [1965] paper.

The collision frequency formulas given by Johler and Berry [1965] were employed in this analysis. However, several alternate formulas were also considered as follows [Knapp, 1965]:

$$\nu_{+o} \sim 8(10^{12})\,\rho \tag{2.5}$$

$$\nu_{o+} \sim 4(10^{-10})N_+ \tag{2.6}$$

$$\nu_{-o} \sim 8(10^{12})\,\rho \tag{2.7}$$

$$\nu_{o-} \sim 4(10^{-18})\,N_-. \tag{2.8}$$

Here ρ is the density at the altitude under consideration and can be obtained from the U. S. Standard Atmosphere [1962]. N_+ is the

positive ion density cc^{-1} and N_- is the negative ion density. The effect of these changes on the propagation was found to be small for the models considered.

The terrestrial waveguide propagation is depicted in figure 1. Here several geometric-optical rays are shown for purposes of physical discussion of the propagation as was done in previous papers [Johler, 1966a; 1966b; 1966c; 1967]. The mathematical theory employed, however, is a full wave theory and the geometric optical rays are not necessary for the solution.

Figure 2 illustrates the nuclear environment model developed by Crain and Booker [1964]. Here, the positive ion density, N_i, and the electron density are given in terms of the conductivity parameter $N_{e,i}/\nu_{e,i}\, m_{e,i}$ where conductivity σ, is given by

$$\sigma = \frac{e^2}{m_{e,i}} \quad \frac{N_{e,i}}{\nu_{e,i} + i\omega} \quad . \tag{2.9}$$

Thus, in the lower ionosphere $\nu_{e,i} >> \omega$ for $f << 1000$ kc/s, or

$$\sigma \sim \frac{N_{e,i}\, e^2}{m_{e,i}\, \nu_{e,i}} \propto \frac{N_{e,i}}{\nu_{e,i}\, m_{e,i}} \quad . \tag{2.10}$$

The quantity, σ, in (2.10) is convenient for comparing the relative importance of ions and electrons as a function of altitude as depicted in figure 2. The parameter Q_0 is the production rate of the nuclear debris in ion pairs per cubic centimeter per second per atmosphere. The U. S. Standard Atmosphere [1962] can be employed to calculate the production rate at any altitude. $Q_0 = 10^8$ is a severe disturbance and $Q_0 = 10^6$ and 10^4 are intermediate and weak disturbances, respectively. Note that the curves in general cross at a particular altitude. Thus, at approximately 42 km the effects of ions and electrons are equal for $Q_0 = 10^6$. Above this height, electrons dominate and below this height ions dominate. Electron densities are given in figure 2a and ion densities are given in figure 2b for convenience. Figure 2c illustrates the corresponding nighttime nuclear profits, and the number densities corresponding to these profiles are given in figures 2d and 2e.

3. Transforms for the Nuclear Model Propagation Medium

The previous papers [Johler, 1962; 1964; 1966c] define the basis for the calculation of transforms. The rays corresponding to the rays of the geometric-optical theory are depicted in figure 1. Thus, the solution to the rigorous theory has been expressed as the series,

$$E_r(\omega, d) = \sum_{j=0}^{\infty} E_{r,j}(\omega, d), \tag{3.1}$$

where E_r is the vertical electric component of the propagated field. Corresponding to each term of this rigorous series [Johler, 1964] geometric-optical rays (the principal rays) can be identified with regions of reflection near the points [1, 1], [2, 1], [2, 2], [3, 1], [3, 2] $\cdots$ in figure 1. The angle of incidence on the ionosphere is in general complex, but the real part is the geometric angle φ_1 with the vertical. The precise calculations of the exact theory, however, use the complex angle, φ_1.

At each point [1, 1], [2, 1], [2, 2], [3, 1] $\cdots$ a profile is introduced to determine the reflection process. The profiles employed in this analysis are given in figures 2, 2a, 2b, 2c, 2d, 2e. The normal daytime profile given in the previous paper [Johler, 1966c] forms the basis for the normal propagation model with which the disturbed models are compared.

Figures 3 through 38 present both the amplitude, $|E_j(\omega, d)|$, and the phase correction, $\varphi_c = -\mathrm{Arg}\, E_j(\omega, d) - k_1 d$ as a function of frequency. The sum of the terms of the geometric series, amplitude $|\sum_j E_j(\omega, d)|$ and phase correction $\varphi_c = -\mathrm{Arg} \sum_j E_j(\omega, d) - k_1 d$ for j = 0, 1, 2, 3, 4, 5 or $\sum_{j=0}^{5}$. This curve has significance, for example, when the contribution of the 6th and higher order terms can be neglected. In this case, $\sum_j$ represents the complete field of a CW transmitter. The $\sum_j$ representation is, of course, not necessary to the pulse solution, since each term of the series is integrated separately to the time domain as discussed in the previous paper [Johler, 1966c].

Transforms of the type presented in figures 3 through 38 can be employed to simulate the propagation of almost any shape pulse with energy in the low frequency part of the spectrum. A sferic is an example. This suggests permanent retention of these transforms on data cards or magnetic tape for future use. Figure 7 illustrates a typical amplitude transfer characteristic. Each of the terms of the geometric series, $j = 0, 1, 2, 3, 4, 5$ appear to be a filter characteristic with a maximum centered in the neighborhood of 10 kc/s. The attenuation with frequency is approximately exponential at the high-frequency side of the transfer characteristic. The attenuation with decreasing frequency is less severe on the low frequency side. The corresponding phase correction, φ_c, is illustrated for this case in figure 8. The slope is generally positive and strongly positive with frequency at the high frequency part of the spectrum. An inflection in phase occurs near the crest of the amplitude of the spectrum.

4. Propagation of the Pulse to Great Distances

The theoretical reconstruction of a pulse from a nuclear burst is illustrated at intermediate and great distances in figures 39 through 56. The quantity calculated is the waveform, $\mathrm{Re}\, E(t', d_2)$,

$$\mathrm{Re}\, E(t' d_2) = \mathrm{Re} \sum_{j=0}^{\infty} \frac{1}{2\pi} \int_0^{\infty} \exp(i\omega t') \frac{F_0(\omega, d_1)}{E_0(\omega, d_1)} \times E_j(\omega, d_2)\, d\omega \tag{4.1}$$

where $d_2 \geq d_1$, $t' = t - \eta_1 d/c$, η_1 is the index of refraction, and d_1 is the distance of the observed waveform ($d_1 \sim 44$ km). The observed waveform $\mathrm{Re}\, E(t' d_1)$ is transformed to the frequency domain by calculating F_0,

$$F_0(\omega, d_1) = \int_0^{\infty} \exp(-i\omega t)\, \mathrm{Re}\, E(t', d_1)\, dt. \tag{4.2}$$

$E_0(\omega, d_1)$ is the ground wave to some short distance d_1. $E_j(\omega, d_2)$ comprises the ground wave and the various ionospheric waves, $j = 0, 1, 2, 3 \cdots$. Detailed techniques for evaluating these integrals have been discussed elsewhere [Johler, 1962].

The particular distance, d = 4828 km, $Q_0 = 10^4$, (fig. 42) serves to illustrate the technique. Thus, 300 μs of the composite pulse depicted as the solid line, is obtained by adding the ground wave and the first ionospheric reflection and the higher order reflections, j = 2, 3, 4, ···, in the time domain. Thus, the ground wave, Re $E_0(t', d)$, produces only a very slight ripple in the zero amplitude reference line. A readily perceptable undulation is produced by the sum Re $E_0(t', d)$ + Re $E_1(t', d)$. The second cycle of the pulse is clearly established by the sum Re $E_0(t', d)$ + Re $E_1(t', d)$ + Re $E_2(t', d)$. The third cycle of the pulse is established by the sum Re $E_0(t', d)$ + Re $E_1(t', d)$ + Re $E_2(t', d)$ + Re $E_3(t', d)$. Approximately 200 μs of the pulse is established by the sum, Re $E_0(t', d)$ + Re $E_1(t', d)$ + Re $E_2(t', d)$ + Re $E_3(t', d)$ + Re $E_4(t', d)$. Finally, with the aid of the fifth ionospheric reflection, approximately 300 μs of the pulse is established with the sum, Re $E_0(t', d)$ + Re $E_1(t', d)$ + Re $E_2(t', d)$ + Re $E_3(t', d)$ + Re $E_4(t', d)$ + Re $E_5(t', d)$.

Similar reconstruction of the pulse at various distance between 1609 and 8046 km were developed in figures 39 through 56. The lowering of the ionosphere in the more severe nuclear environment $Q_0 = 10^6$ and 10^8 caused the higher order reflections to arrive earlier. Thus, in addition to dispersion caused by the reflection process involving the ions, dispersion resulting from earlier ionospheric wave delays was noted. A comparison with the normal environment pulse described in other documents [Johler, 1966c; 1967; and Johler and Morgenstern, 1965] is depicted in figure 57. The dispersion of the pulse as a function of distance and as a function of the severity, Q_0, of the nuclear disturbance is clearly evident. It is interesting to note that the disturbance of intermediate severity, $Q_0 = 10^6$, produces the greatest attenuation of the pulse at the greater distances. Thus, further increase in the severity of the disturbance to $Q_0 = 10^8$ increases the amplitude of the pulse.

5. Conclusions

The most distinguishing feature of the pulse dispersion as a consequence of increasing disturbance, Q_0, resulting from uniformly distributed nuclear debris type disturbance is an arrival of the energy of the pulse at earlier time. The lower reflection height in the ionosphere is, in large measure, a consequence of the ions, although the role of the electrons is not negligible in the nuclear environment. Although a particular pulse has been propagated theoretically and the change in form or shape has been illustrated in detail, the transforms developed to propagate such a pulse can be employed to propagate other pulses with energy at low frequencies (< 1000 kc/s).

The author is indebted to Richard S. Greeley, Ted Jarvis, Laurence Jacobs, Nicholas Del Vecchio, John Morgenstern, and other members of the professional staff of the Mitre Corporation for many stimulating discussions which influenced the course of this work. The author also wishes to note the able assistance of Carlene Lilley with the many details of the computer computation.

6. References

Crain, C. M. (1961), Ionization loss rates below 90 km, J. Geophys. Res. 66, No. 4, 1117-1126.

Crain, C. M. (1964), A note on persisting radio propagation effects after high-altitude nuclear bursts, J. Geophys. Res. 66, No. 21, 4-117.

Crain, C. M., and H. G. Booker (1963), The effect of nuclear bursts in space on the propagation of HF radio waves between separated earth terminals, J. Geophys. Res. 68, No. 8, 2159-2166.

Crain, C. M., and H. G. Booker (1964), The effect of ions on LF and VLF propagation in an abnormally ionized atmosphere, J. Geophys. Res. 69, No. 21, 4713-4716.

Johler, J. R. (1962), Propagation of the low-frequency radio signal, Proc. IRE 50, No. 4, 404-427.

Johler, J. R. (1964), Concerning limitations and further corrections to geometric-optical theory for LF, VLF propagation between the ionosphere and the ground, Radio Sci. J. Res. NBS/USNC-URSI 66D, No. 1, 67-78.

Johler, J. R. (1966a), Zonal harmonics in low frequency terrestrial radio wave propagation, NBS Technical Note 335.

Johler, J. R. (1966b), Theory of propagation of low frequency terrestrial radio waves--mathematical techniques for the interpretation of D-region propagation studies, Conference on Ground-Based Radio Wave Propagation Studies of the Lower Ionosphere, April 11-15, 1966, Radio Physics Laboratory, DRTE, Ottawa, Canada (to be published).

Johler, J. R. (1966c), Electromagnetic pulse propagation in the normal terrestrial waveguide environment, ESSA Technical Report, IER-21 ITSA-21.EMP Theoretical Note 46 in Volume 3 of AFWL EMP Note 46.

Johler, J. R. (1967), Propagation of an electromagnetic pulse from a nuclear burst, IEEE Trans. on Ant. and Prop. (to be published).

Johler, J. R., and L. A. Berry (1965), On the effect of heavy ions on LF propagation, with special reference to a nuclear environment, NBS Technical Note 313.

Johler, J. R., and J. C. Morgenstern (1965), Propagation of the ground wave electromagnetic signal, with particular reference to a pulse of nuclear origin, Proc. IEEE 53, No. 12, 2043-2053.

Knapp, W. S. (1965), Private communication.

U. S. Standard Atmosphere (1962), U. S. Government Printing Office, Washington, D. C.

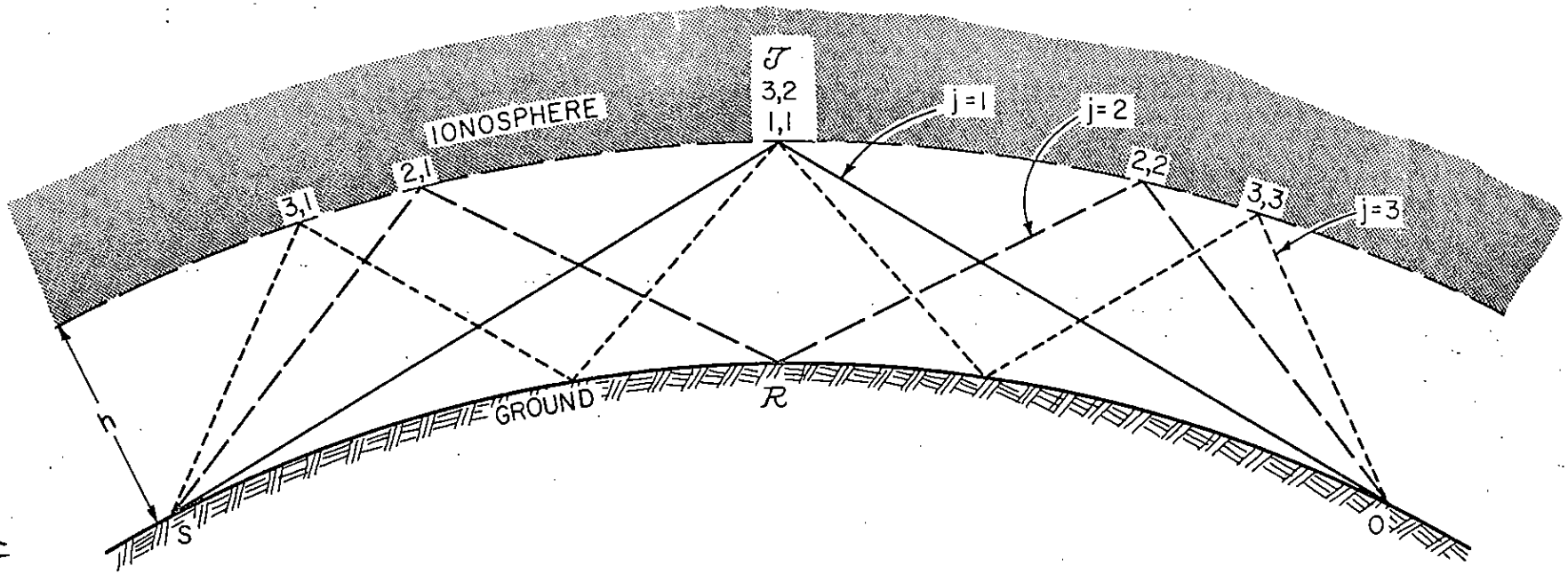

Figure 1. Illustrating approximate geometric-optical rays corresponding to terms of the rigorous geometric-optical series for the theory of propagation in the terrestrial waveguide.

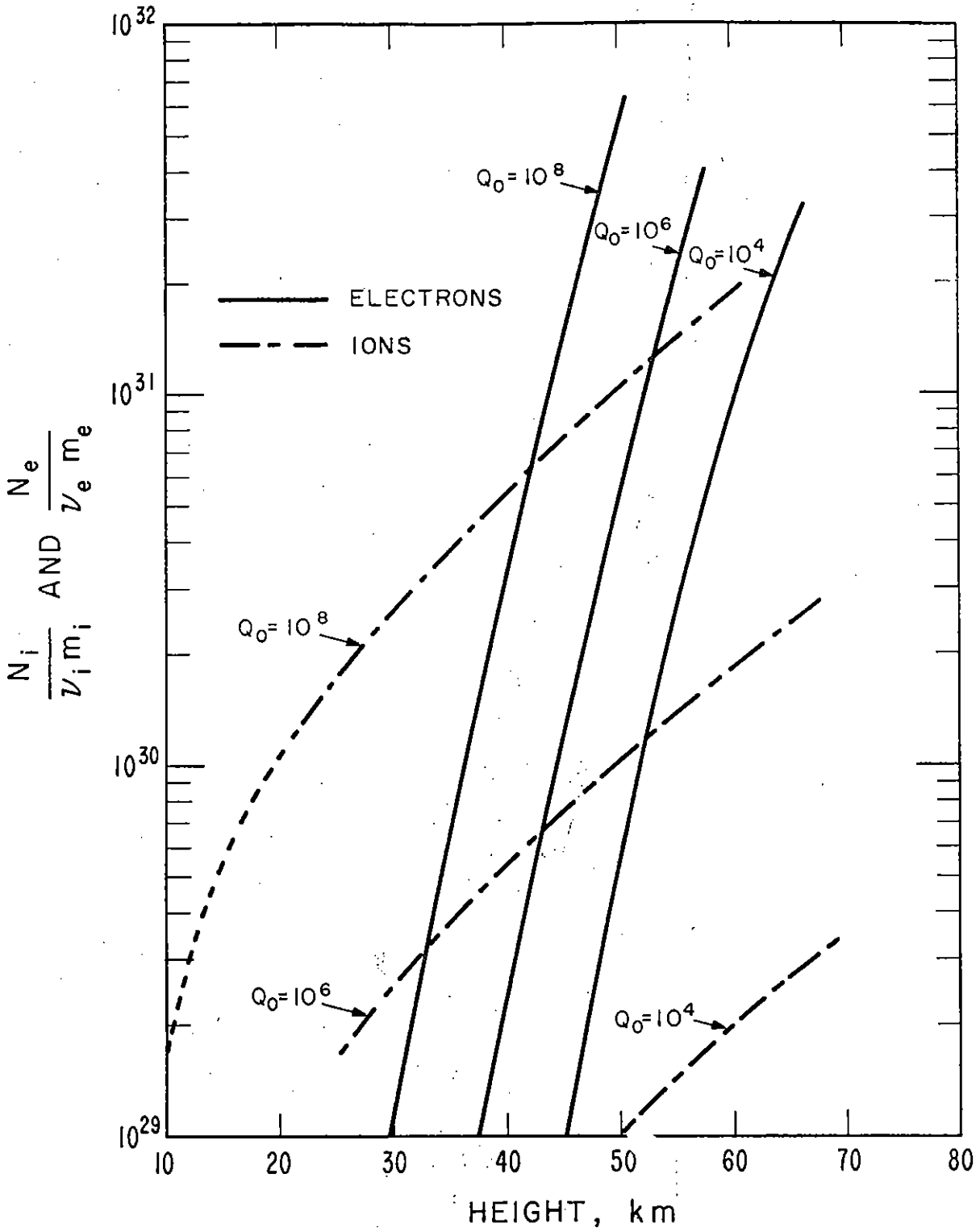

Figure 2. State of electrification of the daytime atmosphere and lower ionosphere in the nuclear environment (after Crain and Booker, 1964) in terms of the parameter $N_{e,i}/\nu_{e,i}m_{e,i}$.

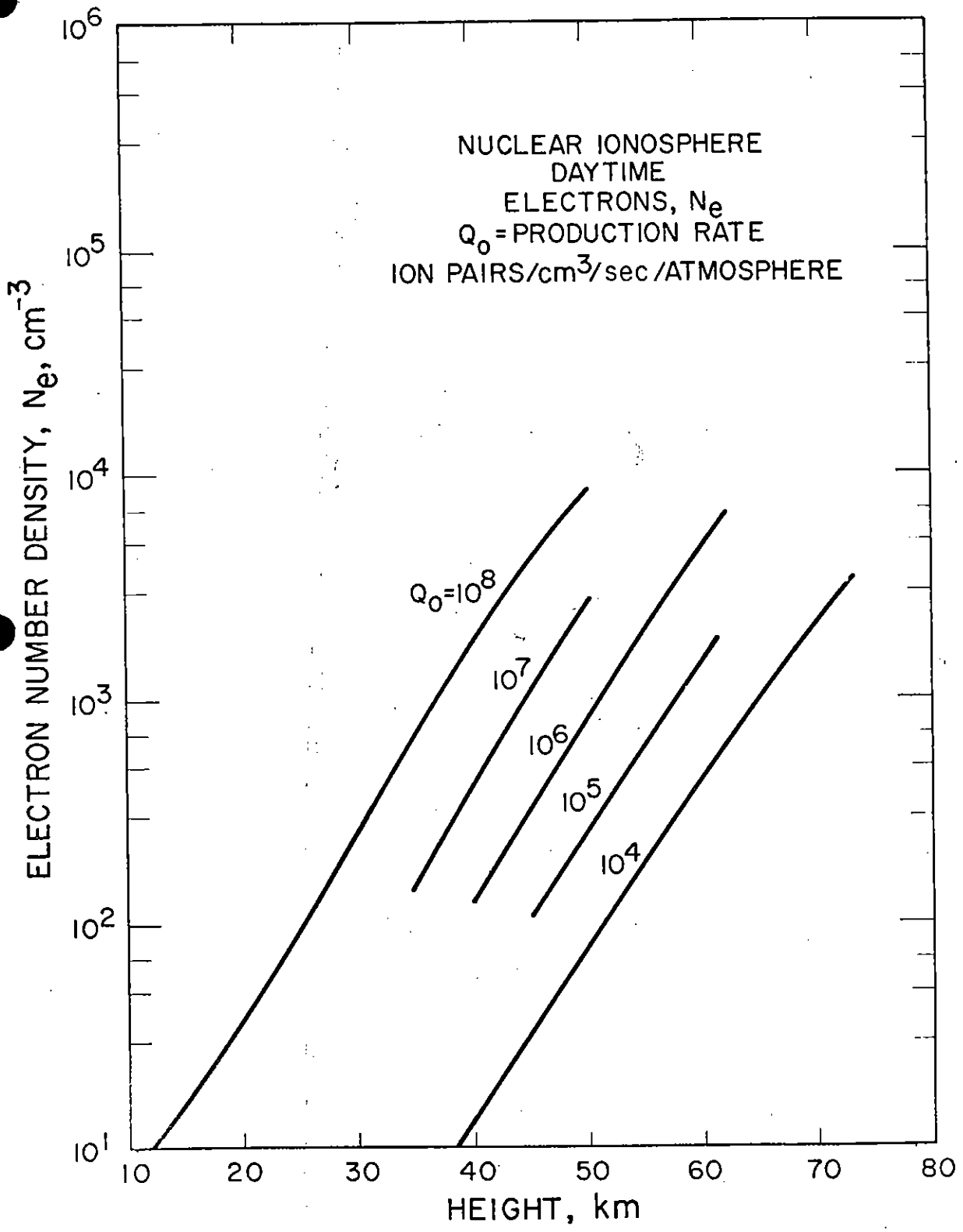

Figure 2a. Electron density in the daytime nuclear environment.

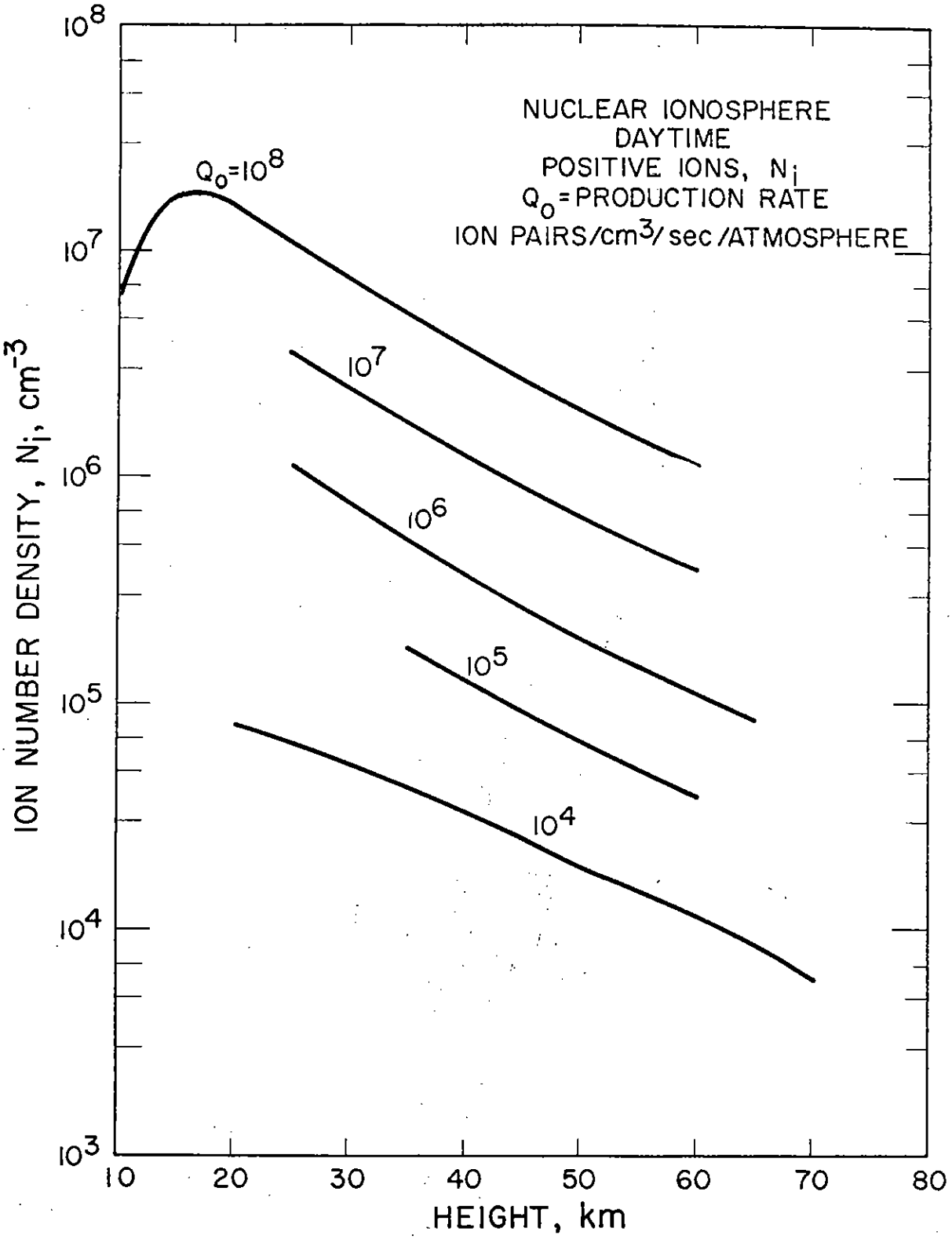

Figure 2b. Ion density in the daytime nuclear environment.

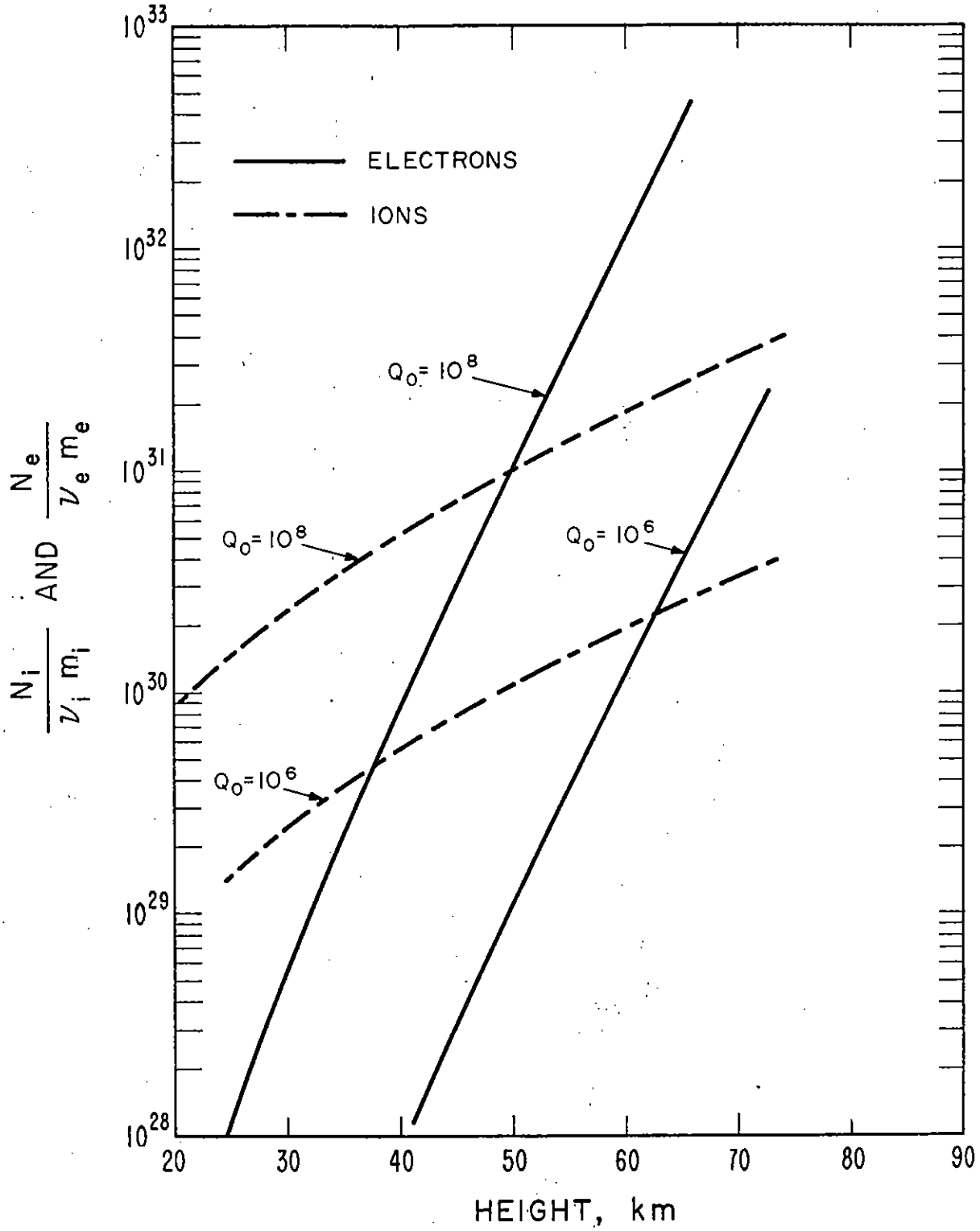

Figure 2c. State of electrification of the nighttime atmosphere and lower ionosphere in the nuclear environment (after Crain and Booker, 1964) in terms of the parameters $N_{e,i}/\nu_{e,i}m_{e,i}$.

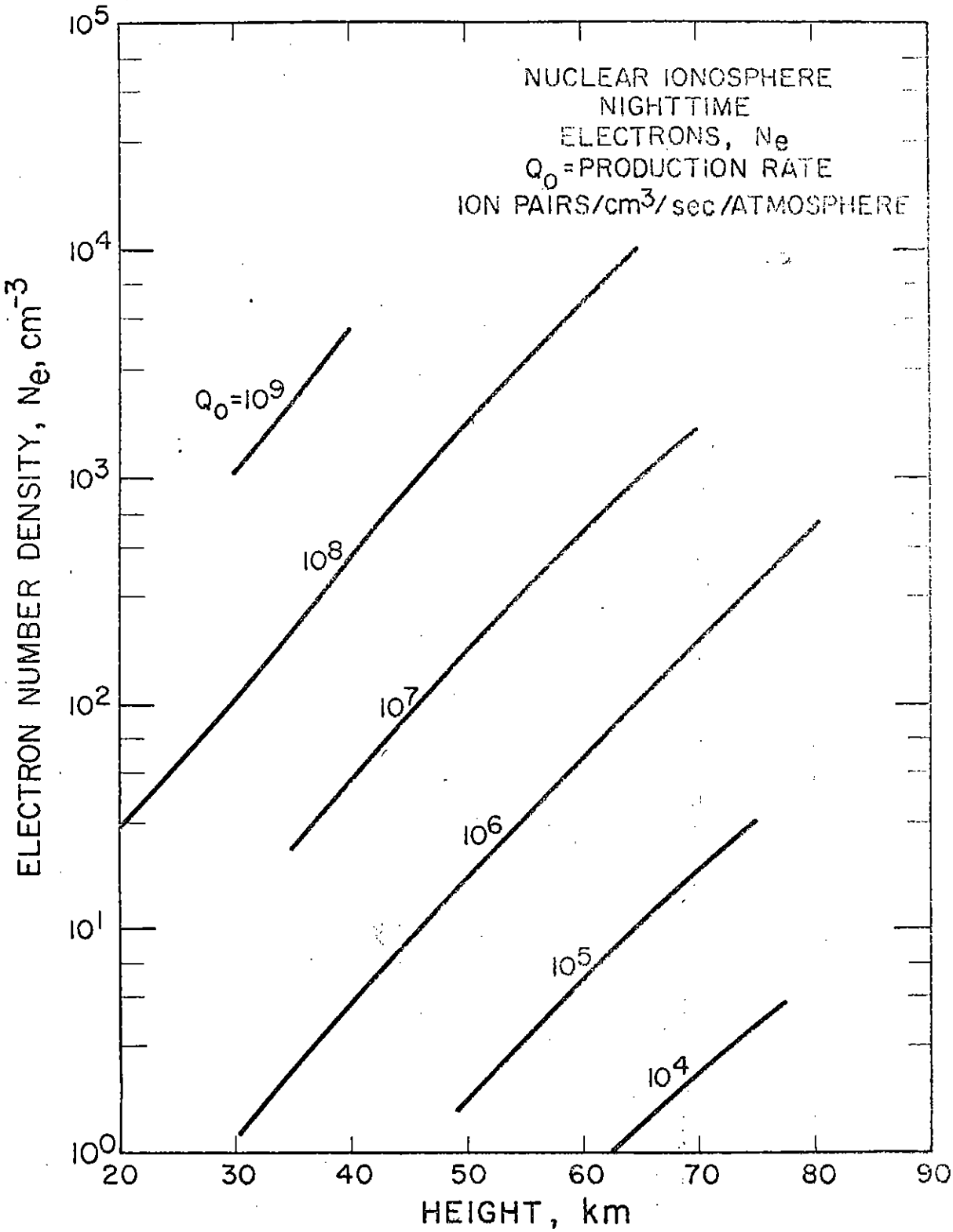

Figure 2d. Electron density in the nighttime nuclear environment.

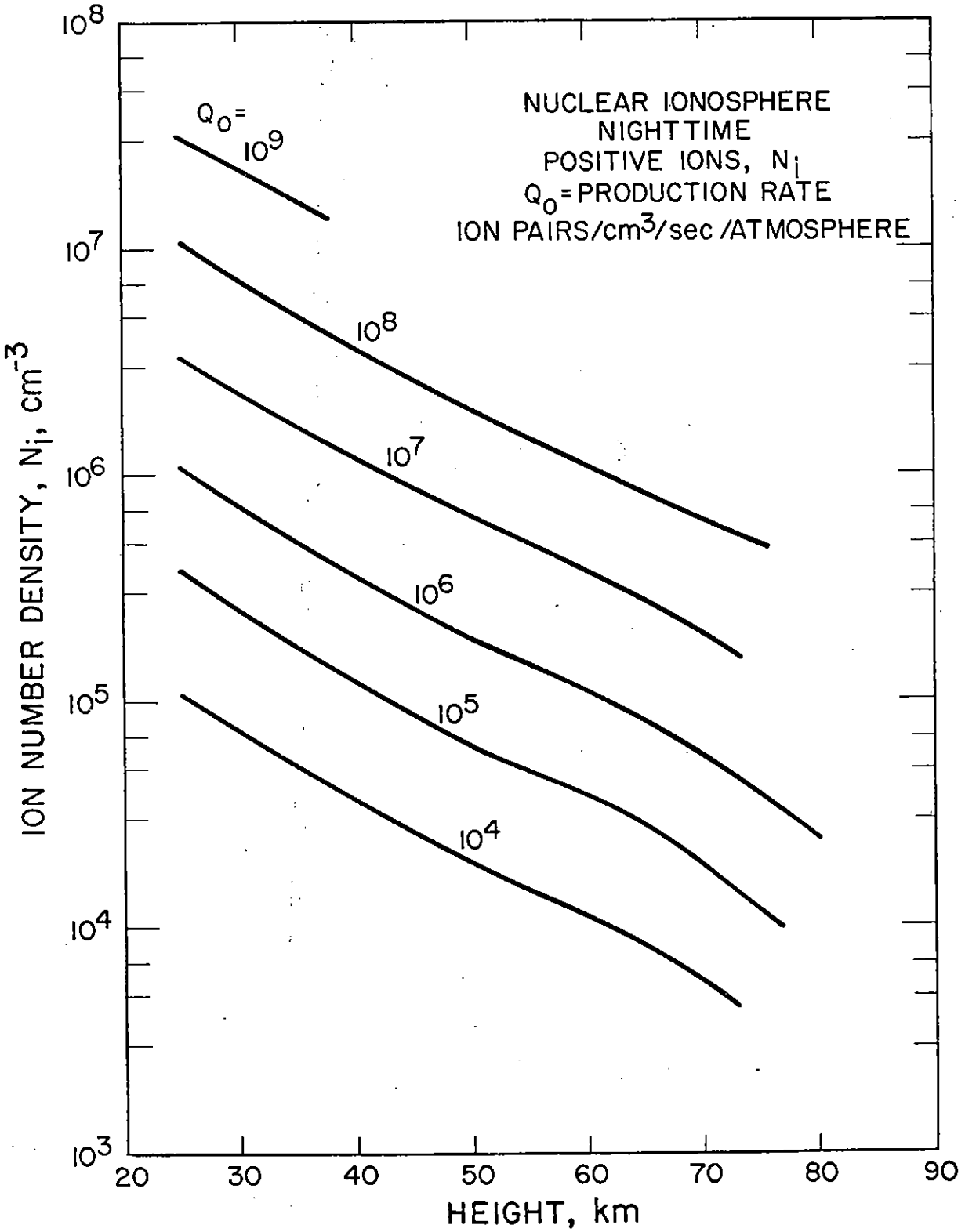

Figure 2e. Ion density in the nighttime nuclear environment.

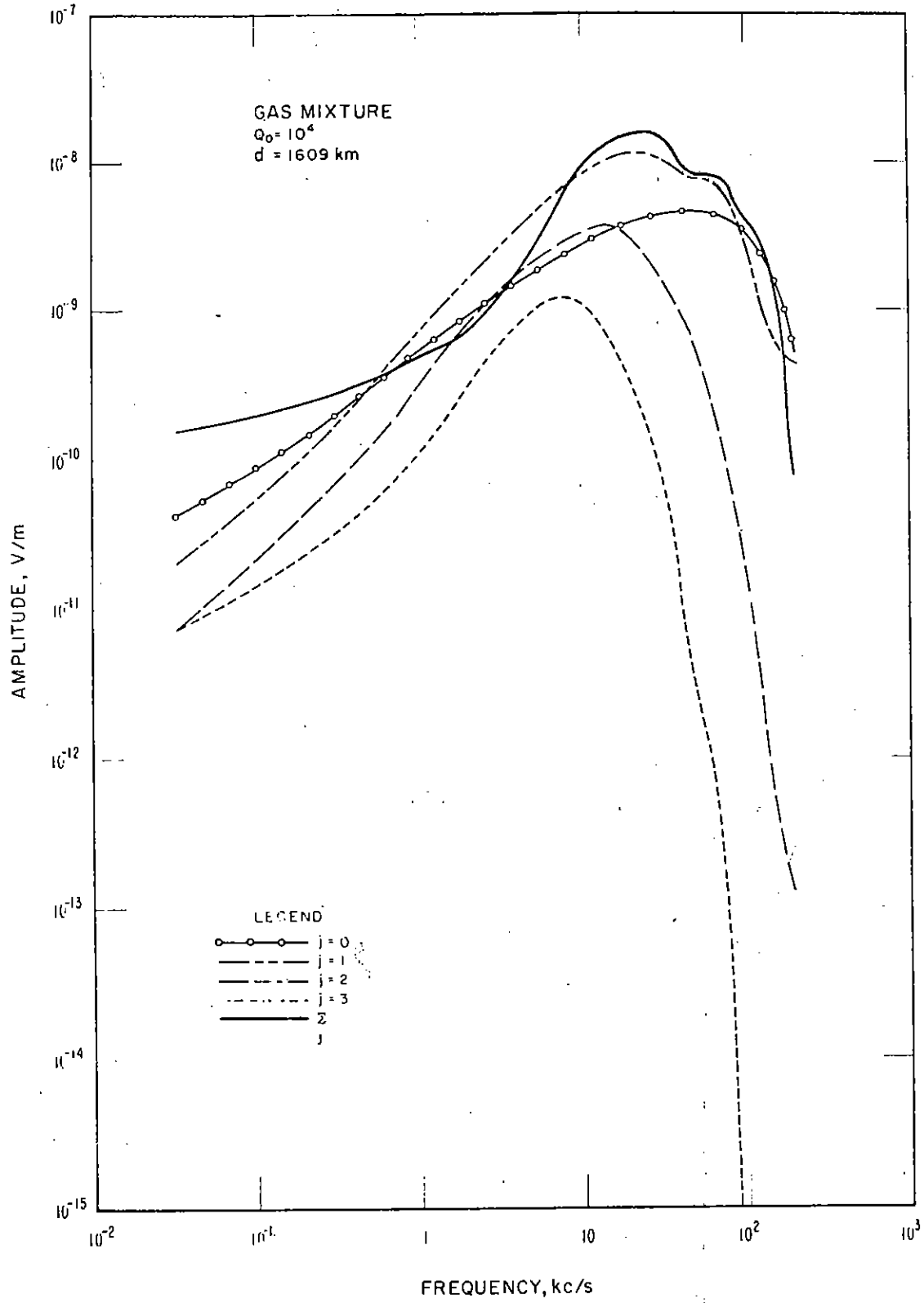

Figure 3. Amplitude of the disturbed propagation medium transform, $d = d_2 = 1609$ km; illustrating the terms of the geometric series $|E_j(\omega, d_2)|$ and the total field $|\sum_j E_j(\omega, d_2)|$ for a nuclear debris production rate, $Q_0 = 10^4$ ion pairs per cubic centimeter per second per atmosphere.

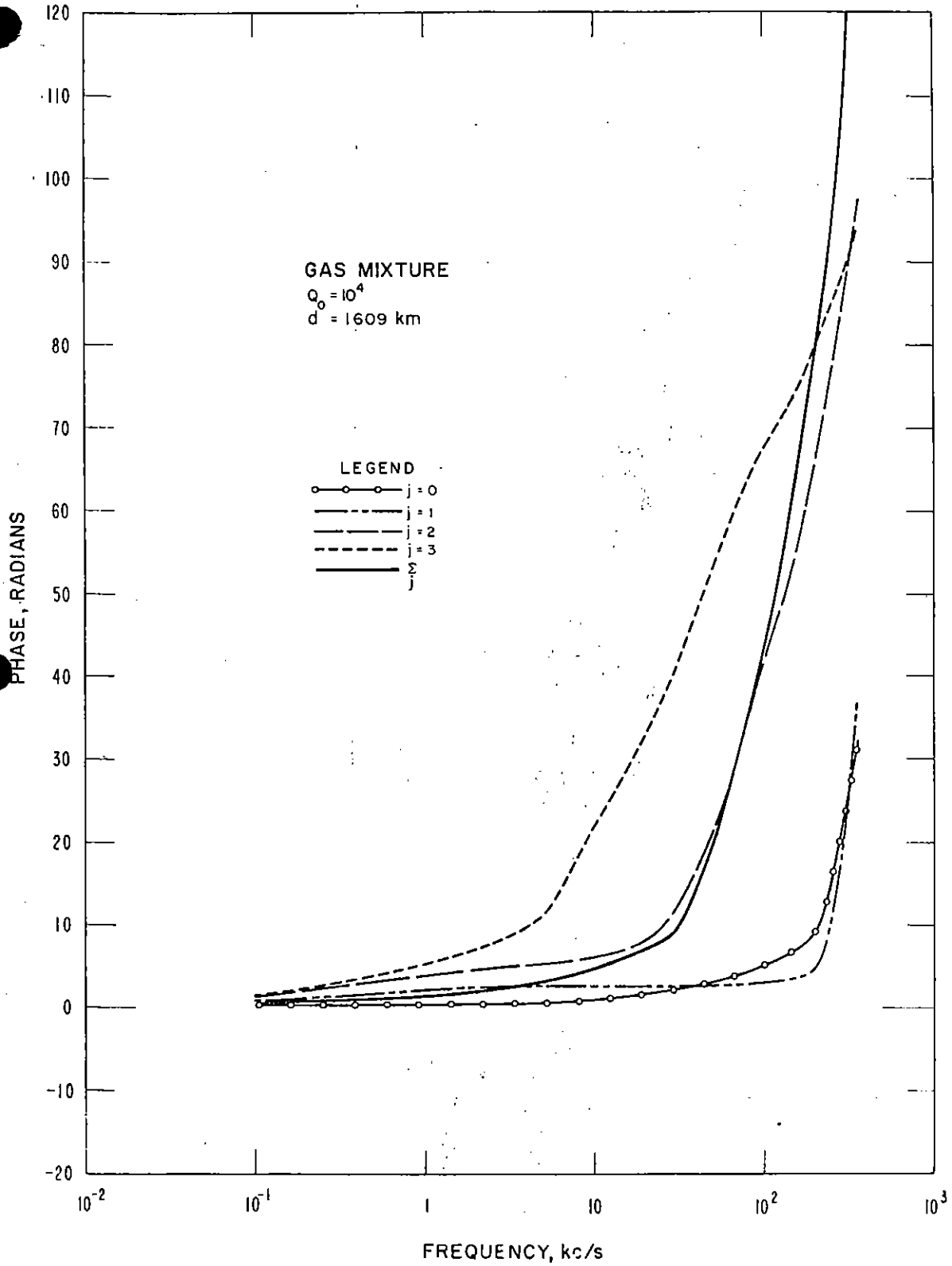

Figure 4. Phase correction of the disturbed propagation medium transform, $d = d_2 = 1609$ km; illustrating the terms of the geometric series $-k_1 d_2 - \text{Arg}\, E_j(\omega, d_2)$ and the total phase $-k_1 d_2 - \text{Arg} \sum_j E_j(\omega, d_2)$ for a nuclear debris production rate, $Q_0 = 10^4$ ion pairs per cubic centimeter per second per atmosphere.

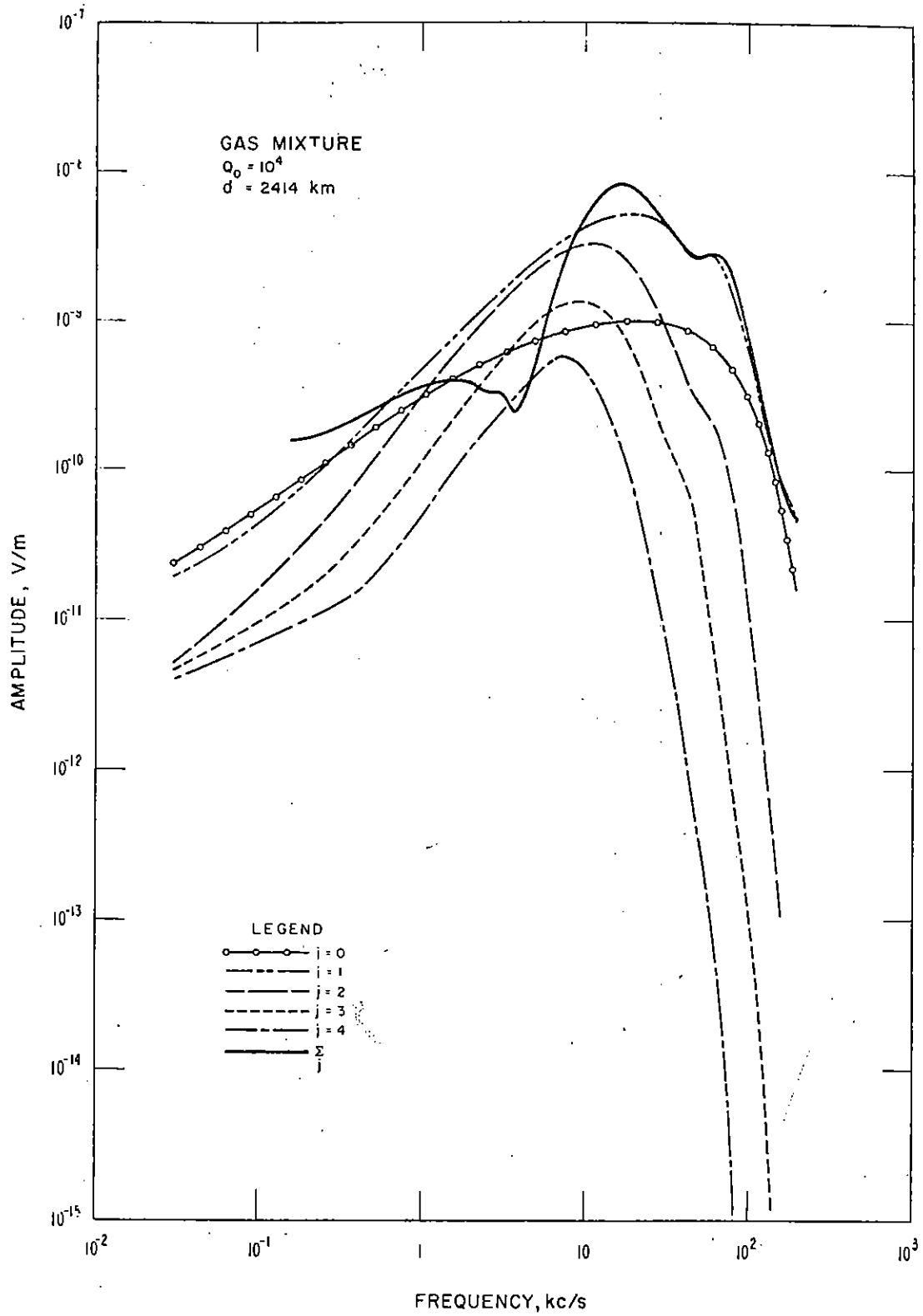

Figure 5. Amplitude of the disturbed propagation medium transform, $d = d_2 = 2414$ km; illustrating the terms of the geometric series $|E_j(\omega, d_2)|$ and the total field $|\sum_j E_j(\omega, d_2)|$ for a nuclear debris production rate, $Q_0 = 10^4$ ion pairs per cubic centimeter per second per atmosphere.

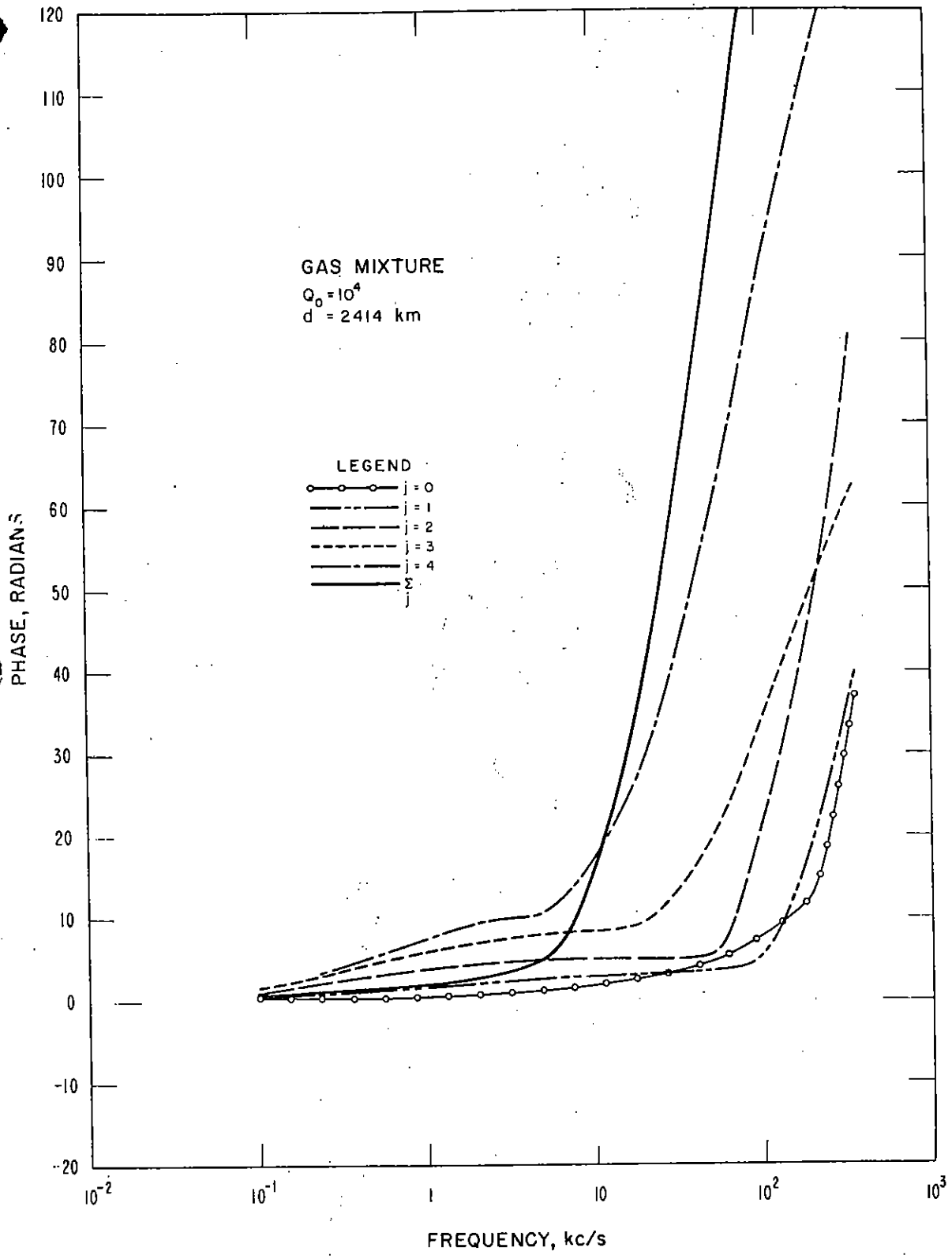

Figure 6. Phase correction of the disturbed propagation medium transform, $d = d_2 = 2414$ km; illustrating the terms of the geometric series $-k_1 d_2 - \text{Arg}\, E_j(\omega, d_2)$ and the total phase $-k_1 d_2 - \text{Arg} \sum_j E_j(\omega, d_2)$ for a nuclear debris production rate, $Q_0 = 10^4$ ion pairs per cubic centimeter per second per atmosphere.

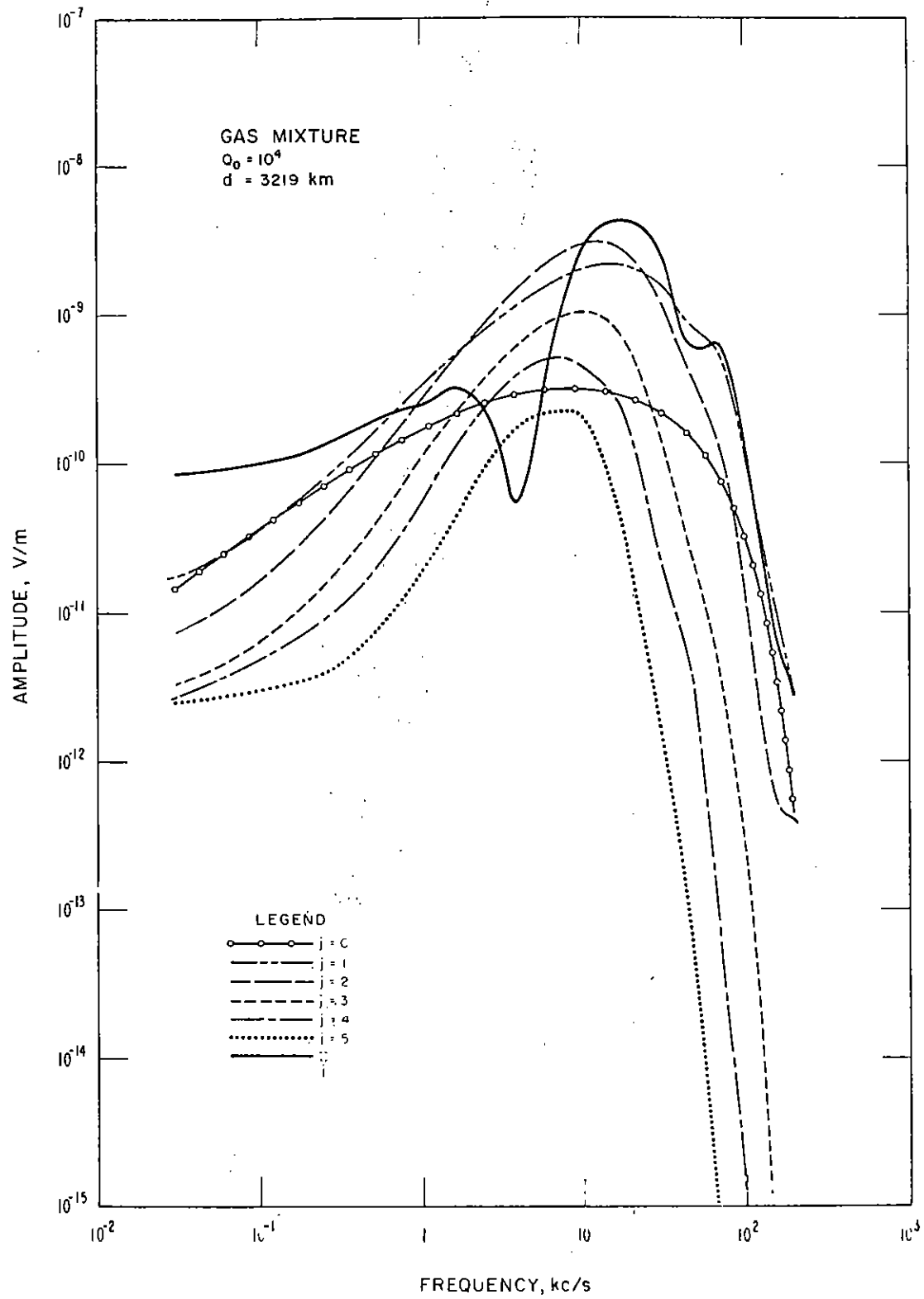

Figure 7. Amplitude of the disturbed propagation medium transform, $d = d_2 = 3219$ km; illustrating the terms of the geometric series $|E_j(\omega, d_2)|$ and the total field $|\sum_j E_j(\omega, d_2)|$ for a nuclear debris production rate, $Q_0 = 10^4$ ion pairs per cubic centimeter per second per atmosphere.

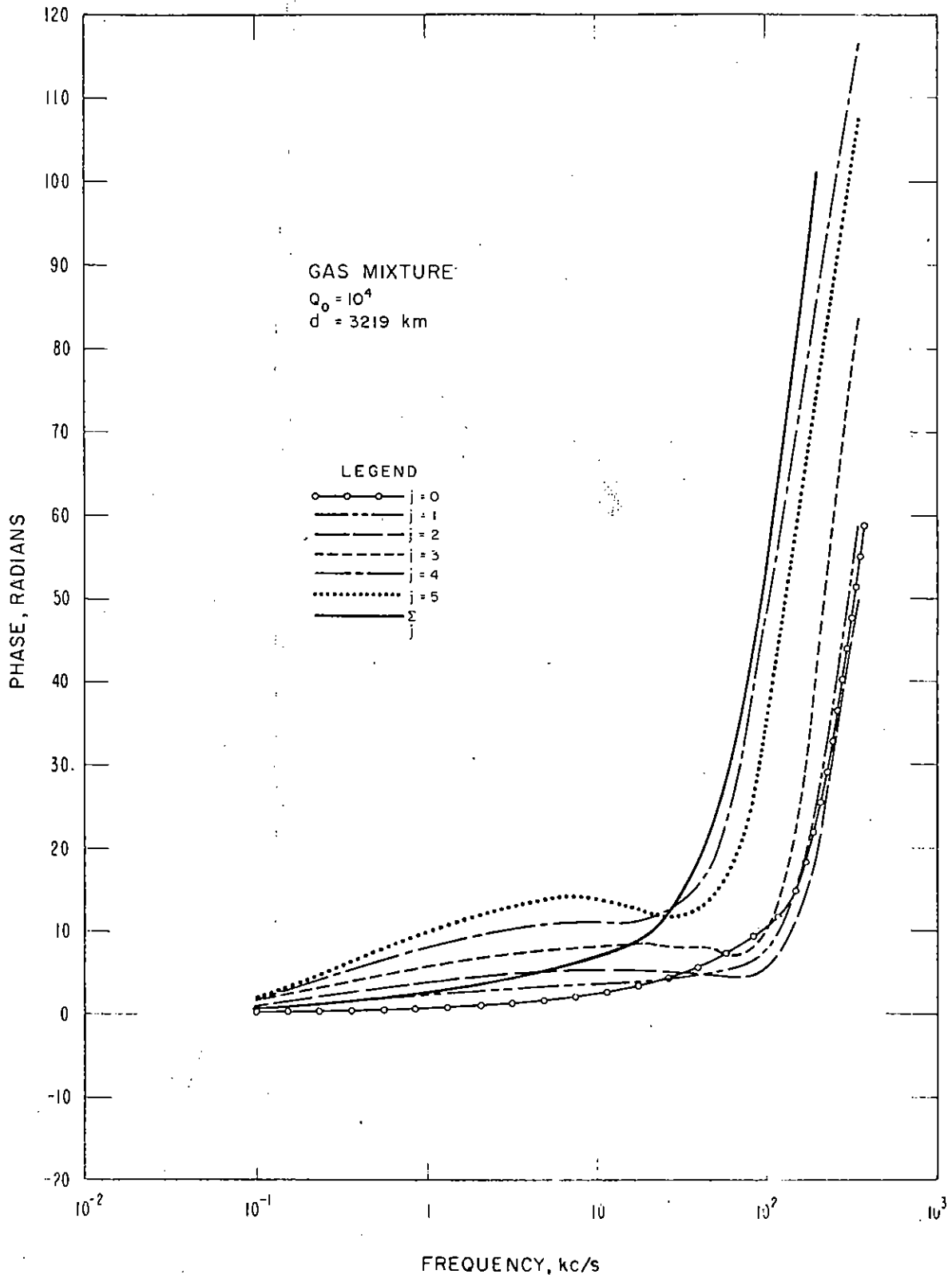

Figure 8. Phase correction of the disturbed propagation medium transform, $d = d_2 = 3219$ km; illustrating the terms of the geometric series $-k_1 d_2 - \mathrm{Arg}\, E_j(\omega, d_2)$ and the total phase $-k_1 d_2 - \mathrm{Arg} \sum_j E_j(\omega, d_2)$ for a nuclear debris production rate, $Q_0 = 10^4$ ion pairs per cubic centimeter per second per atmosphere.

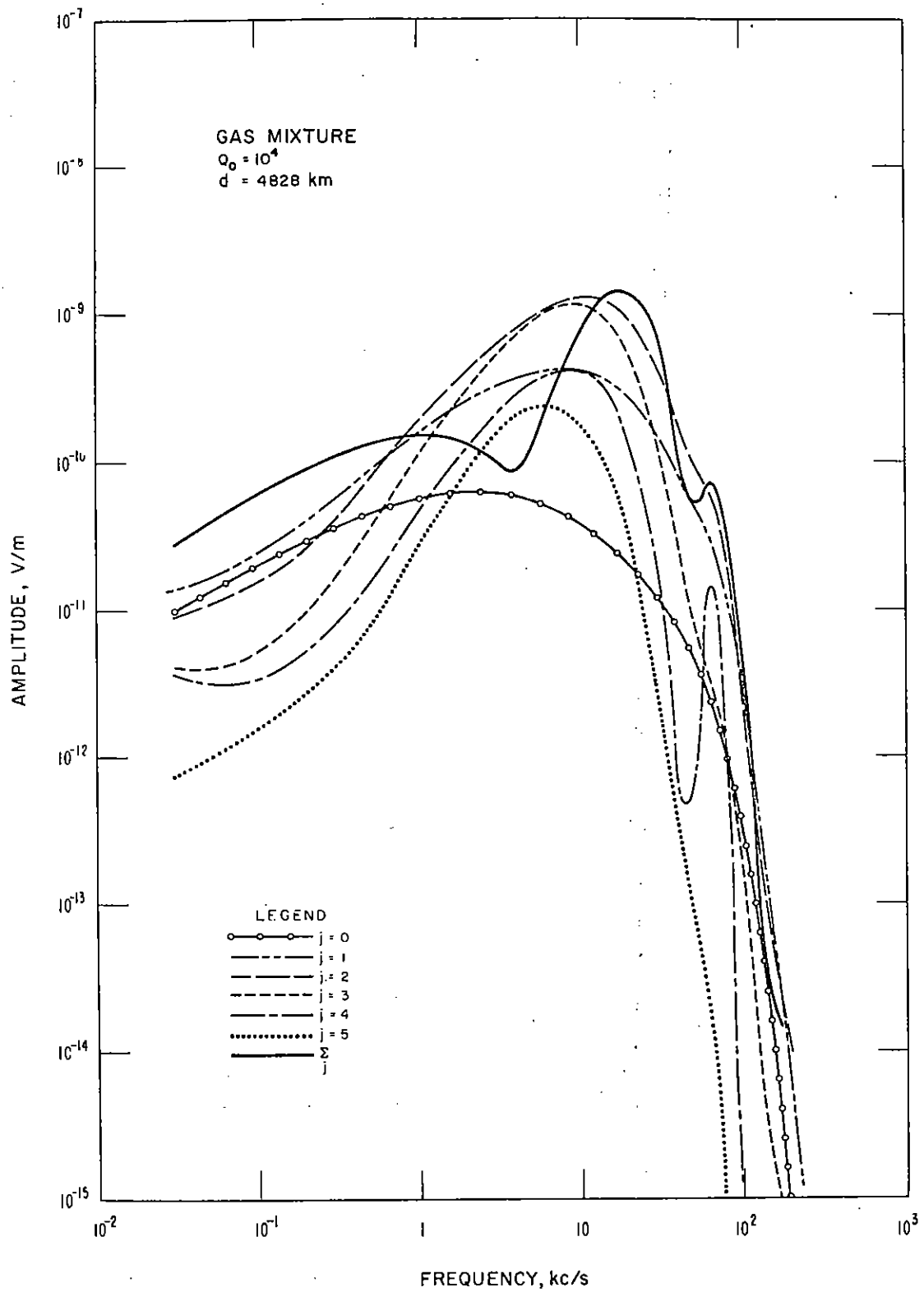

Figure 9. Amplitude of the disturbed propagation medium transform, $d = d_2 = 4828$ km; illustrating the terms of the geometric series $|E_j(\omega, d_2)|$ and the total field $|\sum_j E_j(\omega, d_2)|$ for a nuclear debris production rate, $Q_0 = 10^4$ ion pairs per cubic centimeter per second per atmosphere.

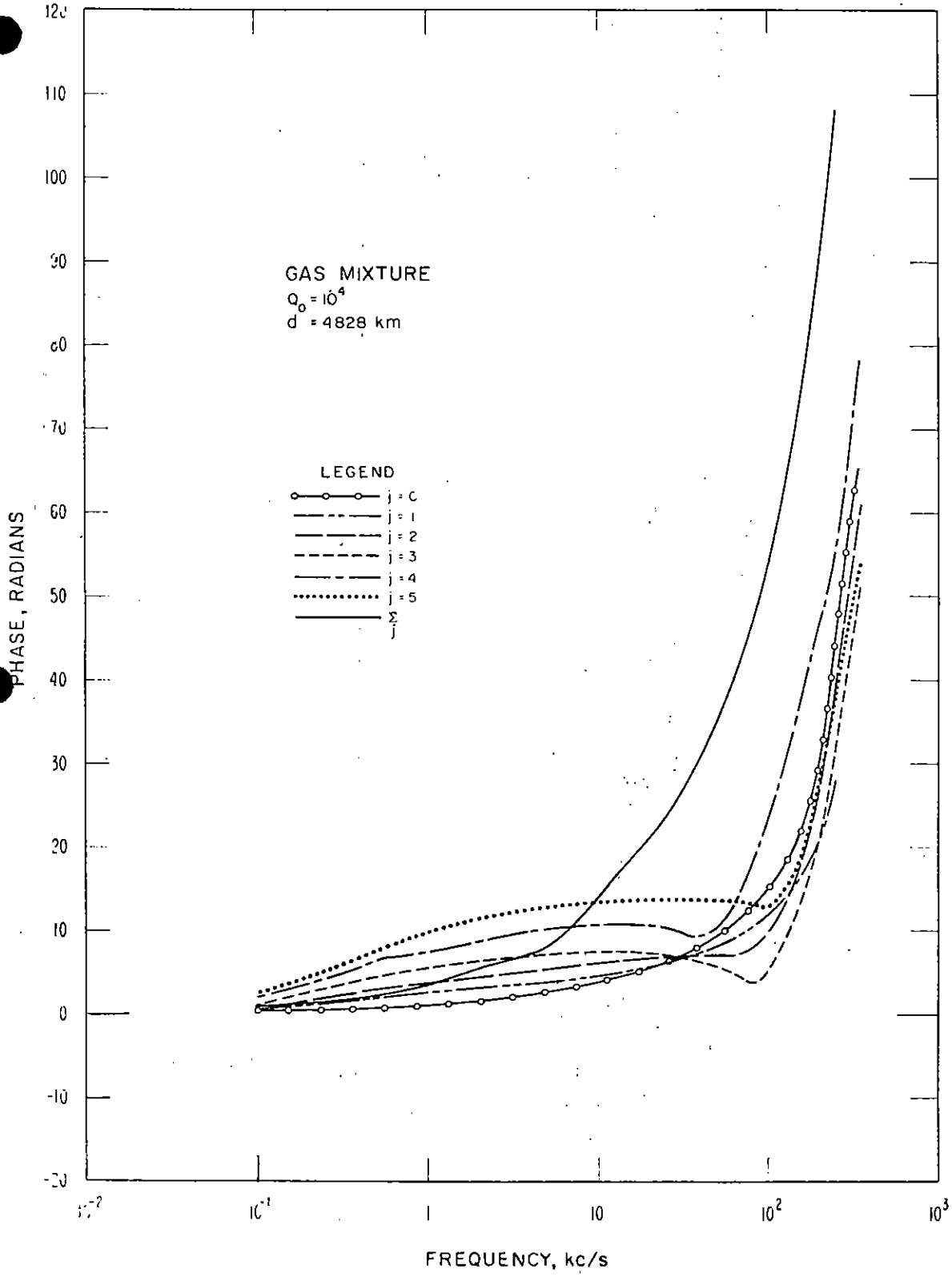

Figure 10. Phase correction of the disturbed propagation medium transform, $d = d_2 = 4828$ km; illustrating the terms of the geometric series $-k_1 d_2 - \mathrm{Arg}\, E_j(\omega, d_2)$ and the total phase $-k_1 d_2 - \mathrm{Arg} \sum_j E_j(\omega, d_2)$ for a nuclear debris production rate, $Q_0 = 10^4$ ion pairs per cubic centimeter per second per atmosphere.

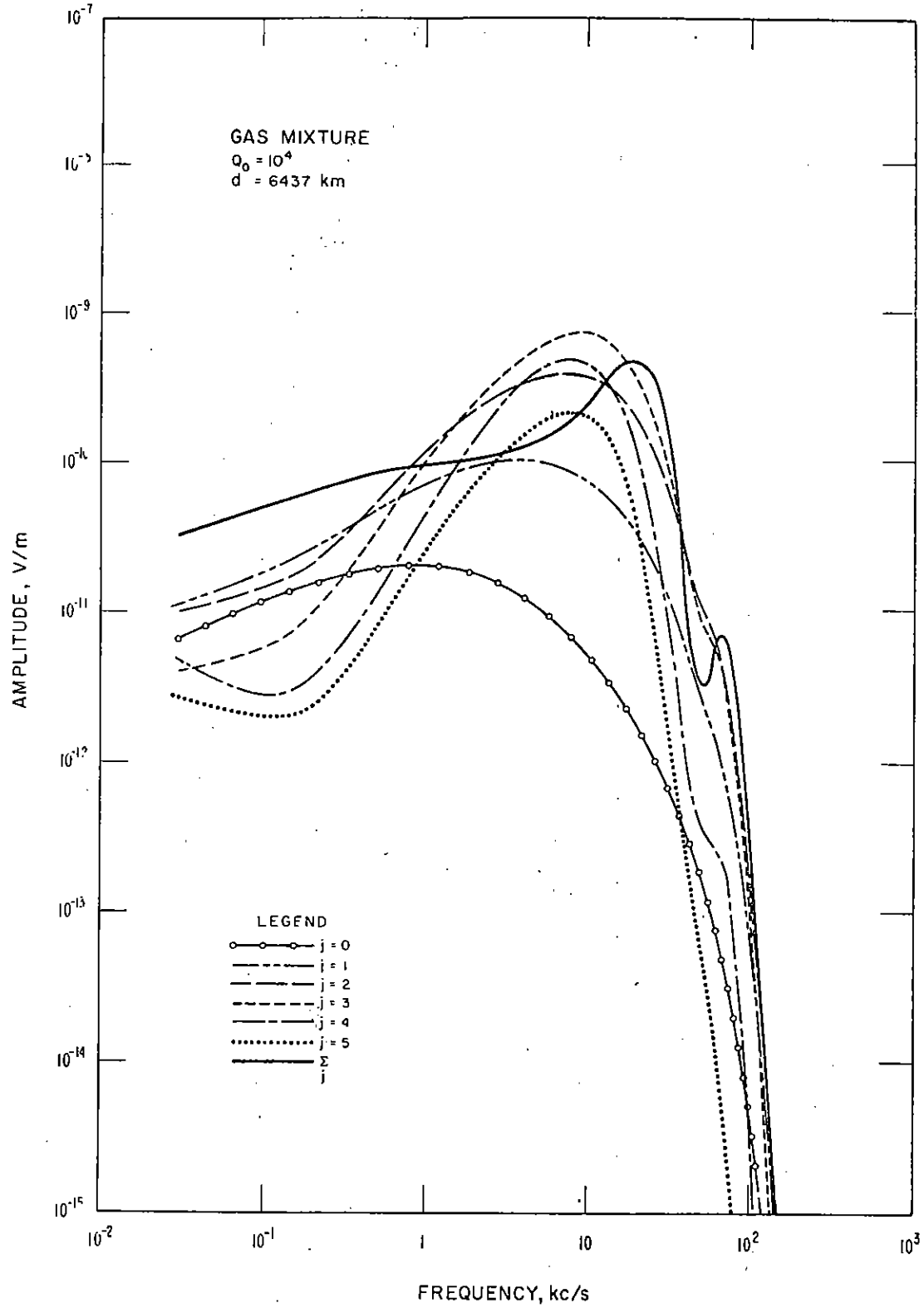

Figure 11. Amplitude of the disturbed propagation medium transform, $d = d_2 = 6437$ km; illustrating the terms of the geometric series $|E_j(\omega, d_2)|$ and the total field $|\sum_j E_j(\omega, d_2)|$ for a nuclear debris production rate, $Q_0 = 10^4$ ion pairs per cubic centimeter per second per atmosphere.

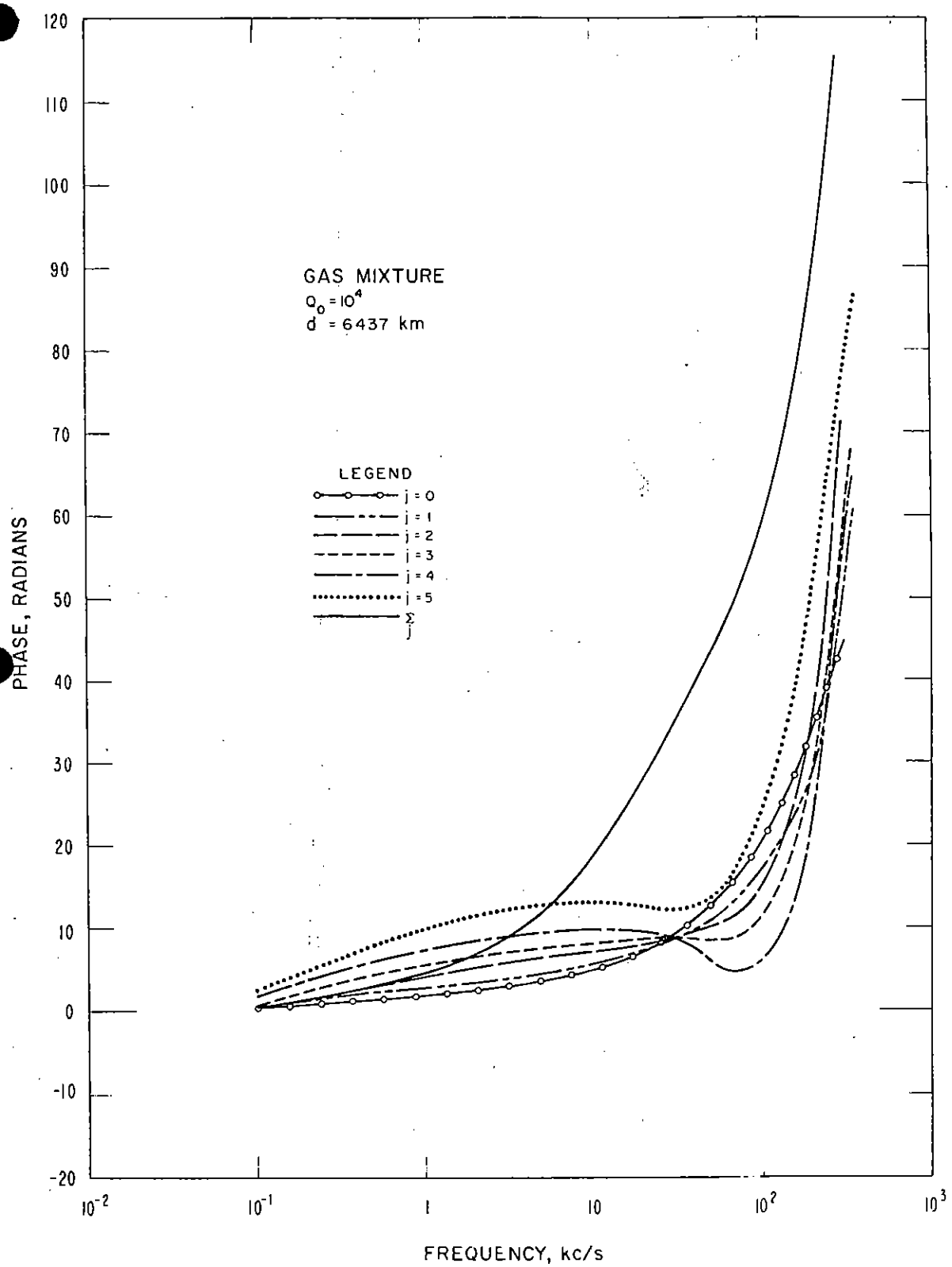

Figure 12. Phase correction of the disturbed propagation medium transform, $d = d_2 = 6437$ km; illustrating the terms of the geometric series $-k_1 d_2 - \text{Arg}\, E_j(\omega, d_2)$ and the total phase $-k_1 d_2 - \text{Arg} \sum_j E_j(\omega, d_2)$ for a nuclear debris production rate, $Q_0 = 10^4$ ion pairs per cubic centimeter per second per atmosphere.

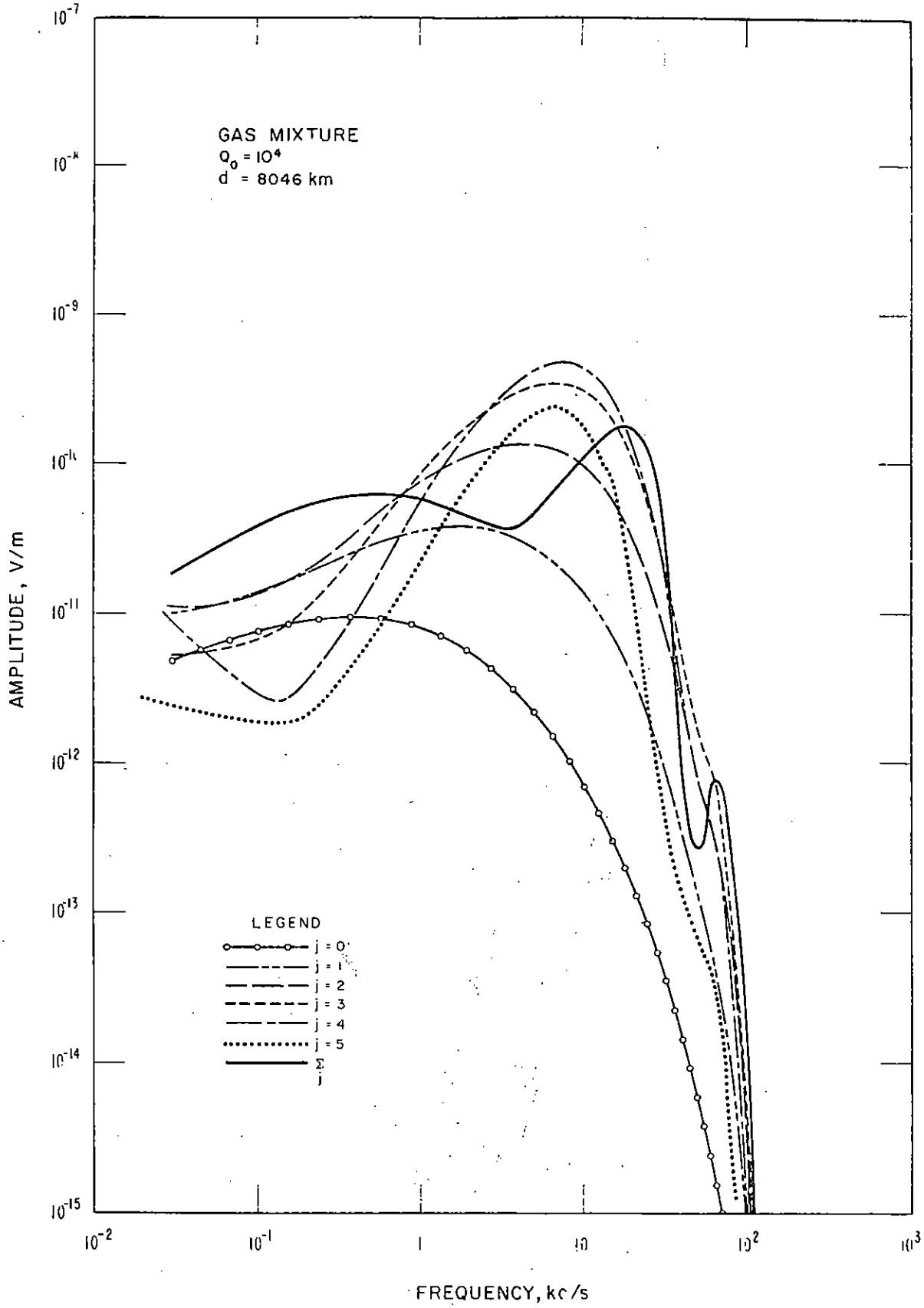

Figure 13. Amplitude of the disturbed propagation medium transform, $d = d_2 = 8046$ km; illustrating the terms of the geometric series $|E_j(\omega, d_2)|$ and the total field $|\sum_j E_j(\omega, d_2)|$ for a nuclear debris production rate, $Q_0 = 10^4$ ion pairs per cubic centimeter per second per atmosphere.

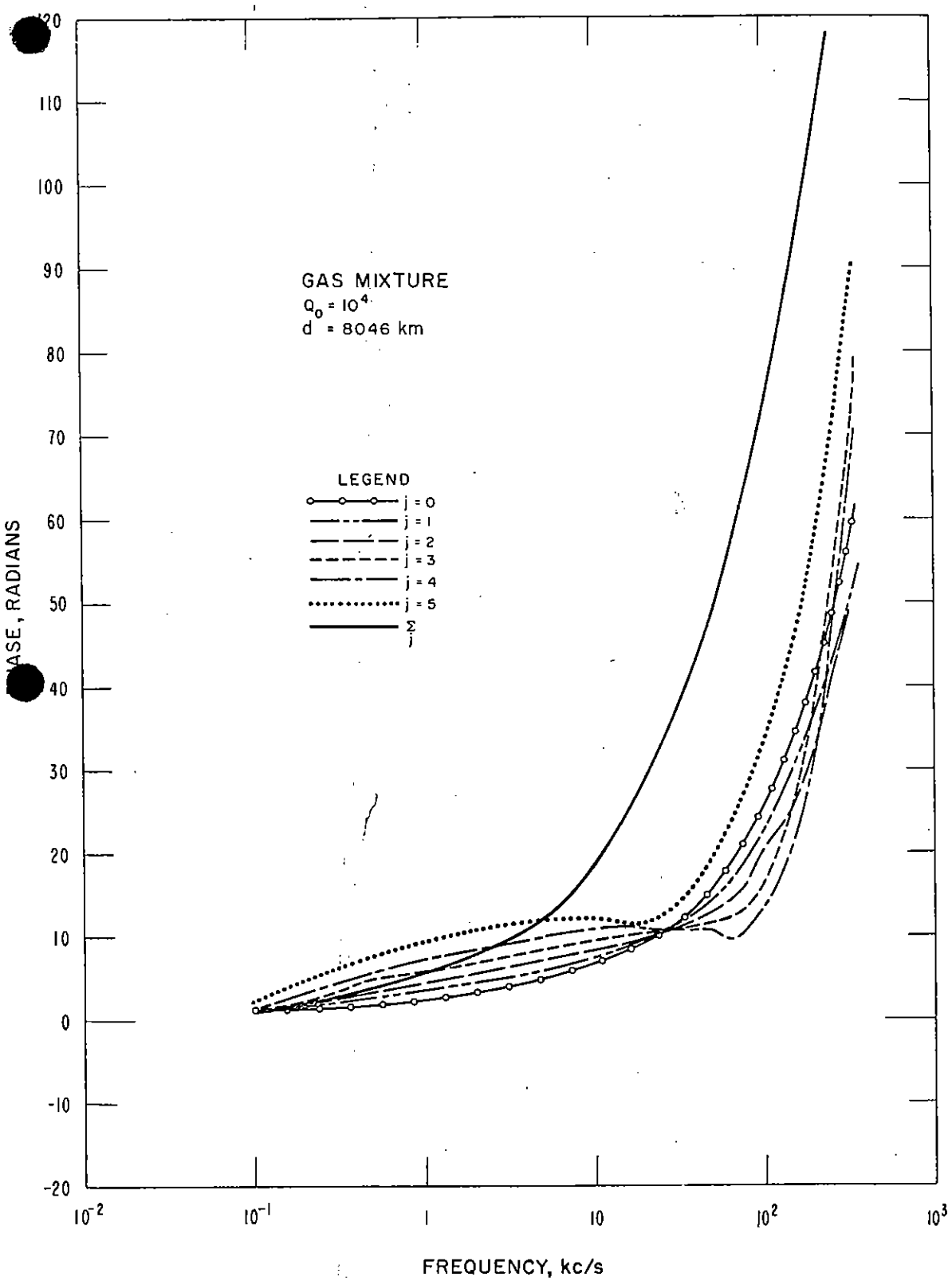

Figure 14. Phase correction of the disturbed propagation medium transform, $d = d_2 = 8046$ km; illustrating the terms of the geometric series $-k_1 d_2 - \mathrm{Arg}\, E_j(\omega, d_2)$ and the total phase $-k_1 d_2 - \mathrm{Arg} \sum_j E_j(\omega, d_2)$ for a nuclear debris production rate, $Q_0 = 10^4$ ion pairs per cubic centimeter per second per atmosphere.

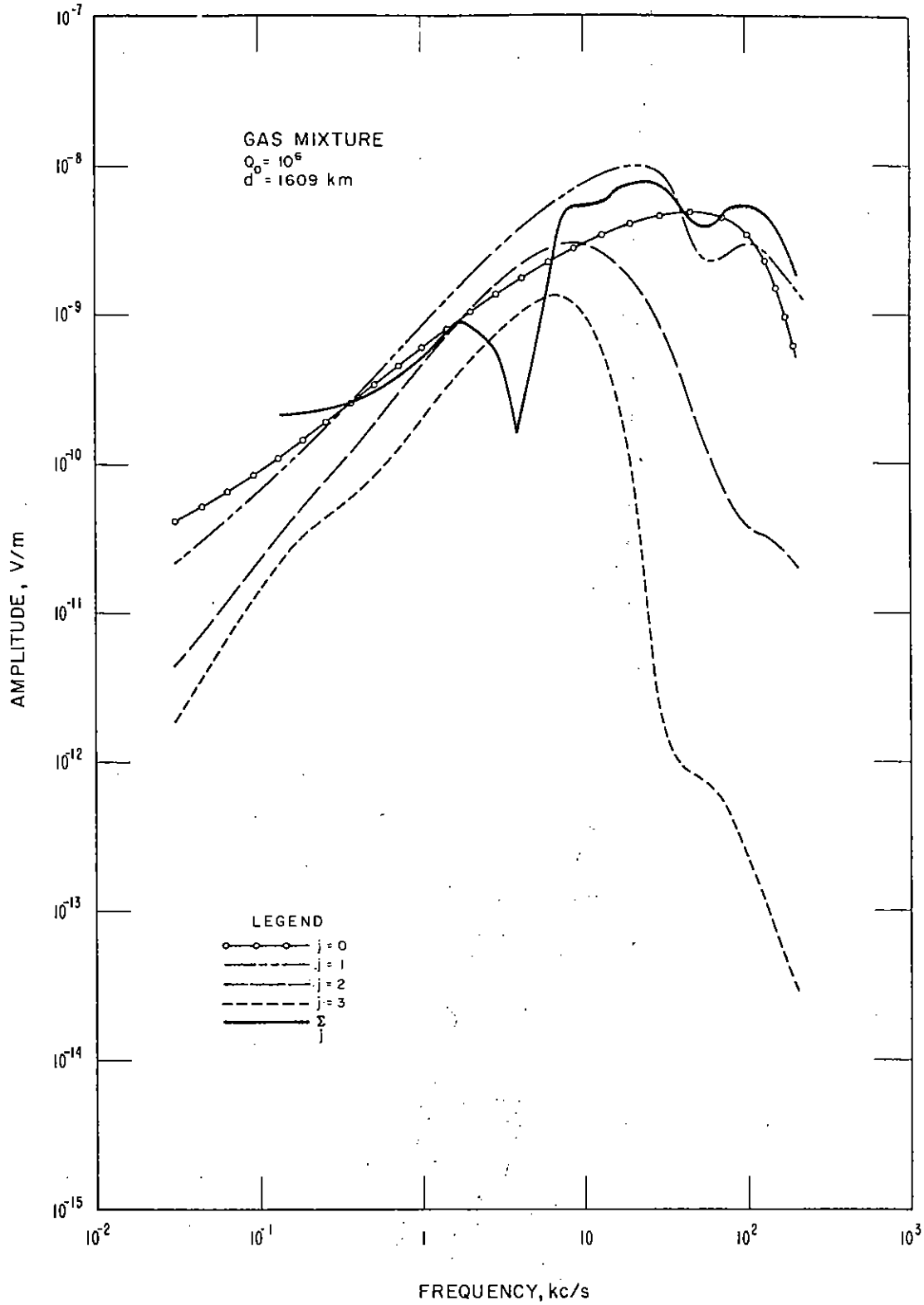

Figure 15. Amplitude of the disturbed propagation medium transform, $d = d_2 = 1609$ km; illustrating the terms of the geometric series $|E_j(\omega, d_2)|$ and the total field $|\sum_j E_j(\omega, d_2)|$ for a nuclear debris production rate, $Q_0 = 10^6$ ion pairs per cubic centimeter per second per atmosphere.

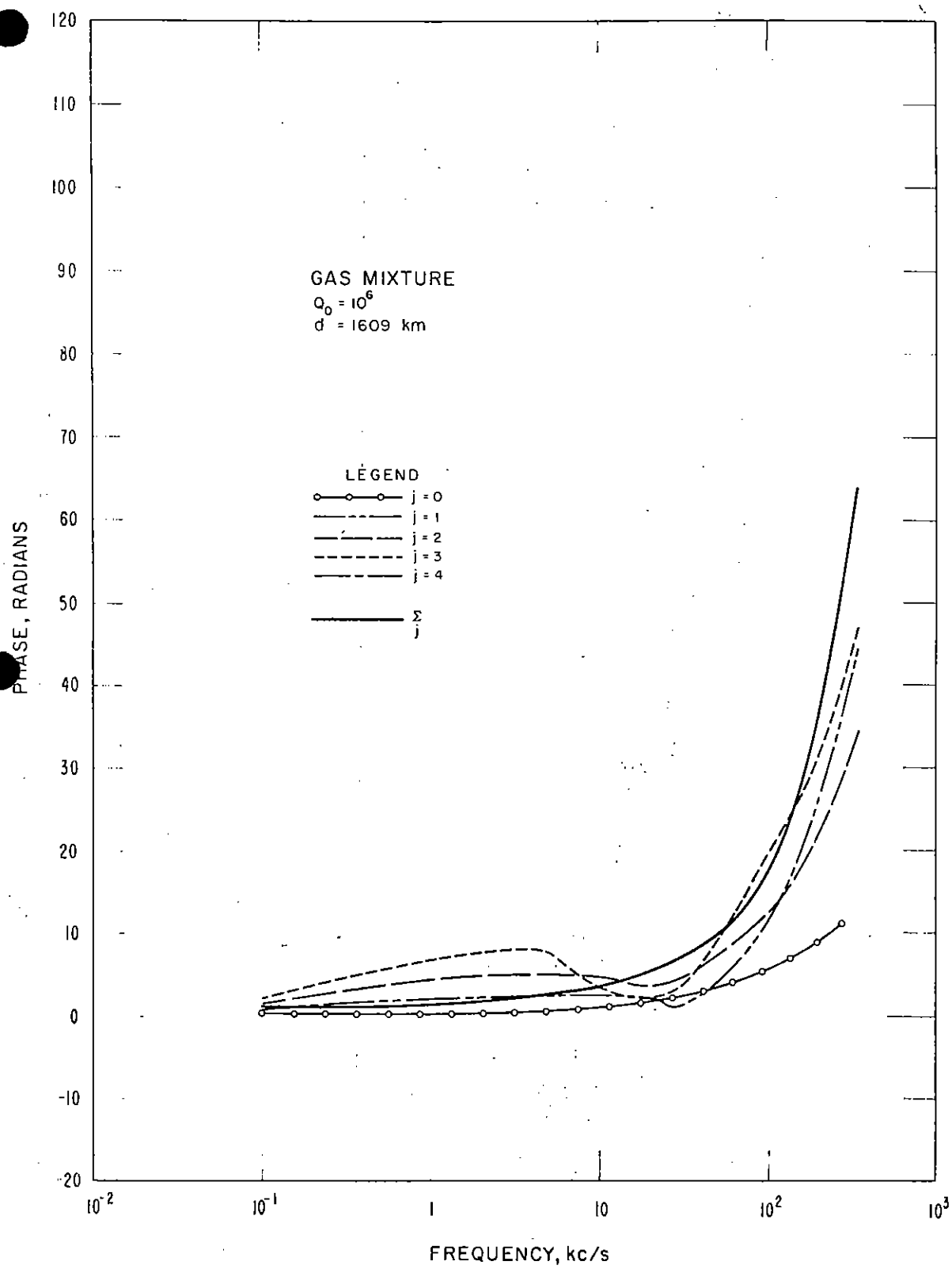

Figure 16. Phase correction of the disturbed propagation medium transform, $d = d_2 = 1609$ km; illustrating the terms of the geometric series $-k_1 d_2 - \text{Arg}\, E_j(\omega, d_2)$ and the total phase $-k_1 d_2 - \text{Arg} \sum_j E_j(\omega, d_2)$ for a nuclear debris production rate, $Q_0 = 10^6$ ion pairs per cubic centimeter per second per atmosphere.

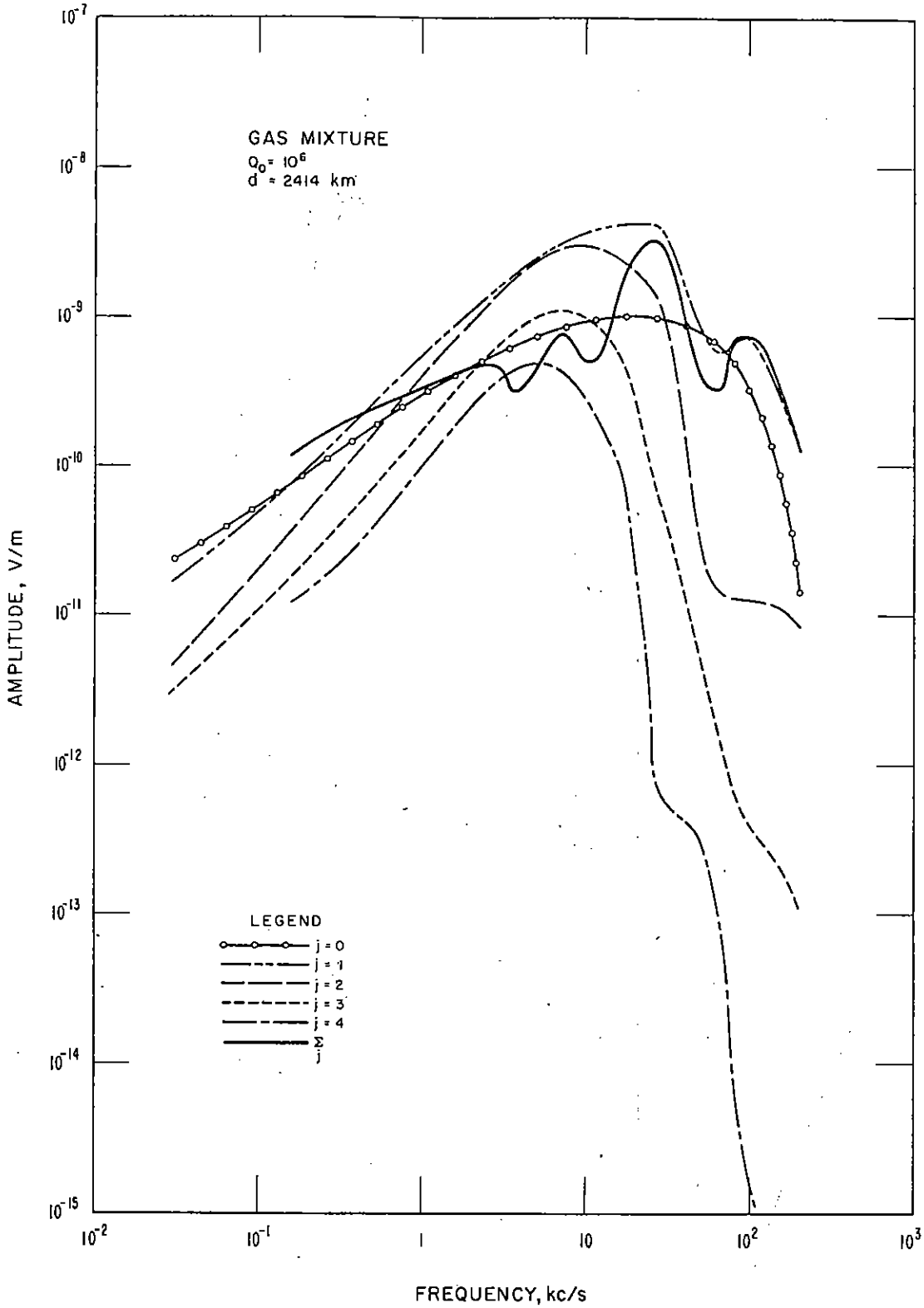

Figure 17. Amplitude of the disturbed propagation medium transform, $d = d_2 = 2414$ km; illustrating the terms of the geometric series $|E_j(\omega, d_2)|$ and the total field $|\sum_j E_j(\omega, d_2)|$ for a nuclear debris production rate, $Q_0 = 10^6$ ion pairs per dubic centimeter per second per atmosphere.

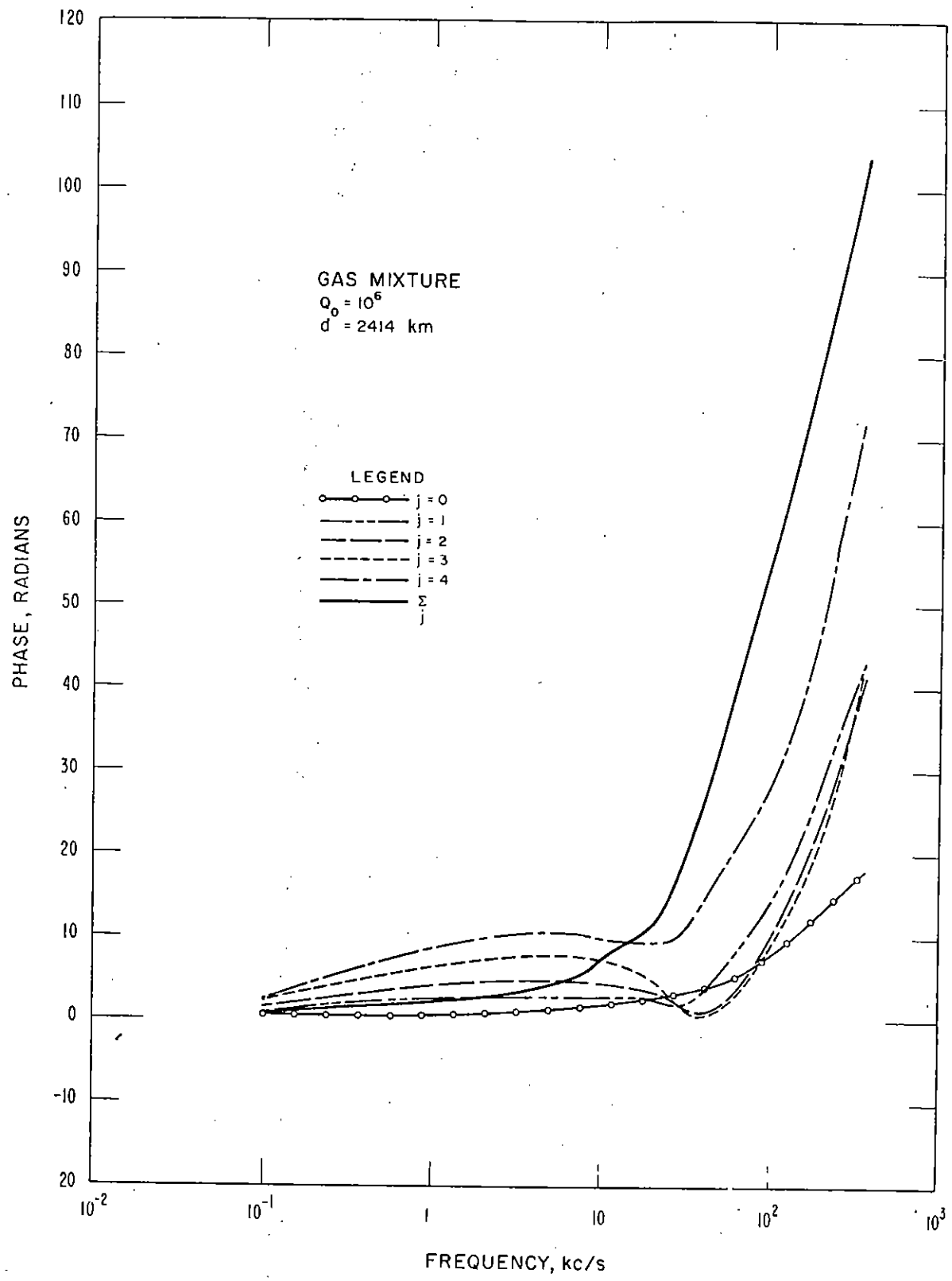

Figure 18. Phase correction of the disturbed propagation medium transform, $d = d_2 = 2414$ km; illustrating the terms of the geometric series $-k_1 d_2 - \text{Arg}\, E_j(\omega, d_2)$ and the total phase $-k_1 d_2 - \text{Arg} \sum_j E_j(\omega, d_2)$ for a nuclear debris production rate, $Q_0 = 10^6$ ion pairs per cubic centimeter per second per atmosphere.

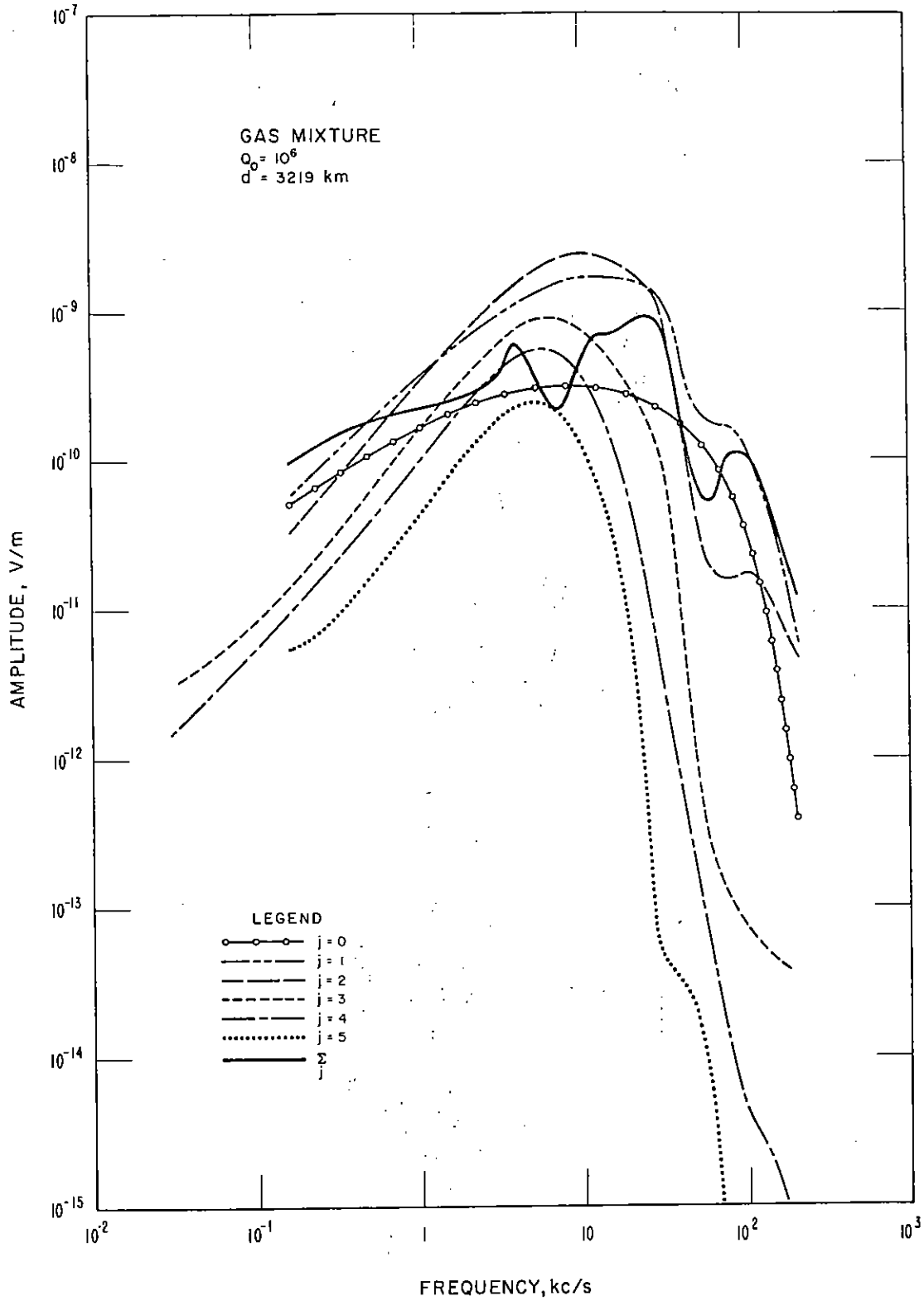

Figure 19. Amplitude of the disturbed propagation medium transform, $d = d_2 = 3219$ km; illustrating the terms of the geometric series $|E_j(\omega, d_2)|$ and the total field $|\sum_j E_j(\omega, d_2)|$ for a nuclear debris production rate, $Q_0 = 10^6$ ion pairs per cubic centimeter per second per atmosphere.

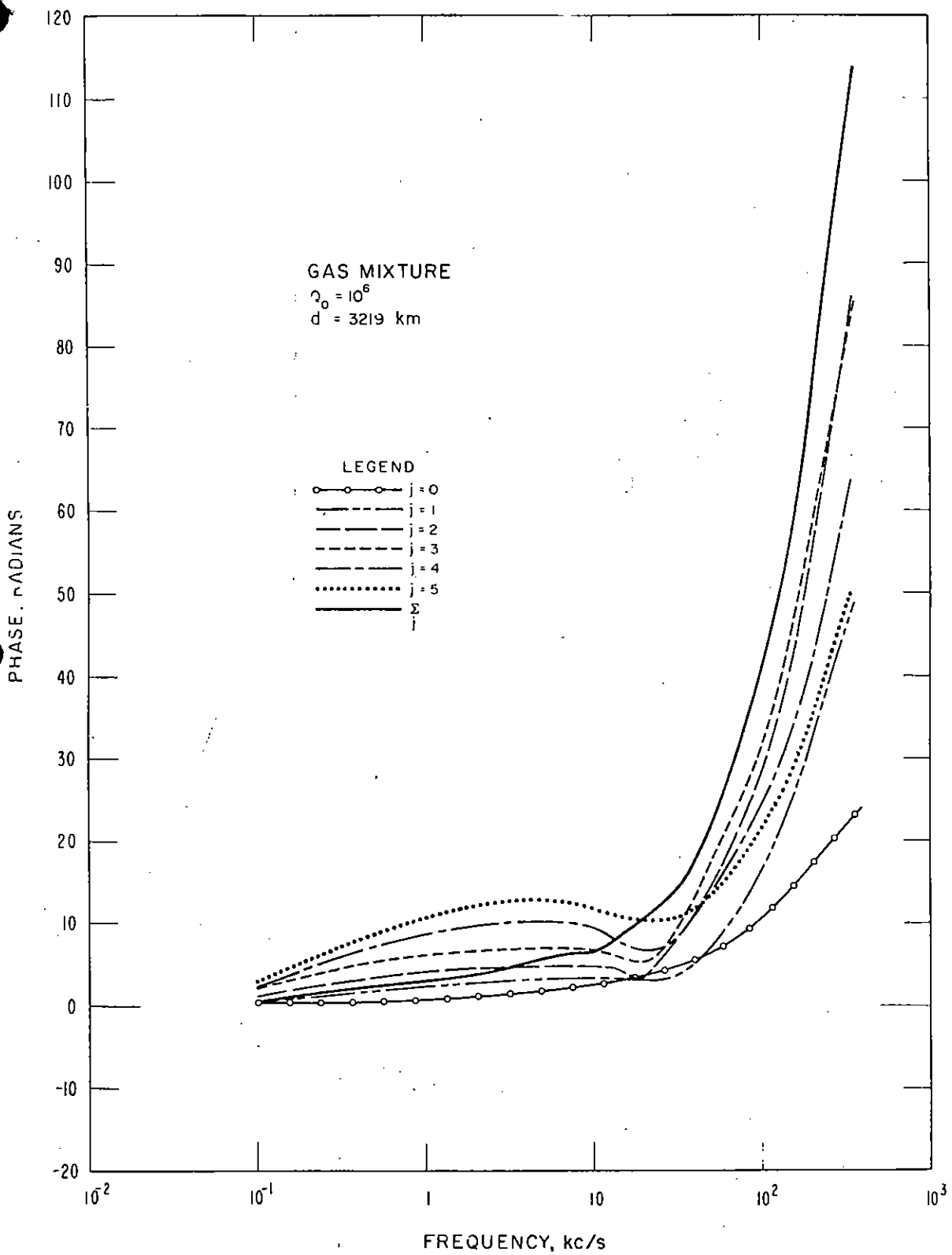

Figure 20. Phase correction of the disturbed propagation medium transform, $d = d_2 = 3219$ km; illustrating the terms of the geometric series $-k_1 d_2 - \text{Arg } E_j(\omega, d_2)$ and the total phase $-k_1 d_2 - \text{Arg } \sum_j E_j(\omega, d_2)$ for a nuclear debris production rate, $Q_0 = 10^6$ ion pairs per cubic centimeter per second per atmosphere.

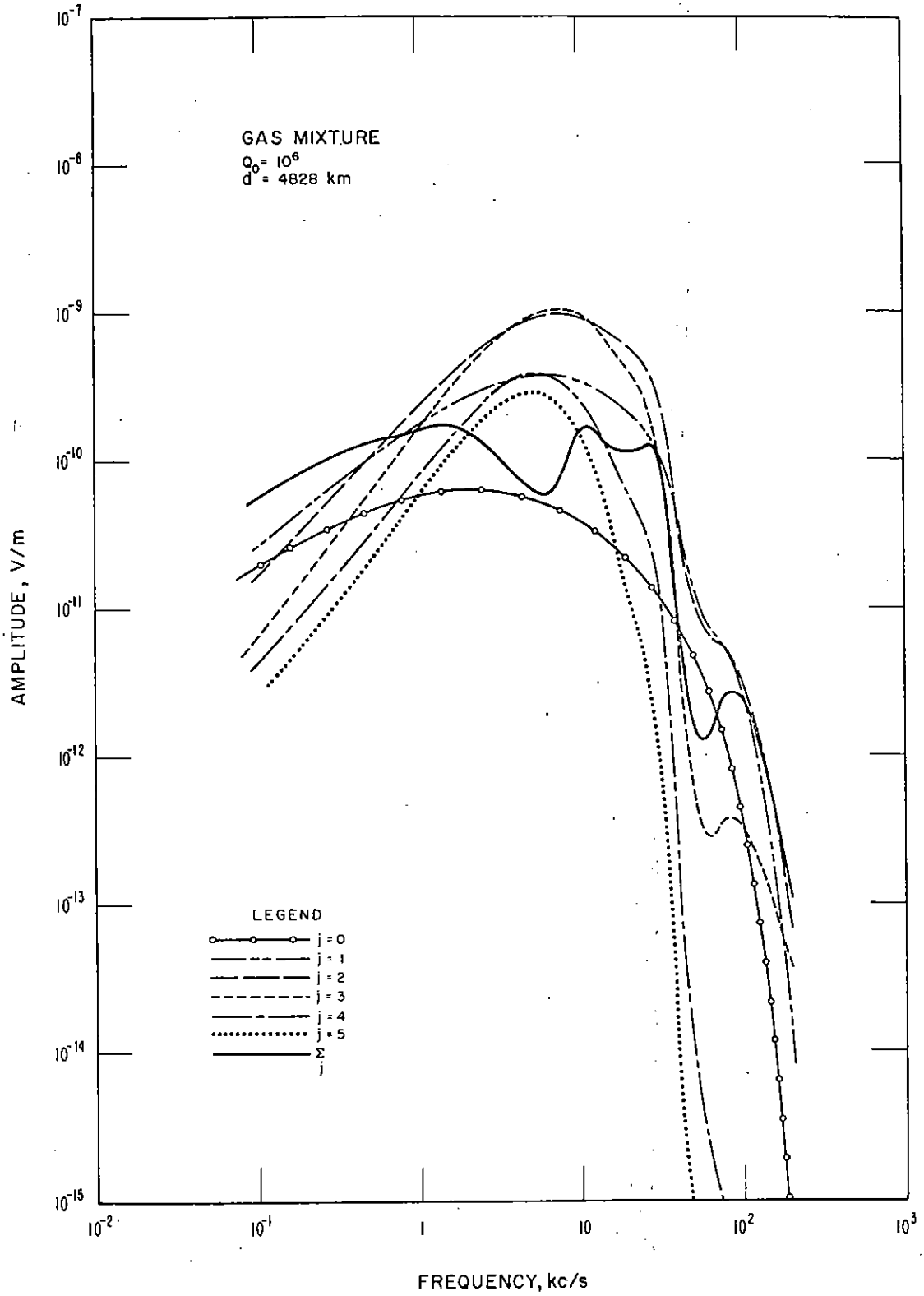

Figure 21. Amplitude of the disturbed propagation medium transform, $d = d_2 = 4828$ km; illustrating the terms of the geometric series $|E_j(\omega, d_2)|$ and the total field $|\sum_j E_j(\omega, d_2)|$ for a nuclear debris production rate, $Q_0 = 10^6$ ion pairs per cubic centimeter per second per atmosphere.

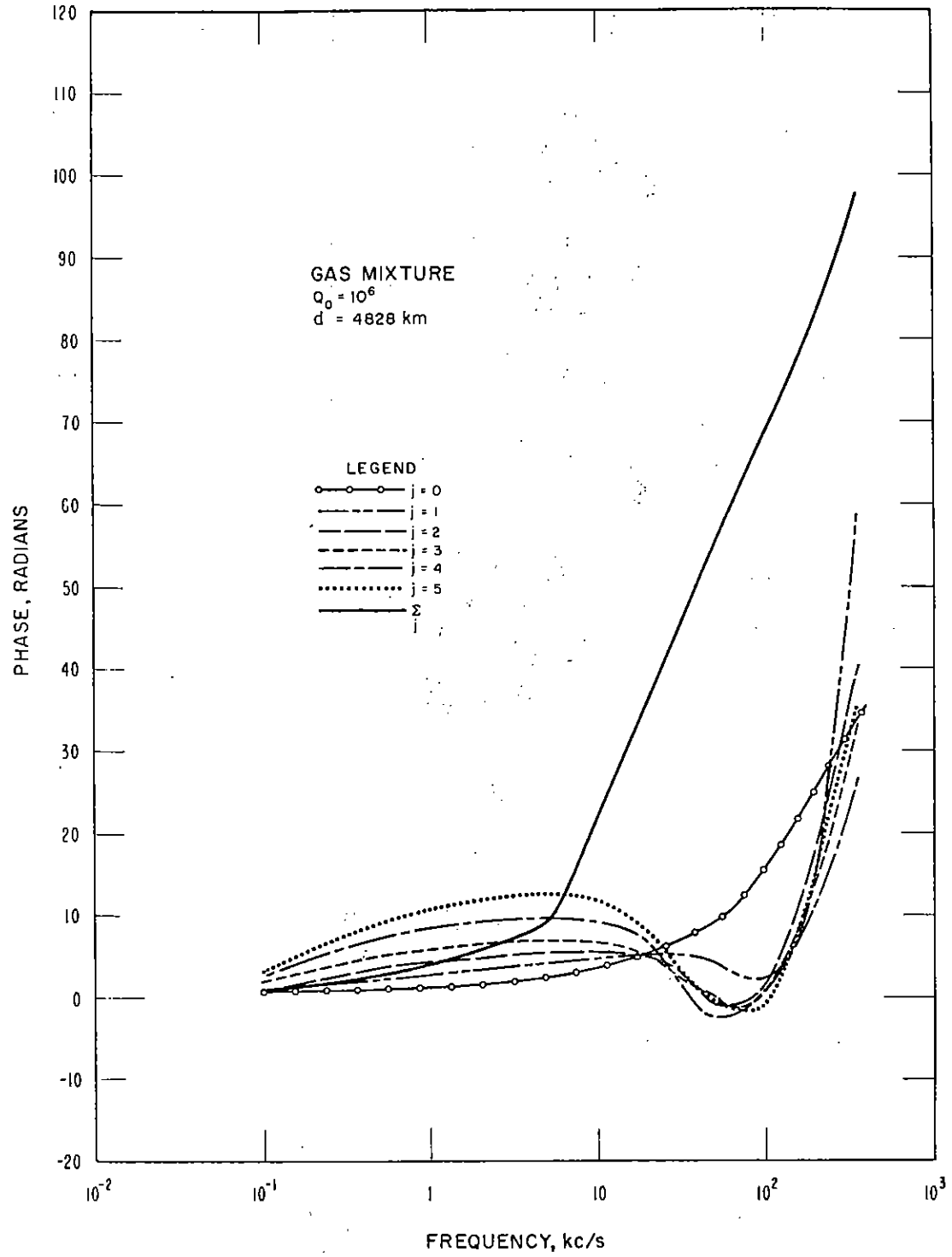

Figure 22. Phase correction of the disturbed propagation medium transform $d = d_2 = 4828$ km; illustrating the terms of the geometric series $-k_1 d_2 - \text{Arg}\, E_j(\omega, d_2)$ and the total phase $-k_1 d_2 - \text{Arg} \sum_j E_j(\omega, d_2)$ for a nuclear debris production rate, $Q_0 = 10^6$ ion pairs per cubic centimeter per second per atmosphere.

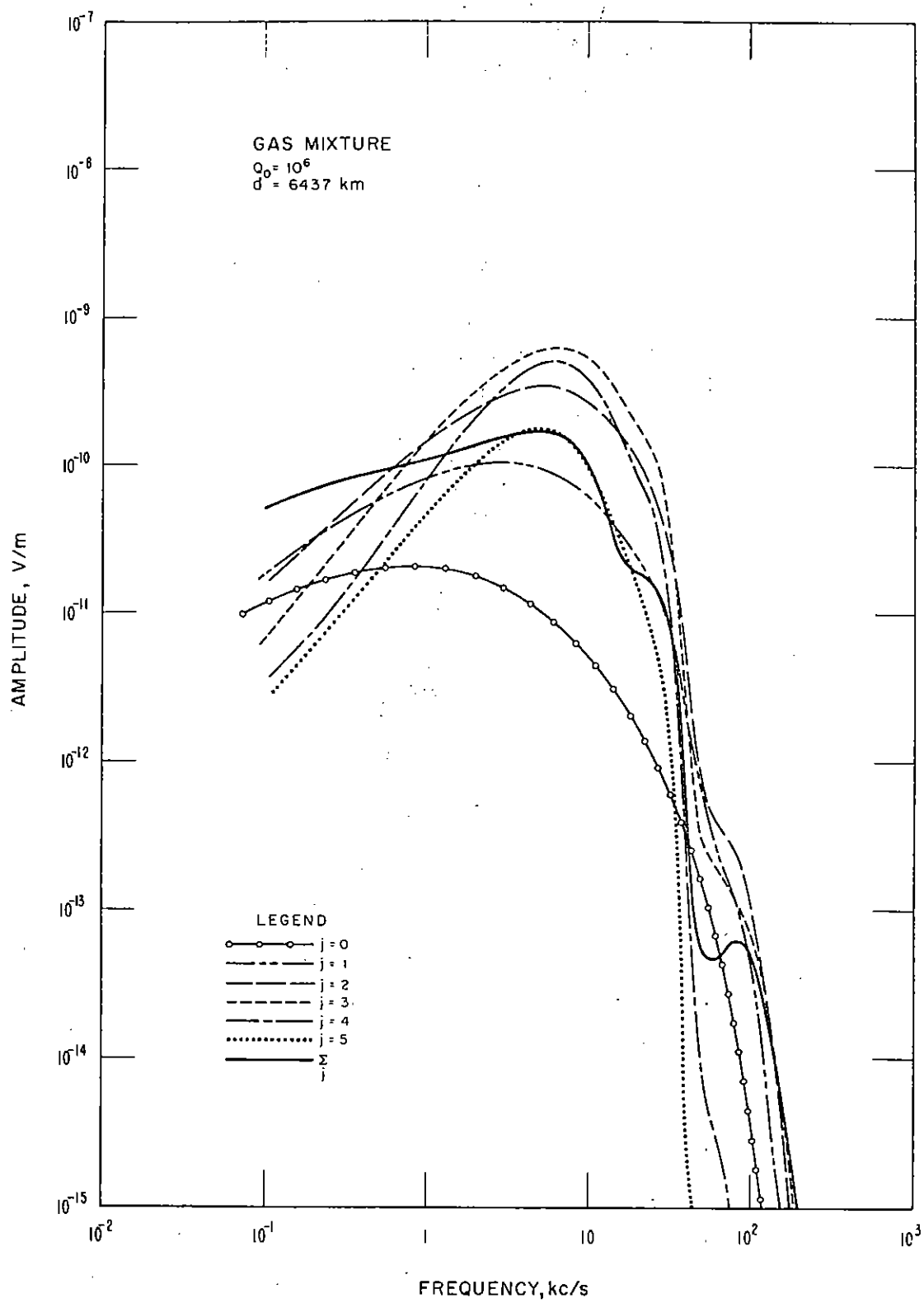

Figure 23. Amplitude of the disturbed propagation medium transform, $d = d_2 = 6437$ km; illustrating the terms of the geometric series $\left|\sum_j E_j(\omega, d_2)\right|$ and the total field $\left|\sum_j E_j(\omega, d_2)\right|$ for a nuclear debris production rate, $Q_0 = 10^6$ ion pairs per cubic centimeter per second per atmosphere.

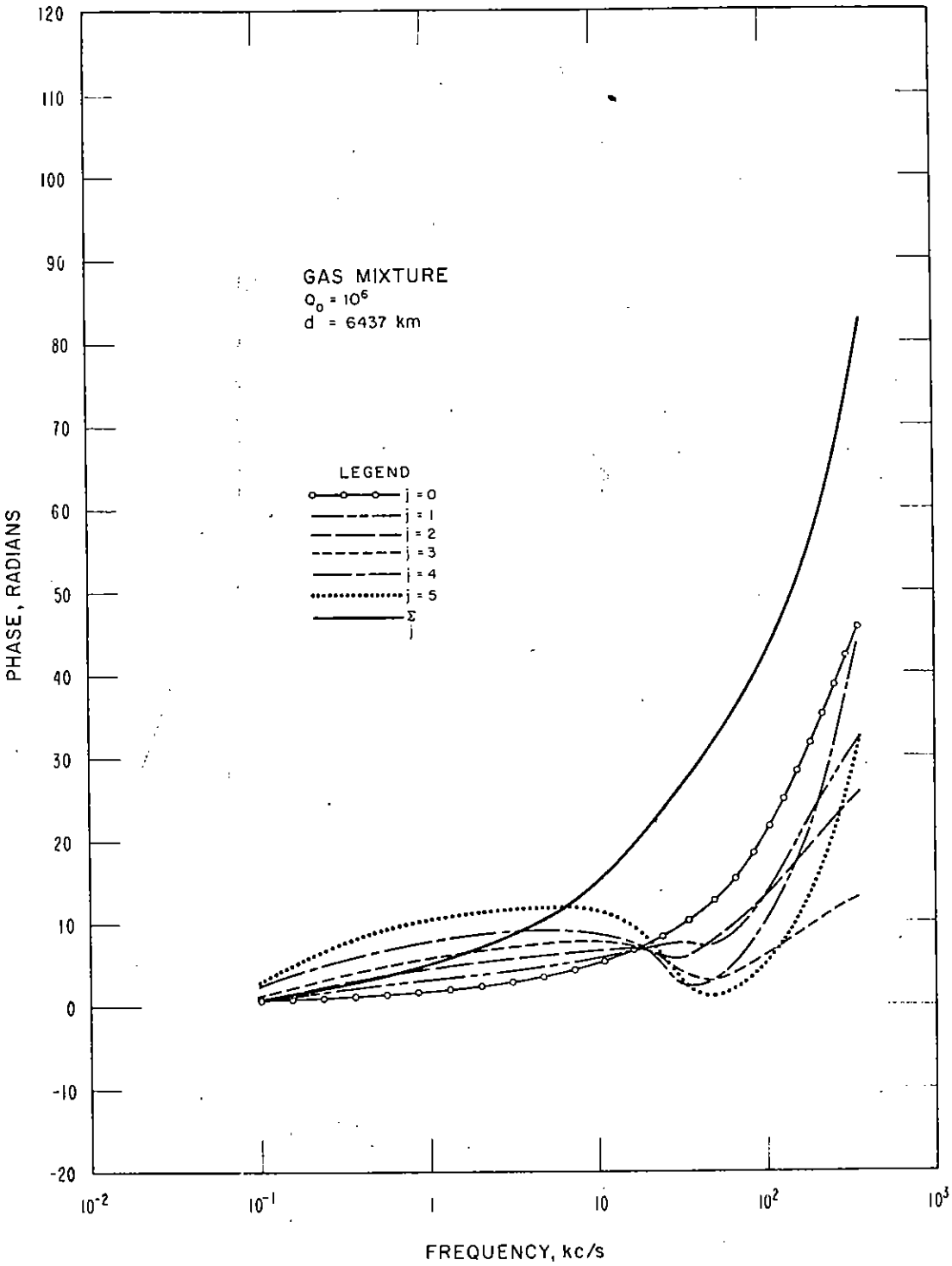

Figure 24. Phase correction of the disturbed propagation medium transform, $d = d_2 = 6437$ km; illustrating the terms of the geometric series $-k_1 d_2 - \text{Arg } E_j(\omega, d_2)$ and the total phase $-k_1 d_2 - \text{Arg } \sum_j E_j(\omega, d_2)$ for a nuclear debris production rate, $Q_0 = 10^6$ ion pairs per cubic centimeter per second per atmosphere.

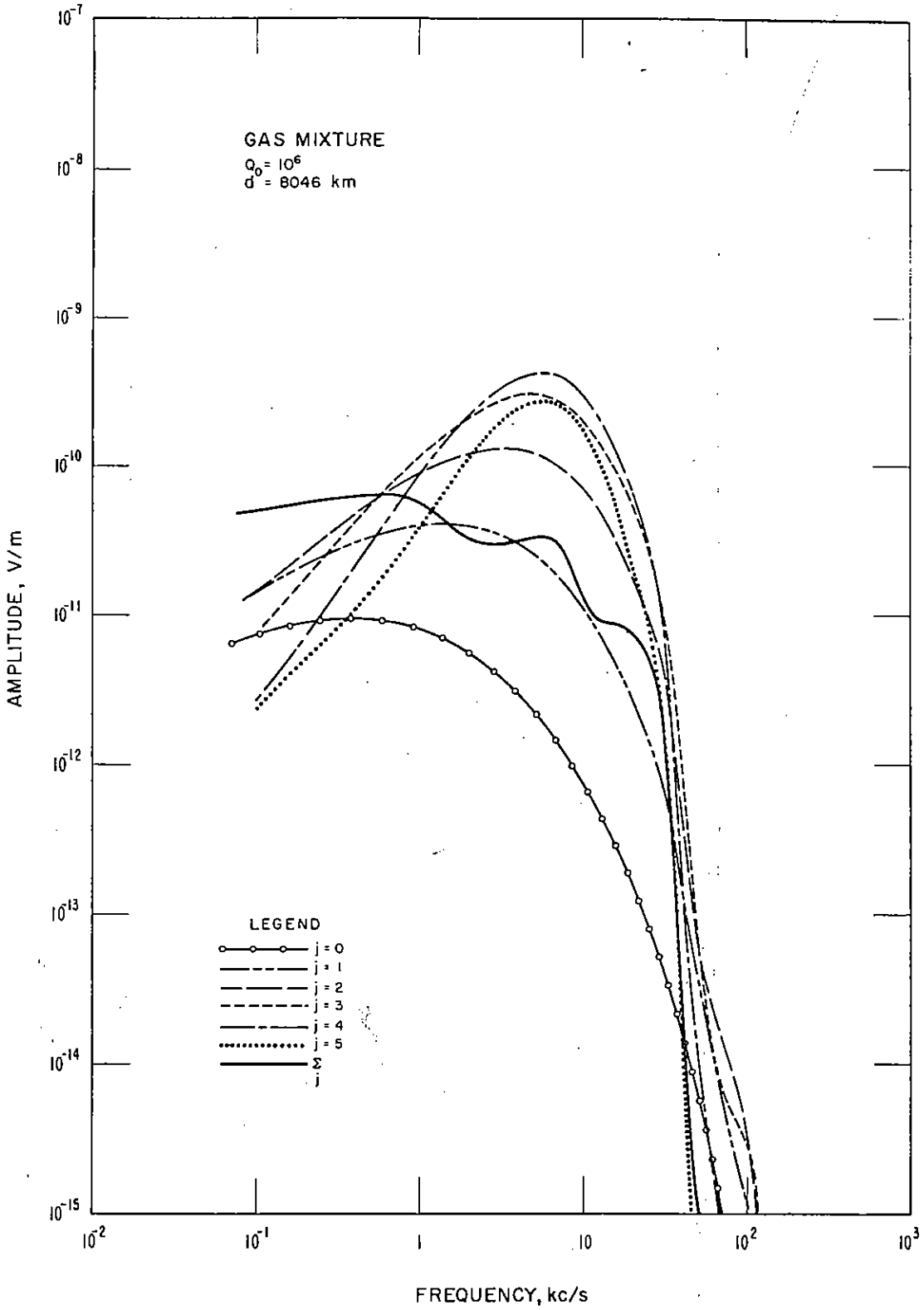

Figure 25. Amplitude of the disturbed propagation medium transform, $d = d_2 = 8046$ km; illustrating the terms of the geometric series $|E_j(\omega, d_2)|$ and the total field $|\sum_j E_j(\omega, d_2)|$ for a nuclear debris production rate, $Q_0 = 10^6$ ion pairs per cubic centimeter per second per atmosphere.

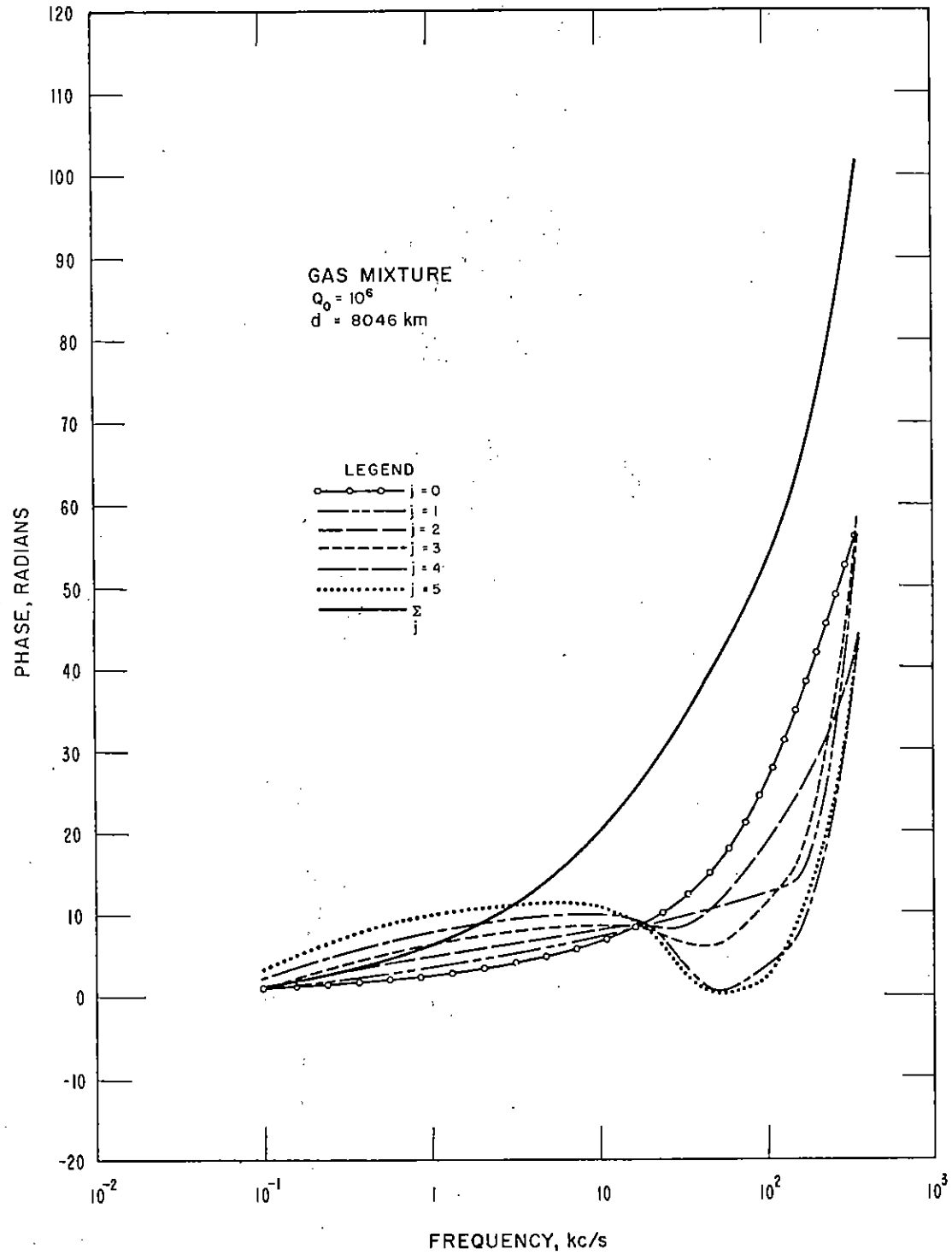

Figure 26. Phase correction of the disturbed propagation medium transform, $d = d_2 = 8046$ km; illustrating the terms of the geometric series $-k_1 d_2 - \text{Arg}\, E_j(\omega, d_2)$ and the total phase $-k_1 d_2 - \text{Arg} \sum_j E_j(\omega, d_2)$ for a nuclear debris production rate, $Q_0 = 10^6$ ion pairs per cubic centimeter per second per atmosphere.

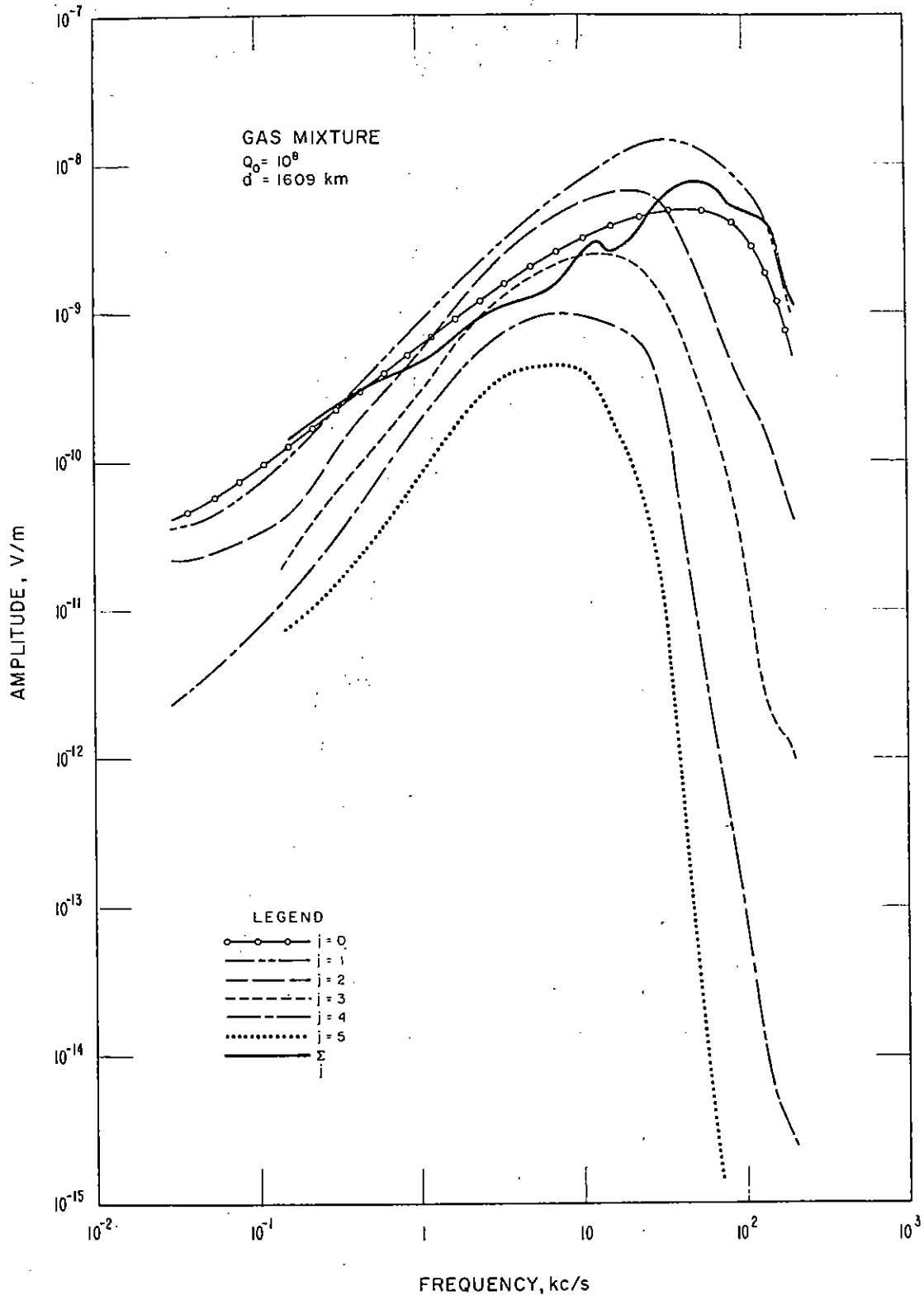

Figure 27. Amplitude of the disturbed propagation medium transform, $d = d_2 = 1609$ km; illustrating the terms of the geometric series $|E_j(\omega, d_2)|$ and the total field $|\sum_j E_j(\omega, d_2)|$ for a nuclear debris production rate, $Q_0 = 10^8$ ion pairs per cubic centimeter per second per atmosphere.

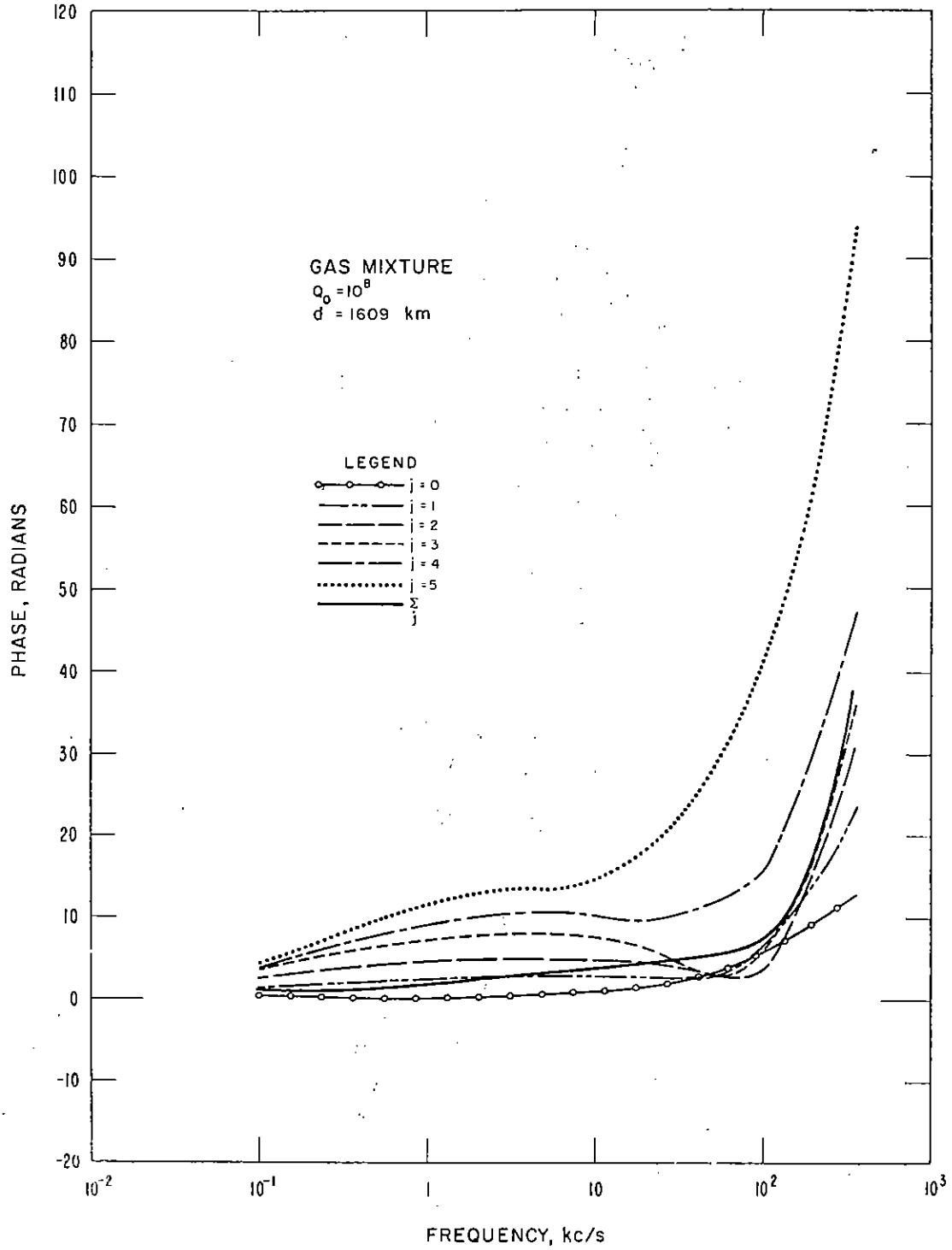

Figure 28. Phase correction of the disturbed propagation medium transform, $d = d_2 = 1609$ km; illustrating the terms of the geometric series $-k_1 d_2 - \text{Arg } E_j(\omega, d_2)$ and the total phase $-k_1 d_2 - \text{Arg} \sum_j E_j(\omega, d_2)$ for a nuclear debris production rate, $Q_0 = 10^8$ ion pairs per cubic centimeter per second per atmosphere.

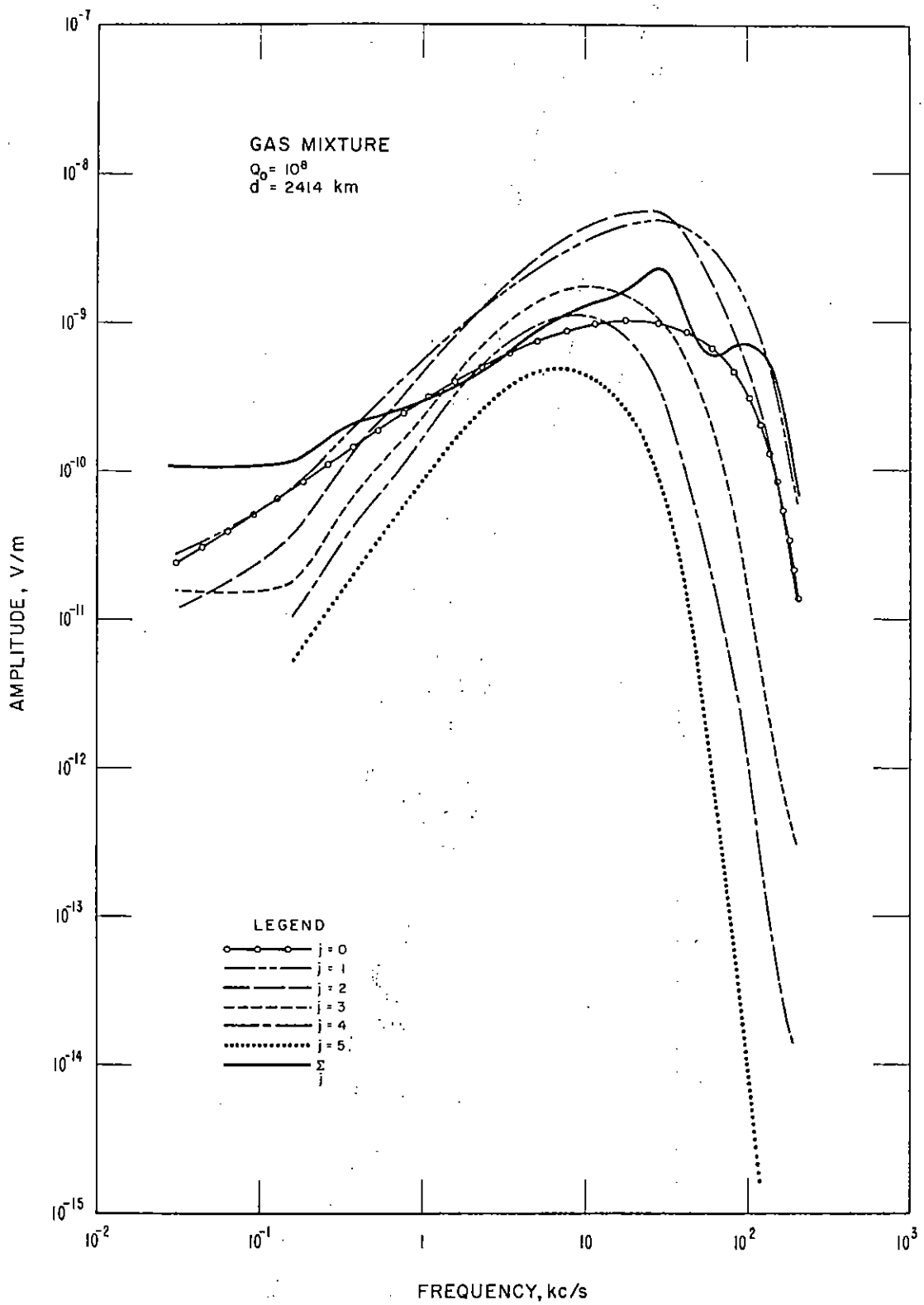

Figure 29. Amplitude of the disturbed propagation medium transform, $d = d_2 = 2414$ km; illustrating the terms of the geometric series $|E_j(\omega, d_2)|$ and the total field $|\sum_j E_j(\omega, d_2)|$ for a nuclear debris production rate, $Q_0 = 10^8$ ion pairs per cubic centimeter per second per atmosphere.

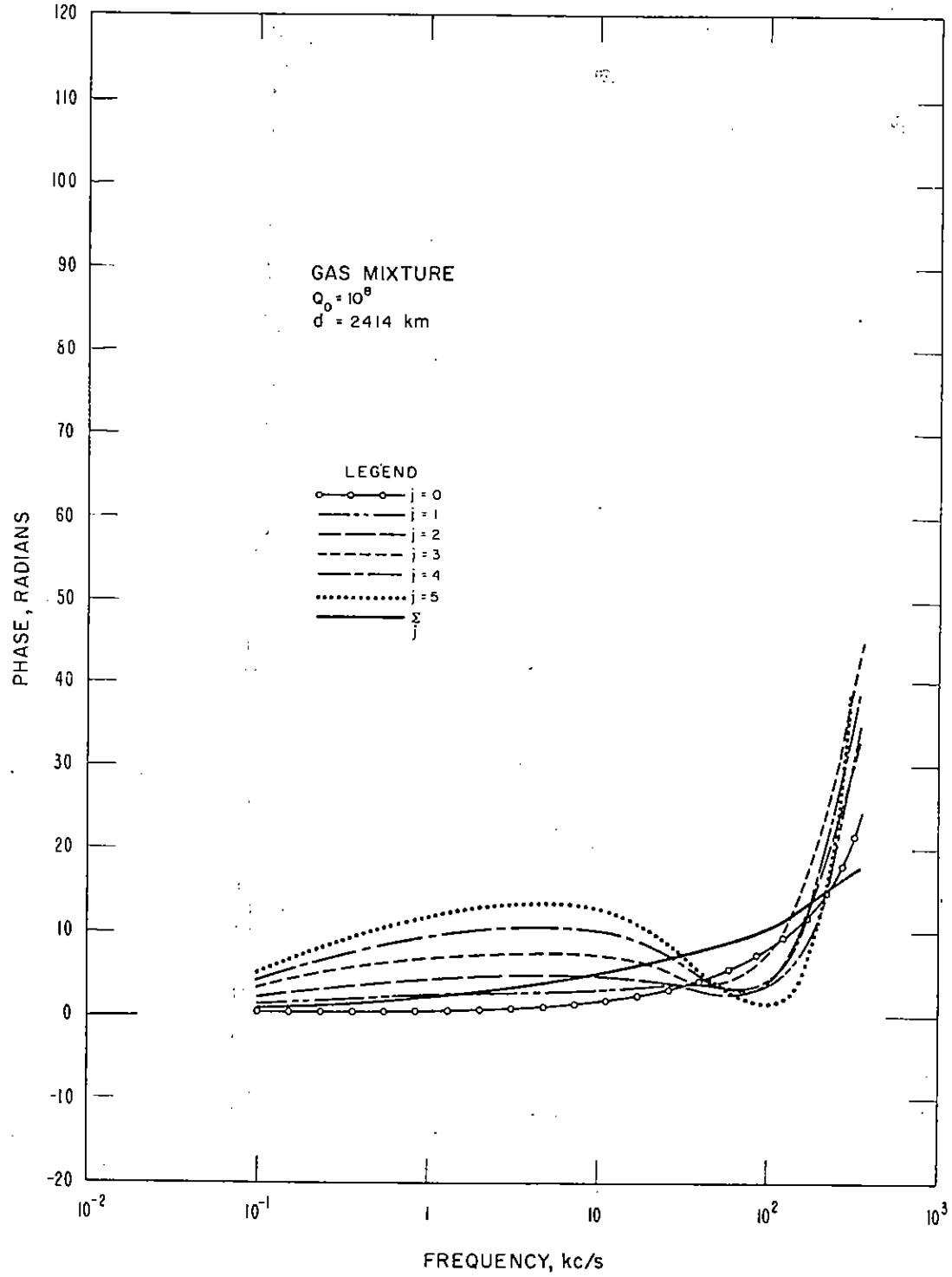

Figure 30. Phase correction of the disturbed propagation medium transform, $d = d_2 = 2414$ km; illustrating the terms of the geometric series $-k_1 d_2 - \text{Arg}\, E_j(\omega, d_2)$ and the total phase $-k_1 d_2 - \text{Arg} \sum_j E_j(\omega, d_2)$ for a nuclear debris production rate, $Q_0 = 10^8$ ion pairs per cubic centimeter per second per atmosphere.

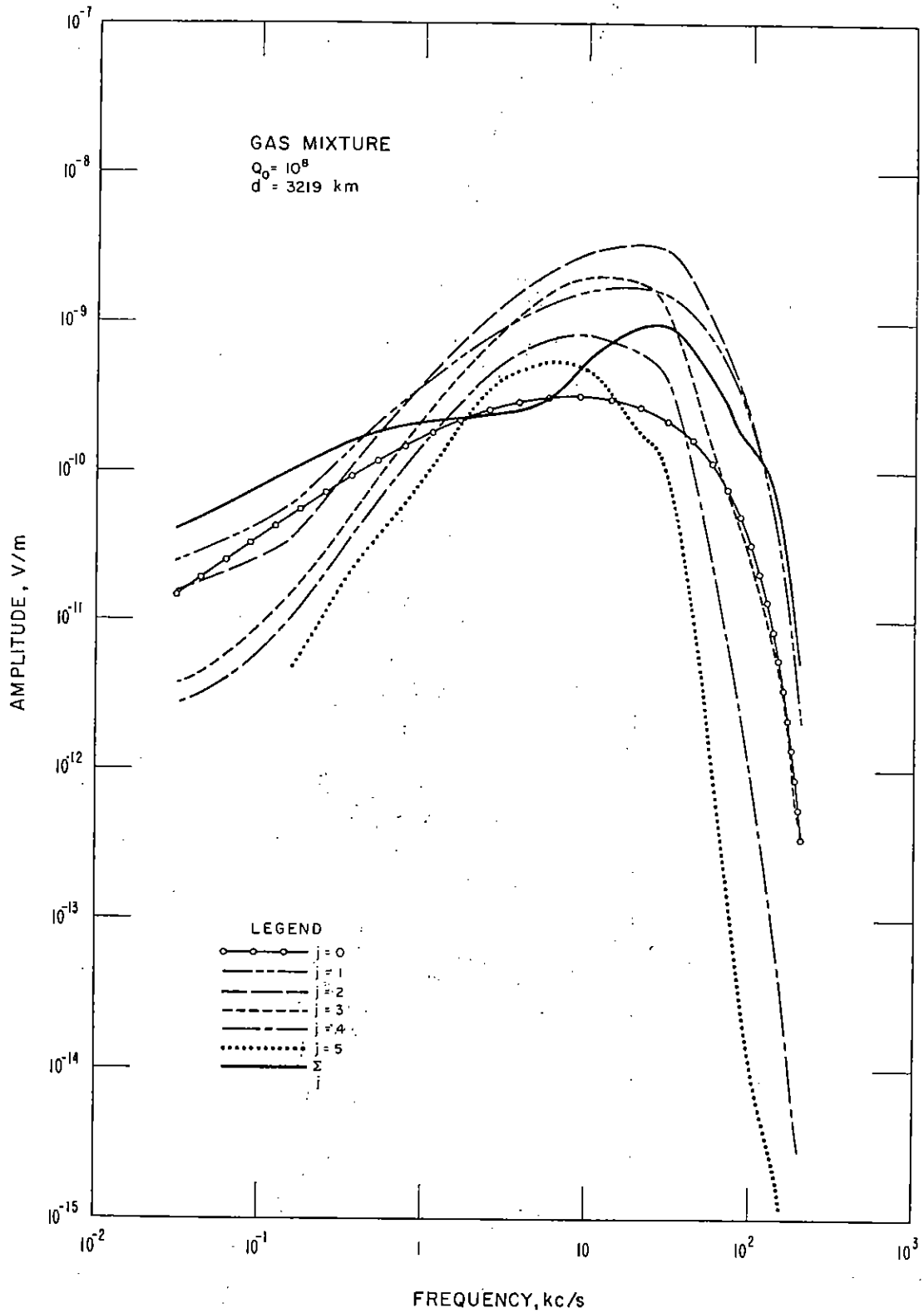

Figure 31. Amplitude of the disturbed propagation medium transform, $d = d_2 = 3219$ km; illustrating the terms of the geometric series $|E_j(\omega, d_2)|$ and the total field $|\sum_j E_j(\omega, d_2)|$ for a nuclear debris production rate, $Q_0 = 10^8$ ion pairs per cubic centimeter per second per atmosphere.

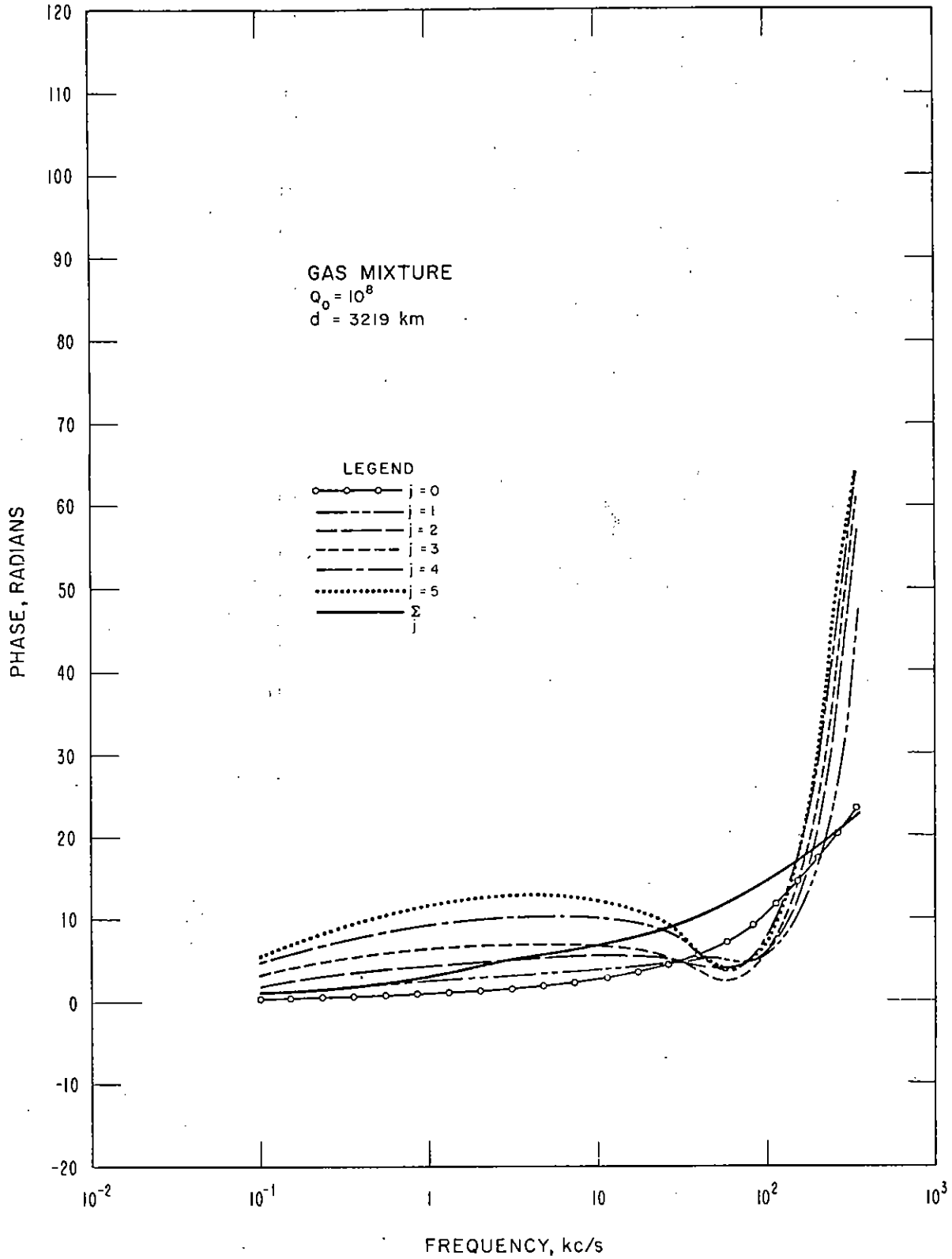

Figure 32. Phase correction of the disturbed propagation medium transform, $d = d_2 = 3219$ km; illustrating the terms of the geometric series $-k_1 d_2 - \text{Arg}\, E_j(\omega, d_2)$ and the total phase $-k_1 d_2 - \text{Arg} \sum_j E_j(\omega, d_2)$ for a nuclear debris production rate, $Q_0 = 10^8$ ion pairs per cubic centimeter per second per atmosphere.

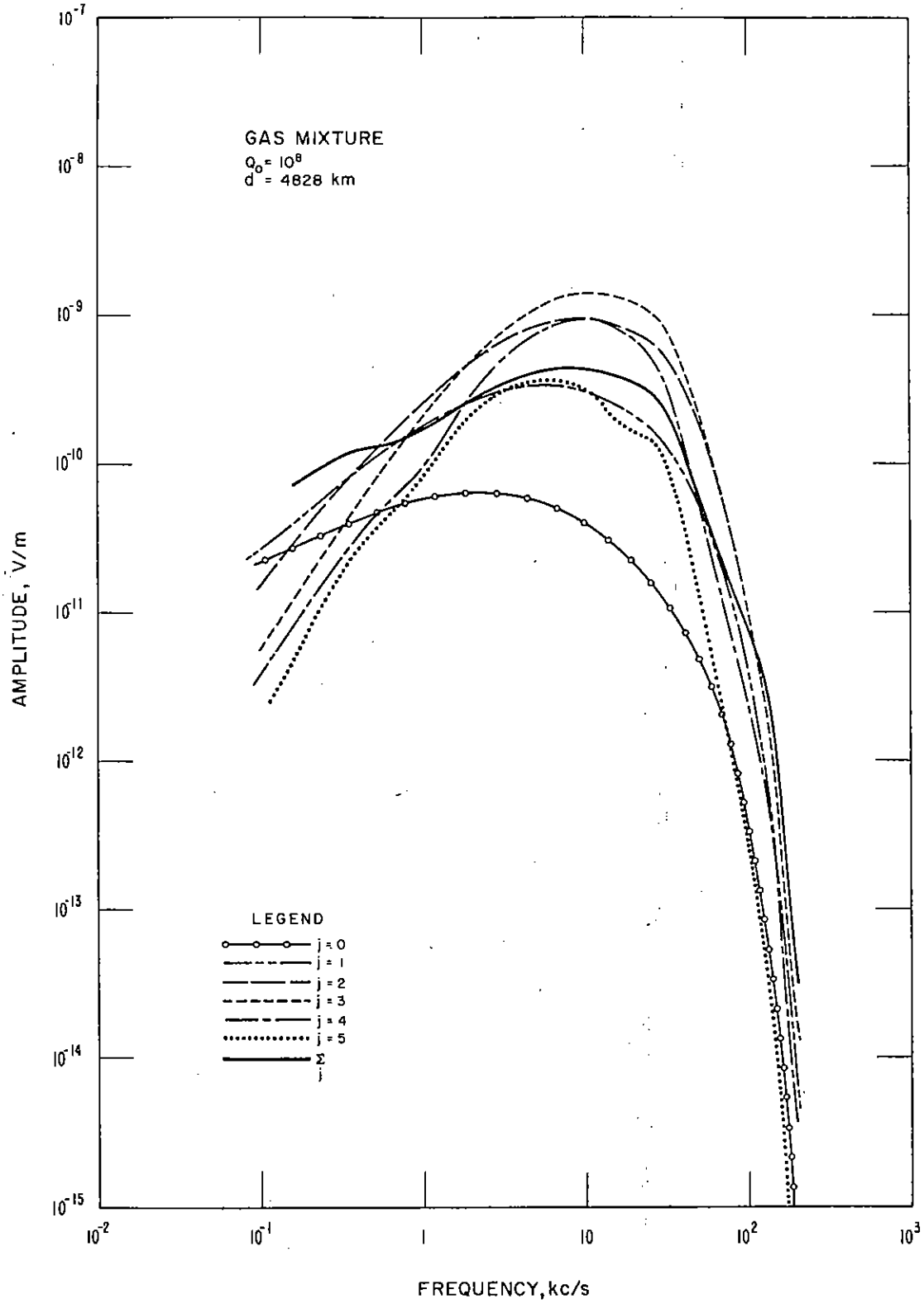

Figure 33. Amplitude of the disturbed propagation medium transform, $d = d_2 = 4828$ km; illustrating the terms of the geometric series $|E_j(\omega, d_2)|$ and the total field $|\sum_j E_j(\omega, d_2)|$ for a nuclear debris production rate, $Q_0 = 10^8$ ion pairs per cubic centimeter per second per atmosphere.

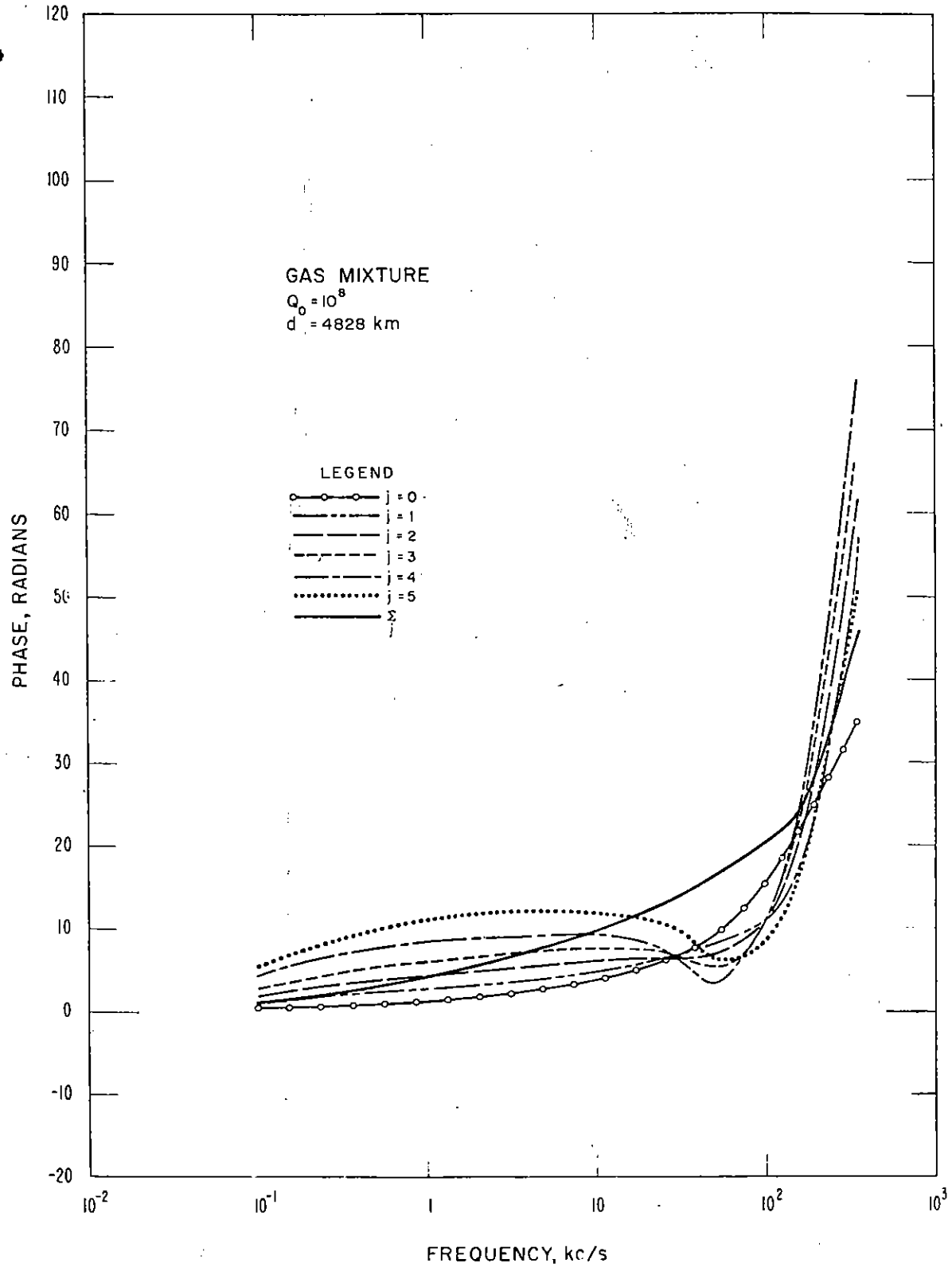

Figure 34. Phase correction of the disturbed propagation medium transform, $d = d_2 = 4828$ km; illustrating the terms of the geometric series $-k_1 d_2 - \text{Arg}\, E_j(\omega, d_2)$ and the total phase $-k_1 d_2 - \text{Arg} \sum_j E_j(\omega, d_2)$ for a nuclear debris production rate, $Q_0 = 10^8$ ion pairs per cubic centimeter per second per atmosphere.

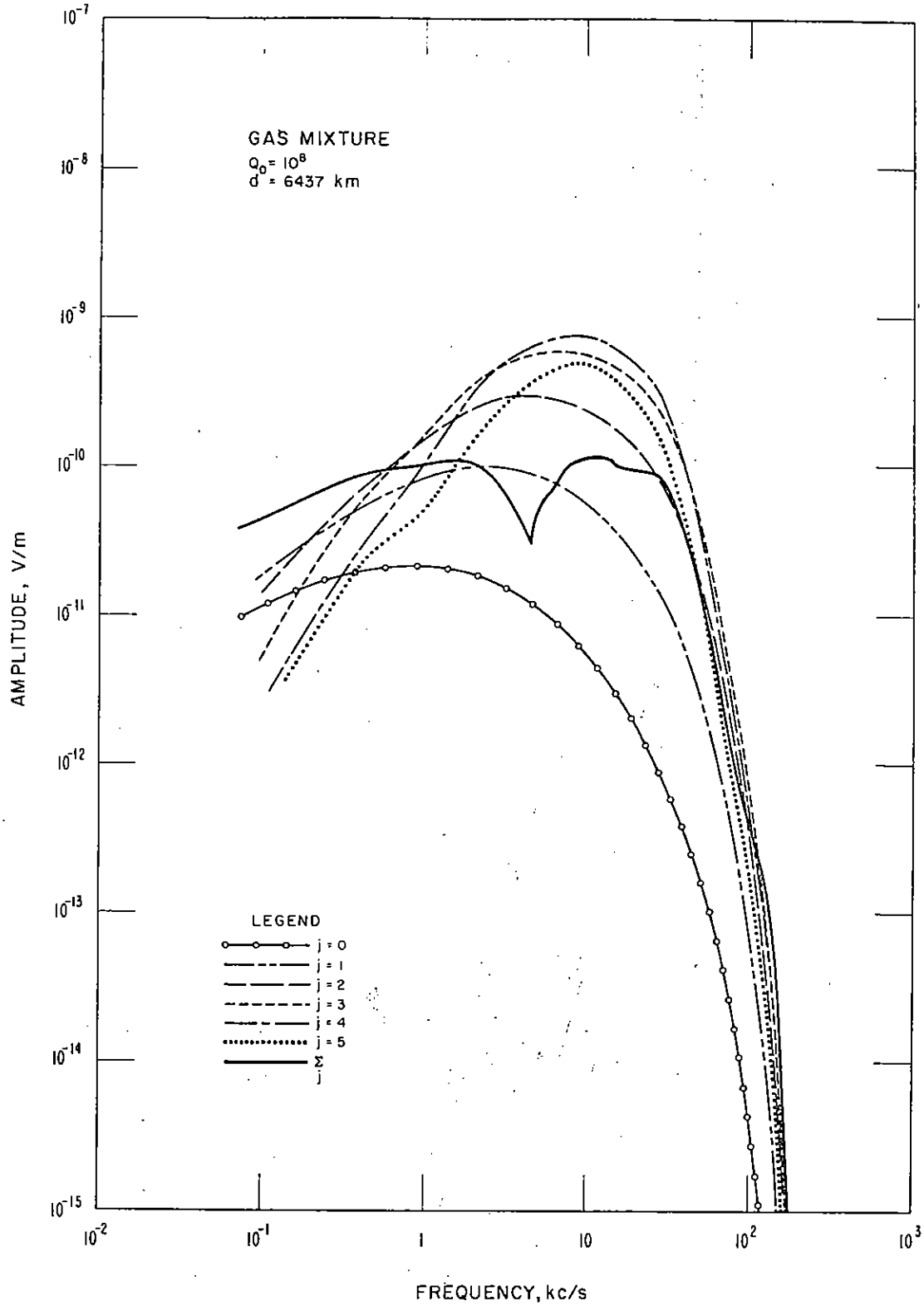

Figure 35. Amplitude of the disturbed propagation medium transform, $d = d_2 = 6437$ km; illustrating the terms of the geometric series $|E_j(\omega, d_2)|$ and the total field $|\sum_j E_j(\omega, d_2)|$ for a nuclear debris production rate, $Q_0 = 10^8$ ion pairs per cubic centimeter per second per atmosphere.

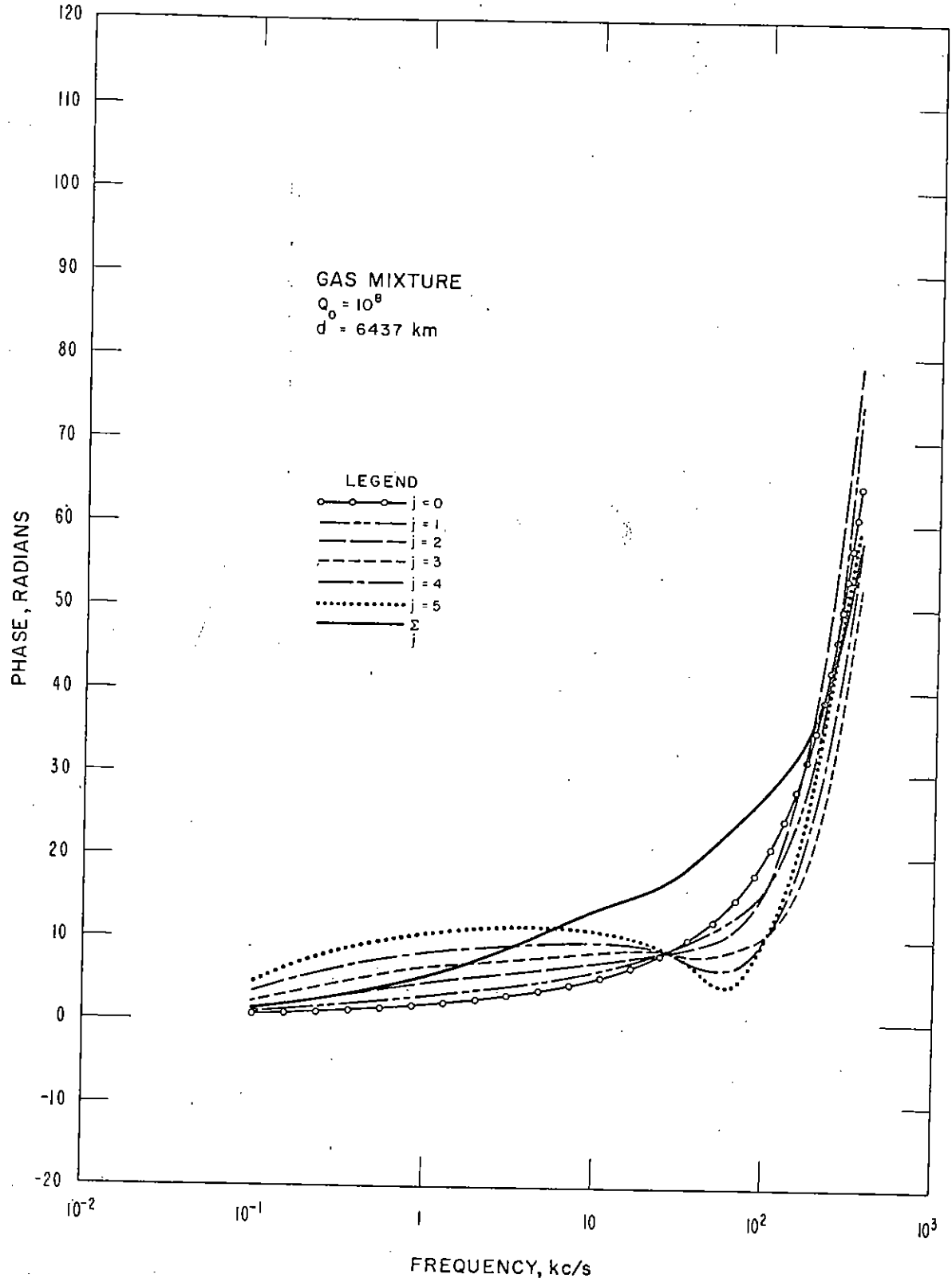

Figure 36. Phase correction of the disturbed propagation medium transform, $d = d_2 = 6437$ km; illustrating the terms of the geometric series $-k_1 d_2 - \text{Arg}\, E_j(\omega, d_2)$ and the total phase $-k_1 d_2 - \text{Arg} \sum_j E_j(\omega, d_2)$ for a nuclear debris production rate, $Q_0 = 10^8$ ion pairs per cubic centimeter per second per atmosphere.

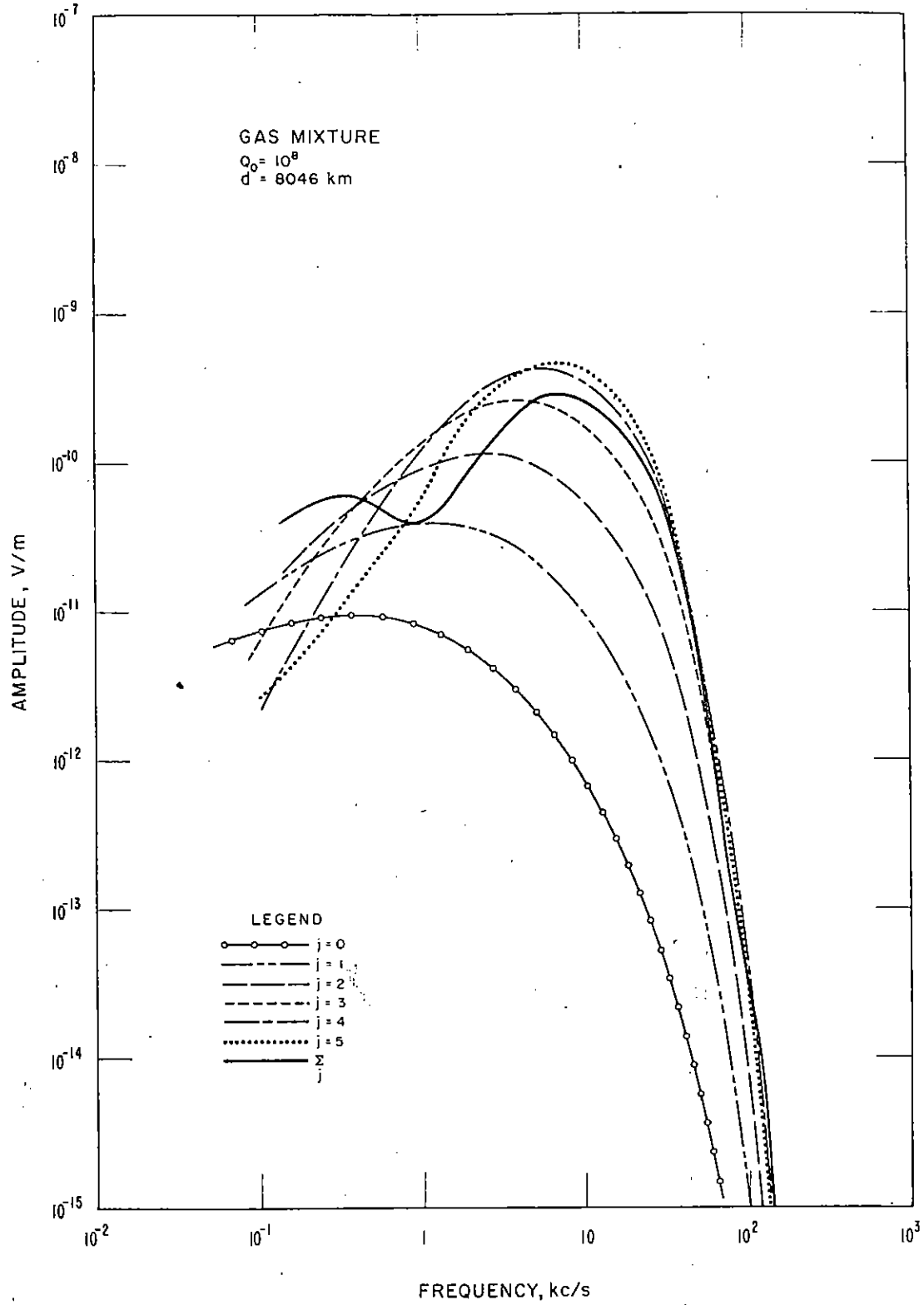

Figure 37. Amplitude of the disturbed propagation medium transform, $d = d_2 = 8046$ km; illustrating the terms of the geometric series $|E_j(\omega, d_2)|$ and the total field $|\sum_j E_j(\omega, d_2)|$ for a nuclear debris production rate, $Q_0 = 10^8$ ion pairs per cubic centimeter per second per atmosphere.

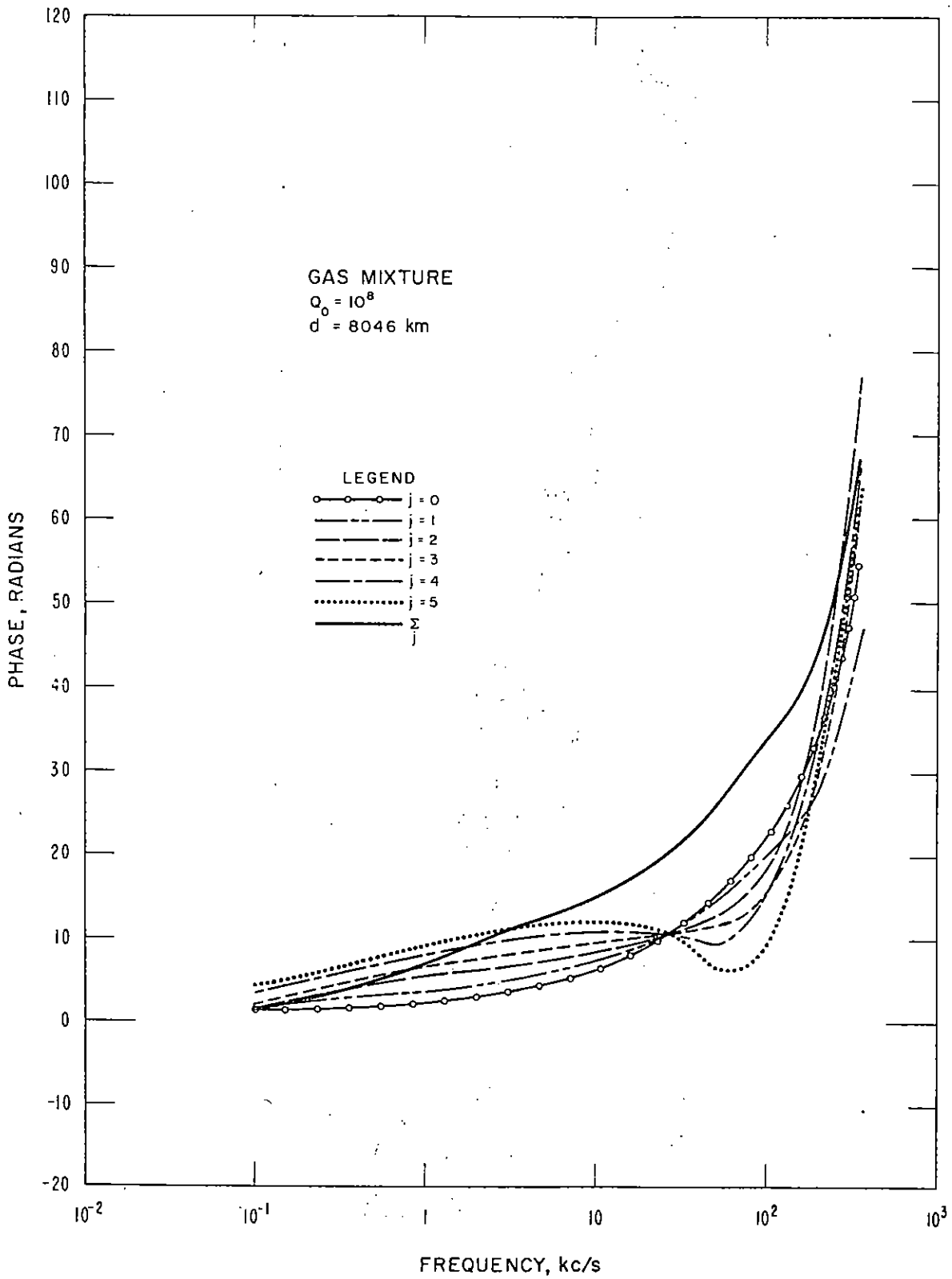

Figure 38. Phase correction of the disturbed propagation medium transform $d = d_2 = 8046$ km; illustrating the terms of the geometric series $-k_1 d_2 - \text{Arg}\, E_j(\omega, d_2)$ and the total phase $-k_1 d_2 - \text{Arg} \sum_j E_j(\omega, d_2)$ for a nuclear debris production rate, $Q_0 = 10^8$ ion pairs per cubic centimeter per second per atmosphere.

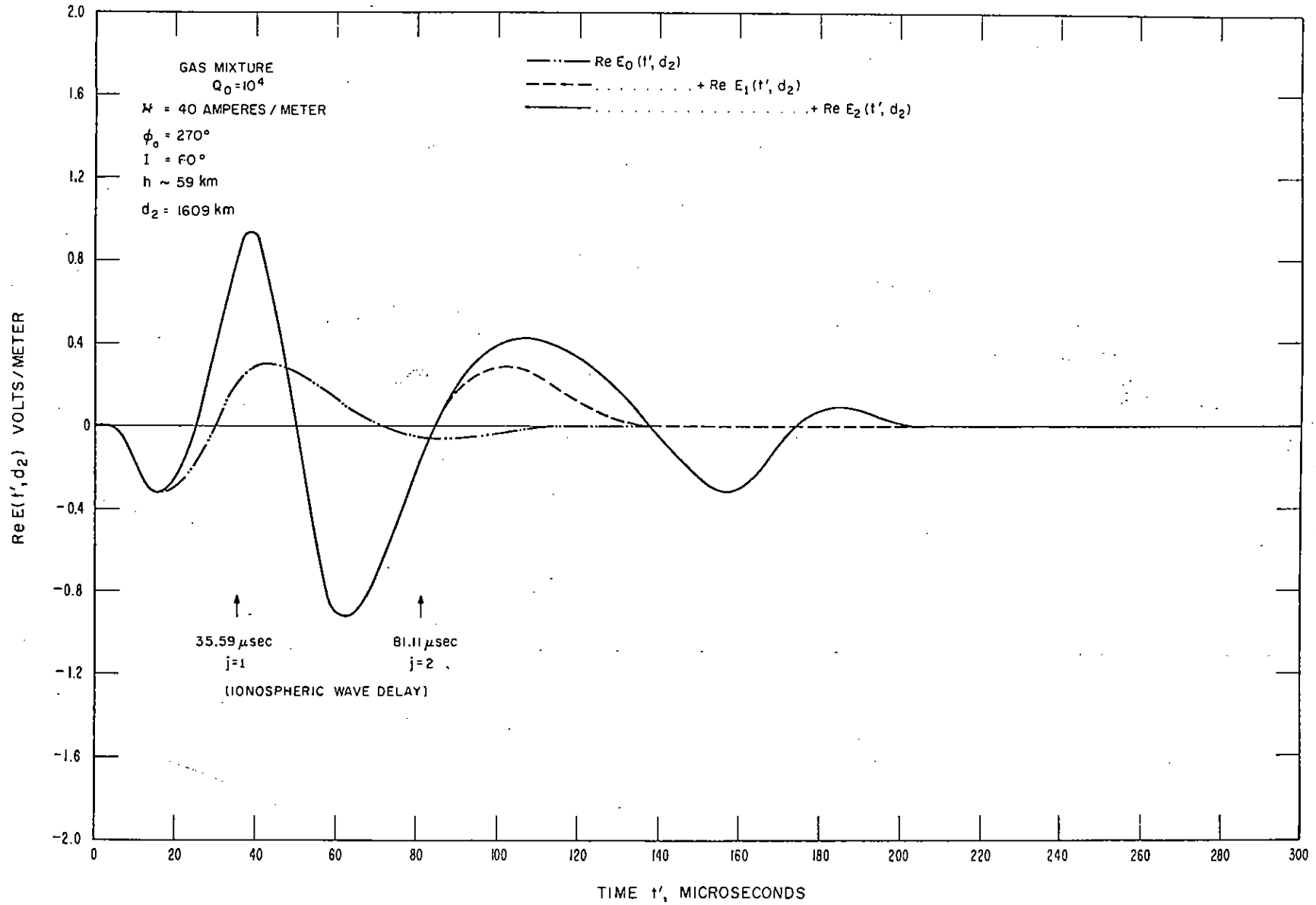

Figure 39. Illustrating theoretical reconstruction of the pulse from a nuclear burst at distance, d = 1609 km, as a sum of pulses in the time domain, where each component pulse corresponds to a term of the geometric series, j = 0, 1, 2, 3 ···. The ionosphere has been disturbed theoretically by the nuclear debris production rate $Q_0 = 10^4$ ion pairs per cubic centimeter per second per atmosphere.

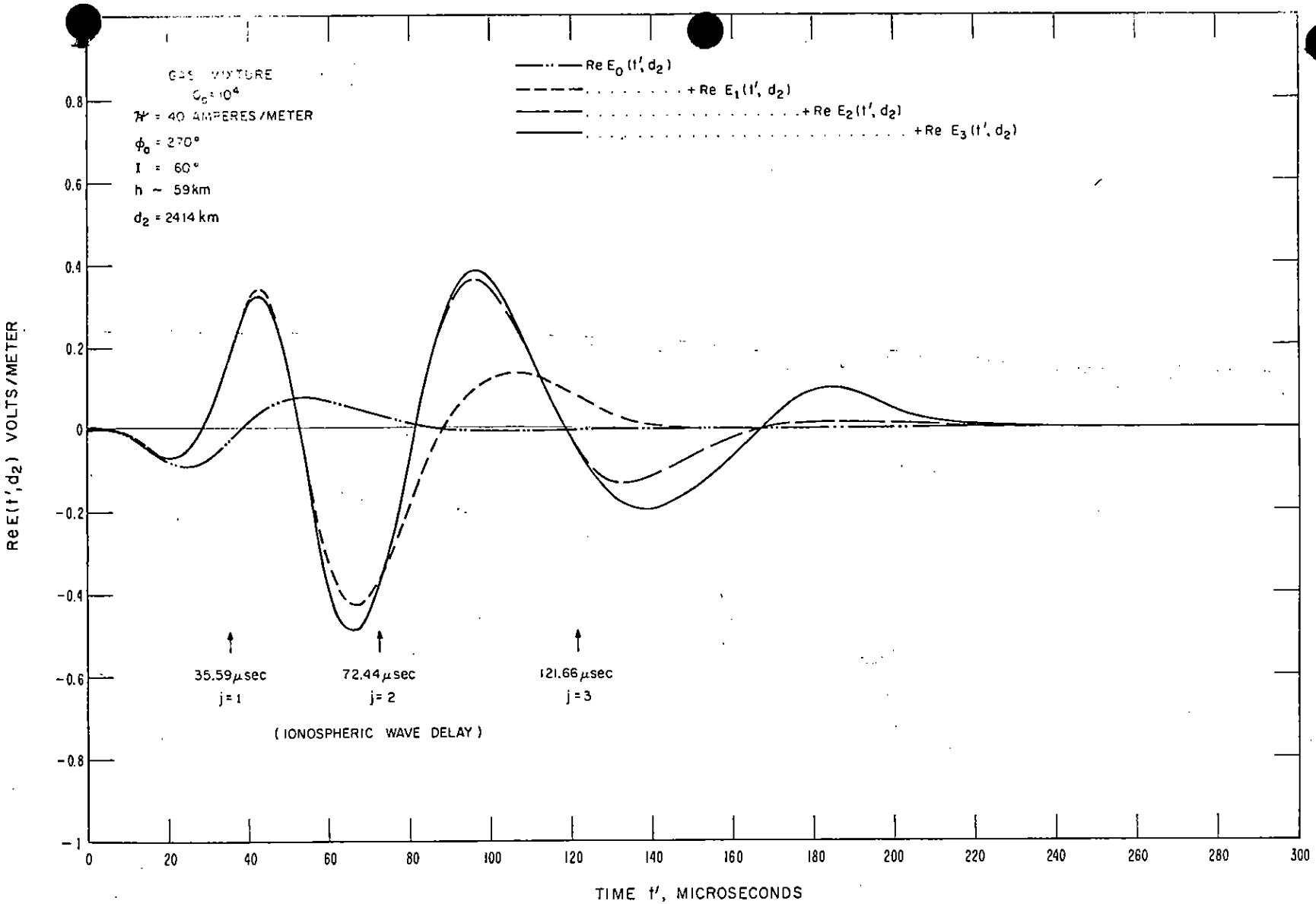

Figure 40. Illustrating theoretical reconstruction of the pulse from a nuclear burst at distance, d = 2414 km, as a sum of pulses in the time domain, where each component pulse corresponds to a term of the geometric series, j = 0, 1, 2, 3···. The ionosphere has been disturbed theoretically by the nuclear debris production rate $Q_0 = 10^4$ ion pairs per cubic centimeter per second per atmosphere.

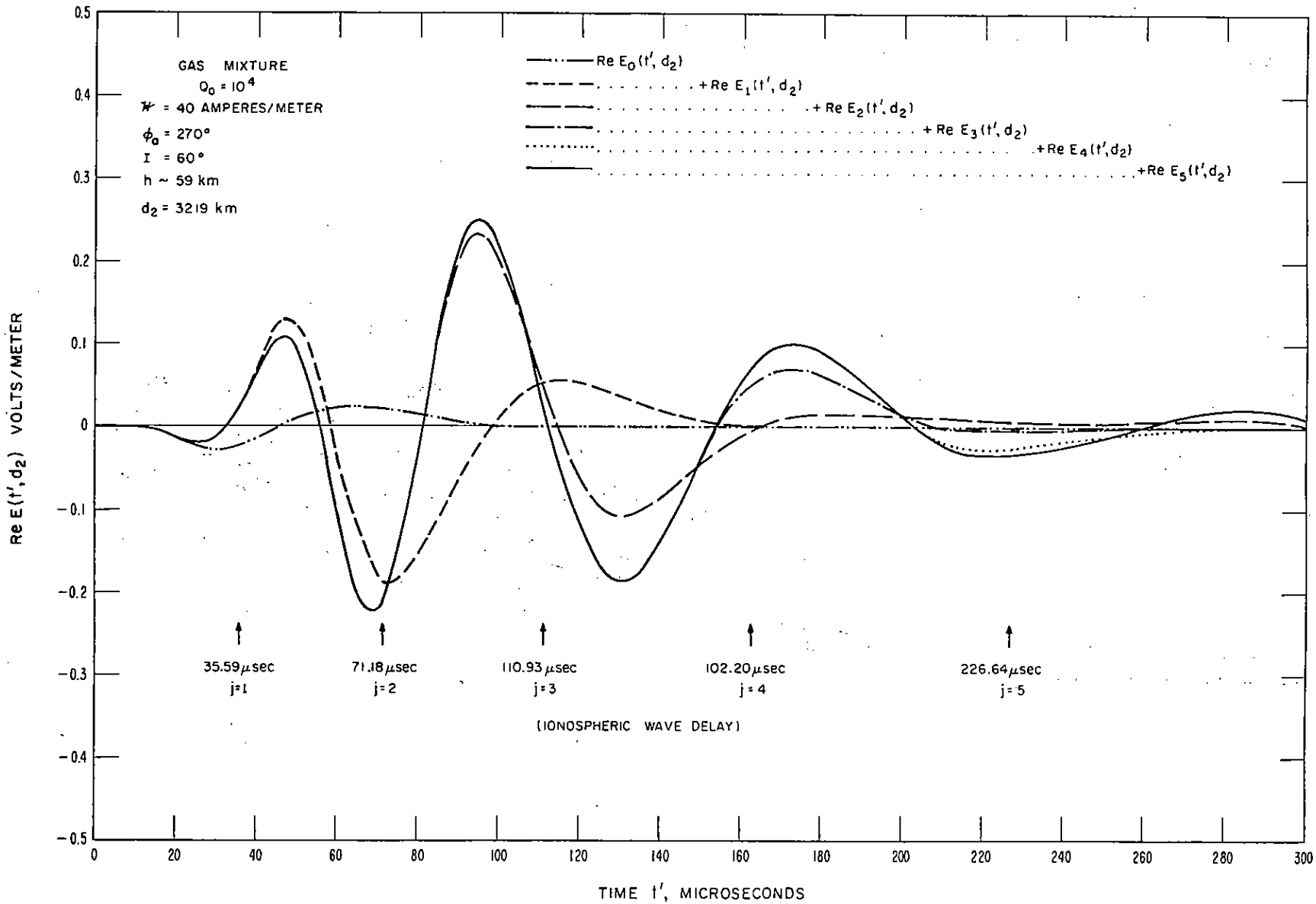

Figure 41. Illustrating theoretical reconstruction of the pulse from a nuclear burst at distance, d = 3219 km, as a sum of pulses in the time domain, where each component pulse corresponds to a term of the geometric series, j = 0, 1, 2, 3 · · ·. The ionosphere has been disturbed theoretically by the nuclear debris production rate $Q_0 = 10^4$ ion pairs per cubic centimeter per second per atmosphere.

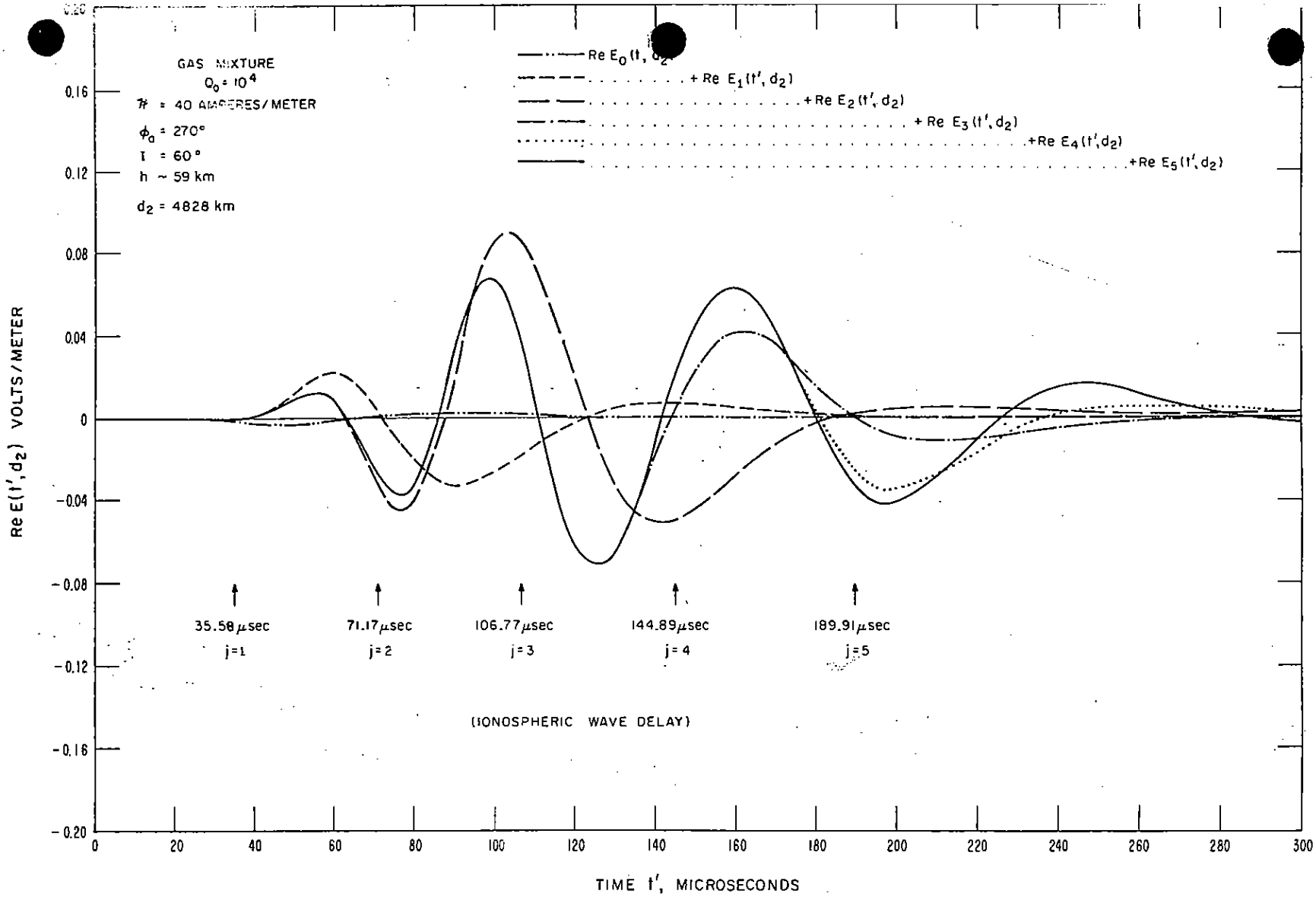

Figure 42. Illustrating theoretical reconstruction of the pulse from a nuclear burst at distance, d = 4828 km, as a sum of pulses in the time domain, where each component pulse corresponds to a term of the geometric series, j = 0, 1, 2, 3 · · · . The ionosphere has been disturbed theoretically by the nuclear debris production rate $Q_0 = 10^4$ ion pairs per cubic centimeter per second per atmosphere.

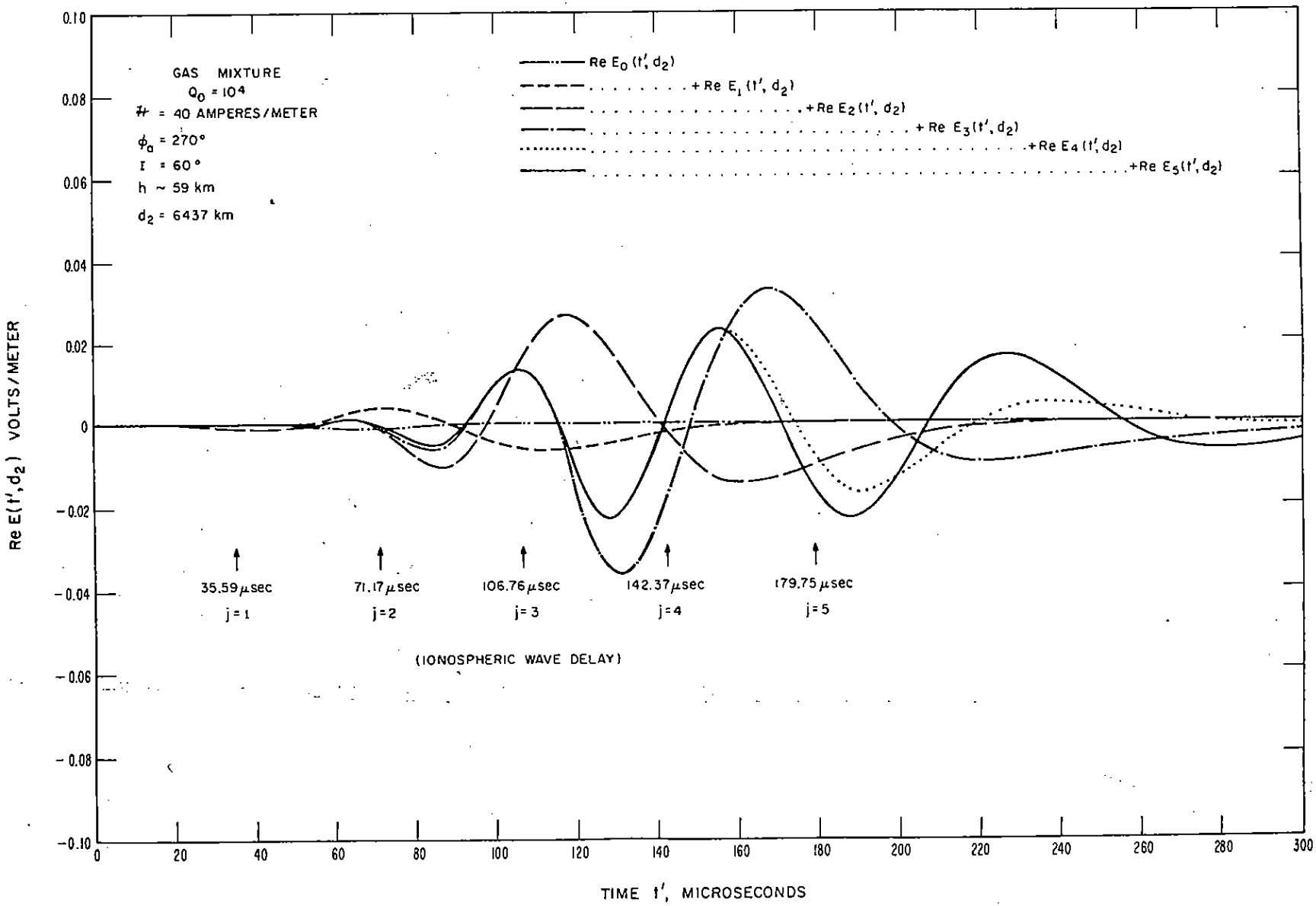

Figure 43. Illustrating theoretical reconstruction of the pulse from a nuclear burst at distance, d = 6437 km, as a sum of pulses in the time domain, where each component pulse corresponds to a term of the geometric series, j = 0, 1, 2, 3 · · ·. The ionosphere has been disturbed theoretically by the nuclear debris production rate $Q_0 = 10^4$ ion pairs per cubic centimeter per second per atmosphere.

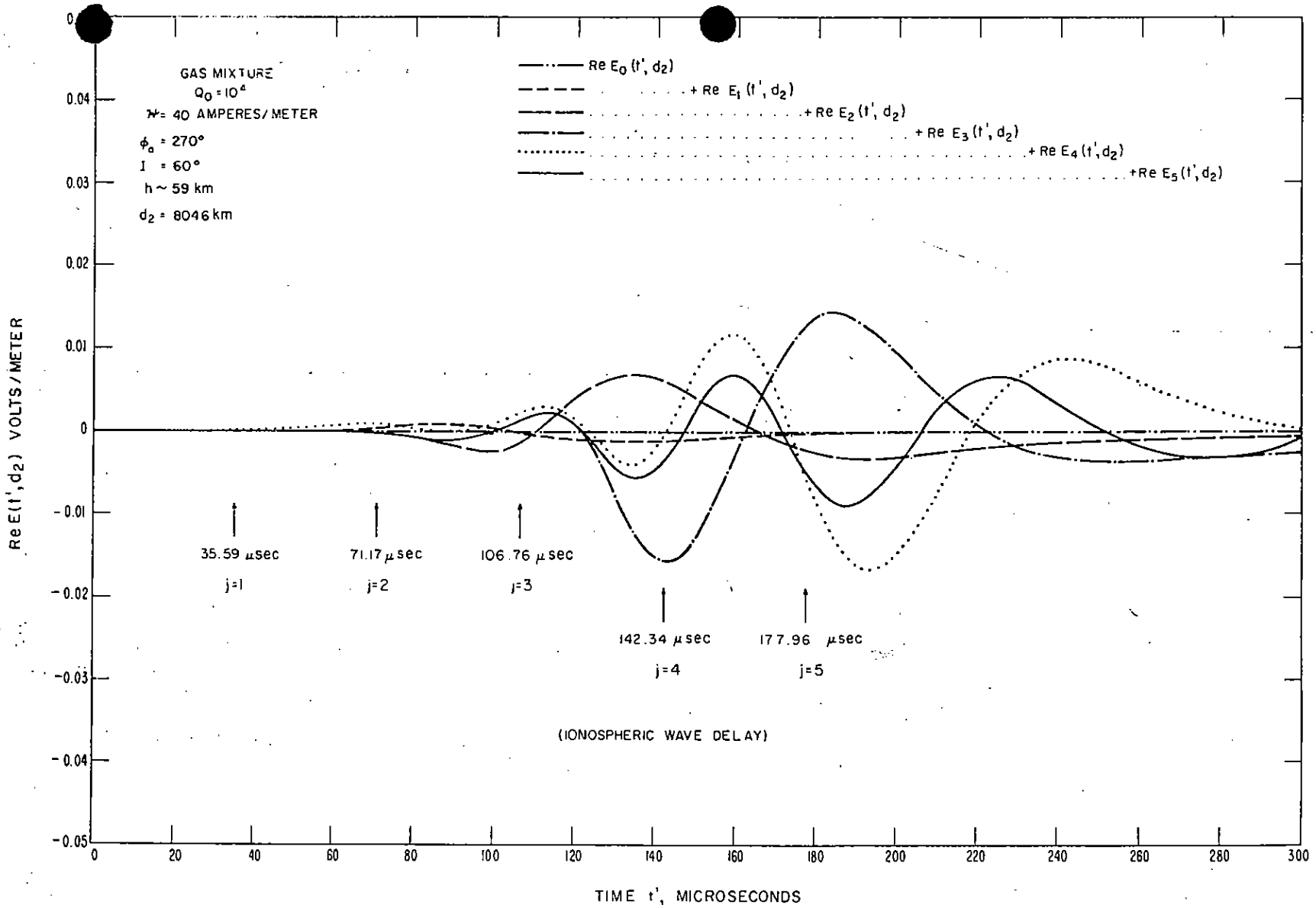

Figure 44. Illustrating theoretical reconstruction of the pulse from a nuclear burst at distance, d = 8046 km, as a sum of pulses in the time domain, where each component pulse corresponds to a term of the geometric series, j = 0, 1, 2, 3 ···. The ionosphere has been disturbed theoretically by the nuclear debris production rate $Q_0 = 10^4$ ion pairs per cubic centimeter per second per atmosphere.

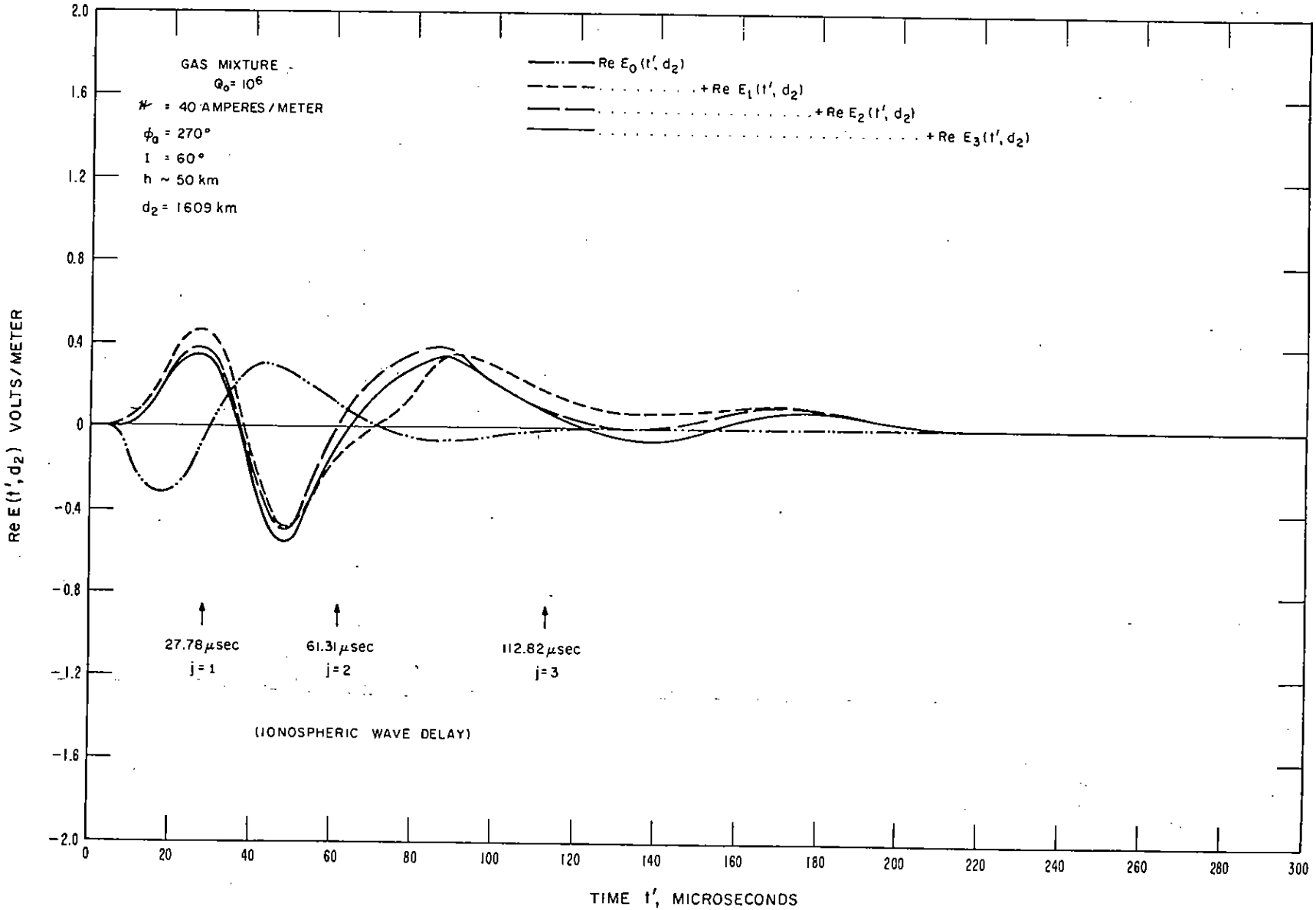

Figure 45. Illustrating theoretical reconstruction of the pulse from a nuclear burst at distance, d = 1609 km, as a sum of pulses in the time domain, where each component pulse corresponds to a term of the geometric series, j = 0, 1, 2, 3 ···. The ionosphere has been disturbed theoretically by the nuclear debris production rate $Q_0 = 10^6$ ion pairs per cubic centimeter per second per atmosphere.

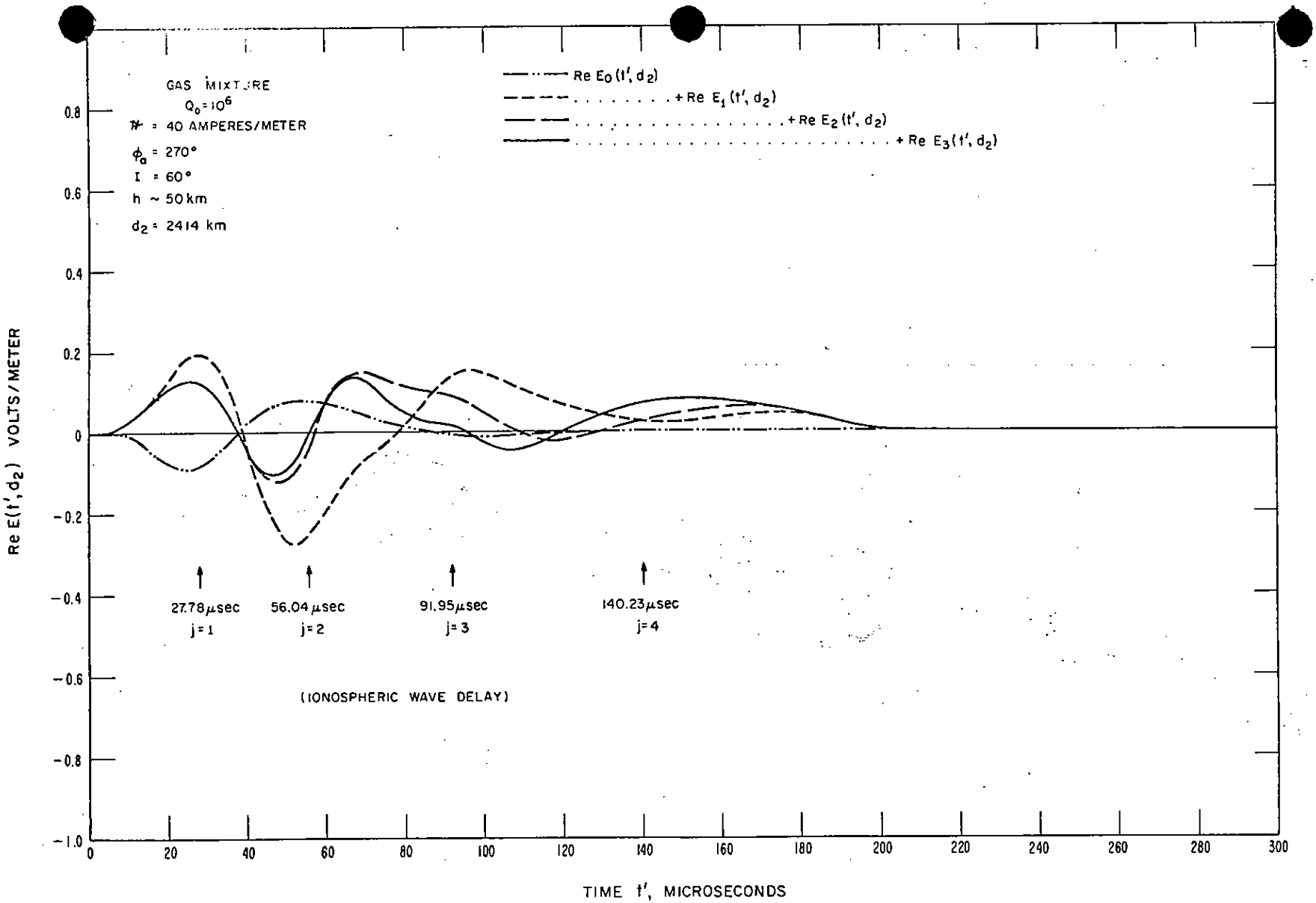

Figure 46. Illustrating theoretical reconstruction of the pulse from a nuclear burst at distance, d = 2414 km, as a sum of pulses in the time domain, where each component pulse corresponds to a term of the geometric series, j = 0, 1, 2, 3 · · · . The ionosphere has been disturbed theoretically by the nuclear debris production rate $Q_0 = 10^6$ ion pairs per cubic centimeter per second per atmosphere.

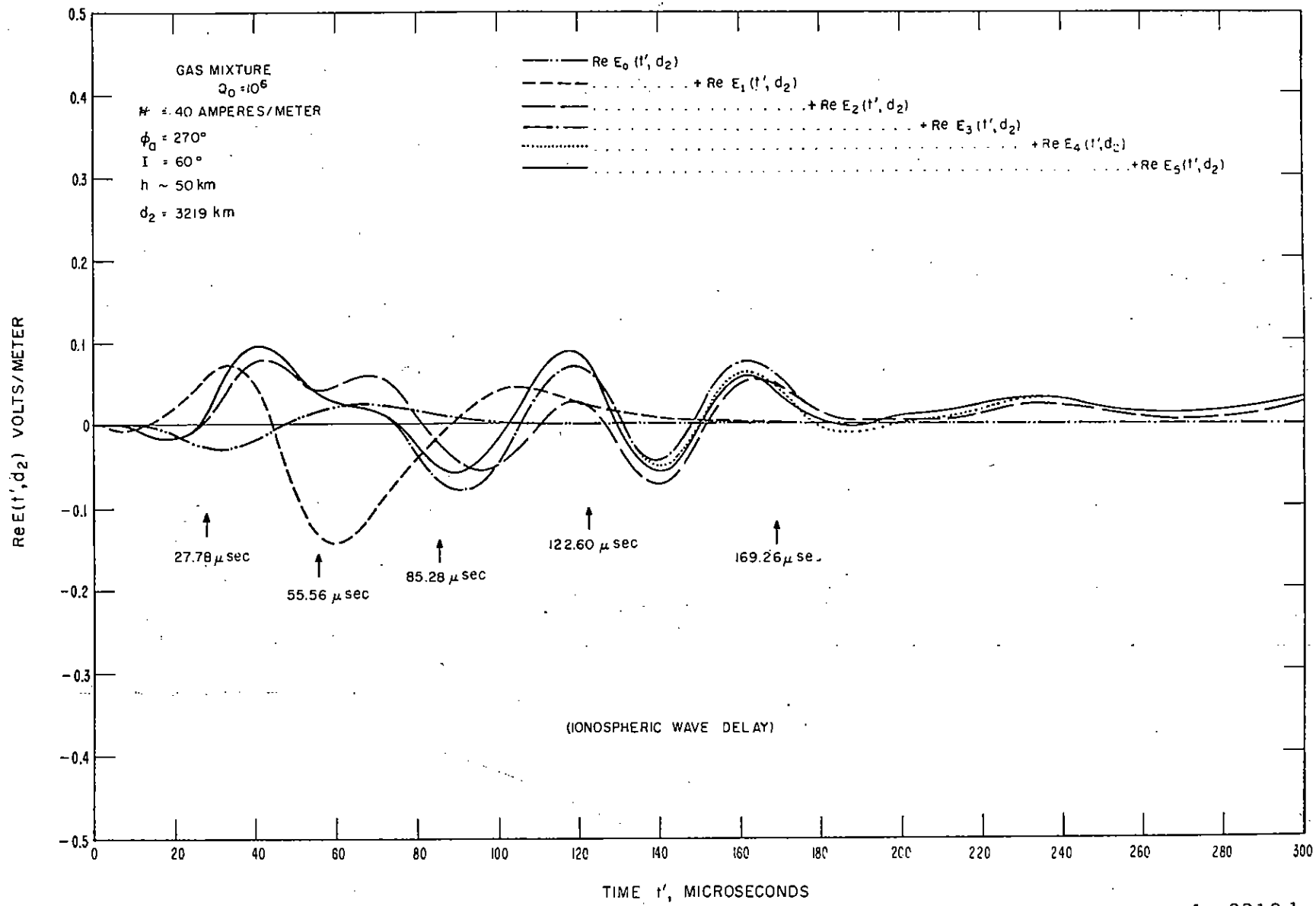

Figure 47. Illustrating theoretical reconstruction of the pulse from a nuclear burst at distance, d = 3219 km, as a sum of pulses in the time domain, where each component pulse corresponds to a term of the geometric series, j = 0, 1, 2, 3 · · · . The ionosphere has been disturbed theoretically by the nuclear debris production rate $Q_0 = 10^6$ ion pairs per cubic centimeter per second per atmosphere.

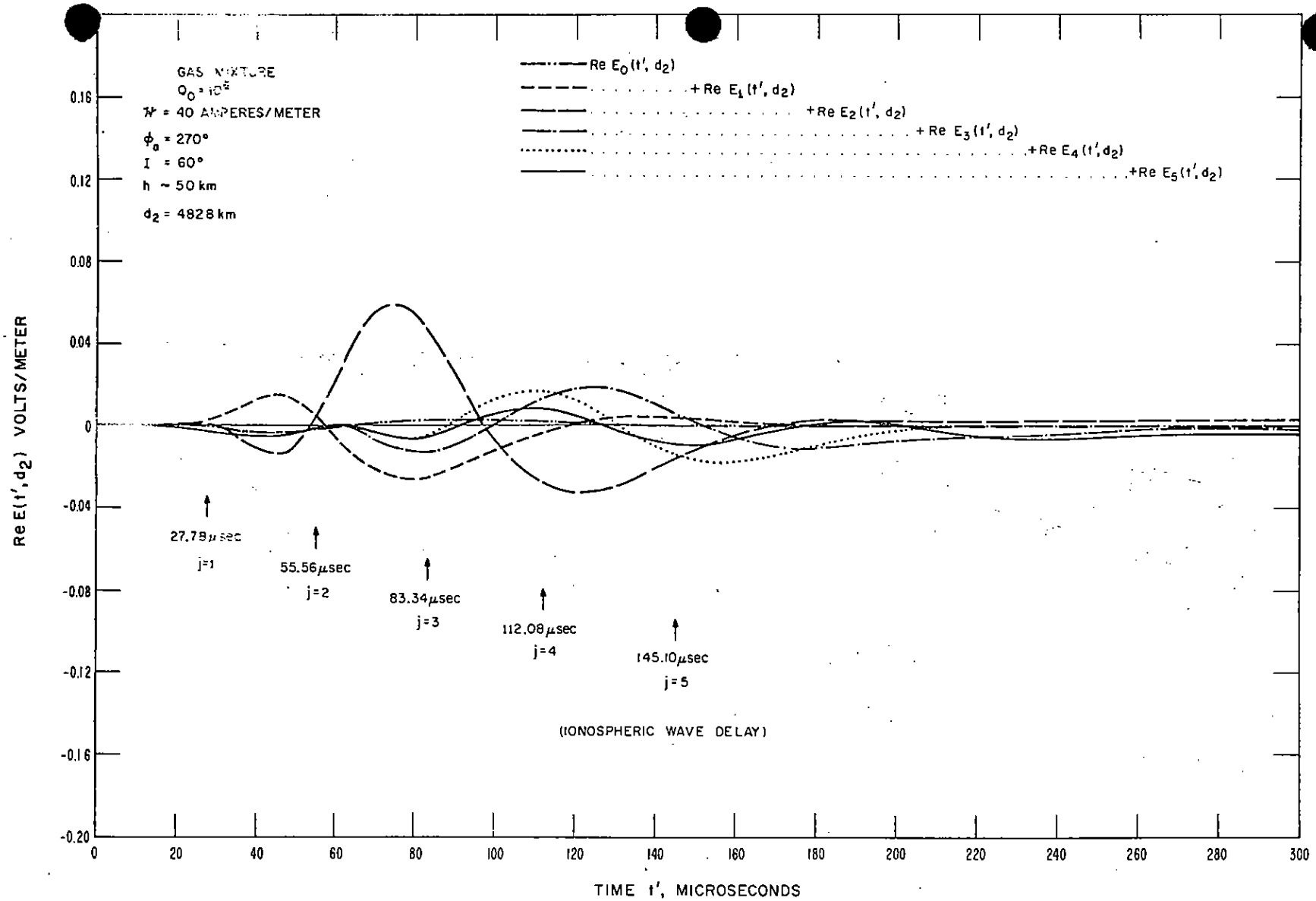

Figure 48. Illustrating theoretical reconstruction of the pulse from a nuclear burst at distance, d = 4828 km, as a sum of pulses in the time domain, where each component pulse corresponds to a term of the geometric series, j = 0, 1, 2, 3 · · ·. The ionosphere has been disturbed theoretically by the nuclear debris production rate $Q_0 = 10^6$ ion pairs per cubic centimeter per second per atmosphere.

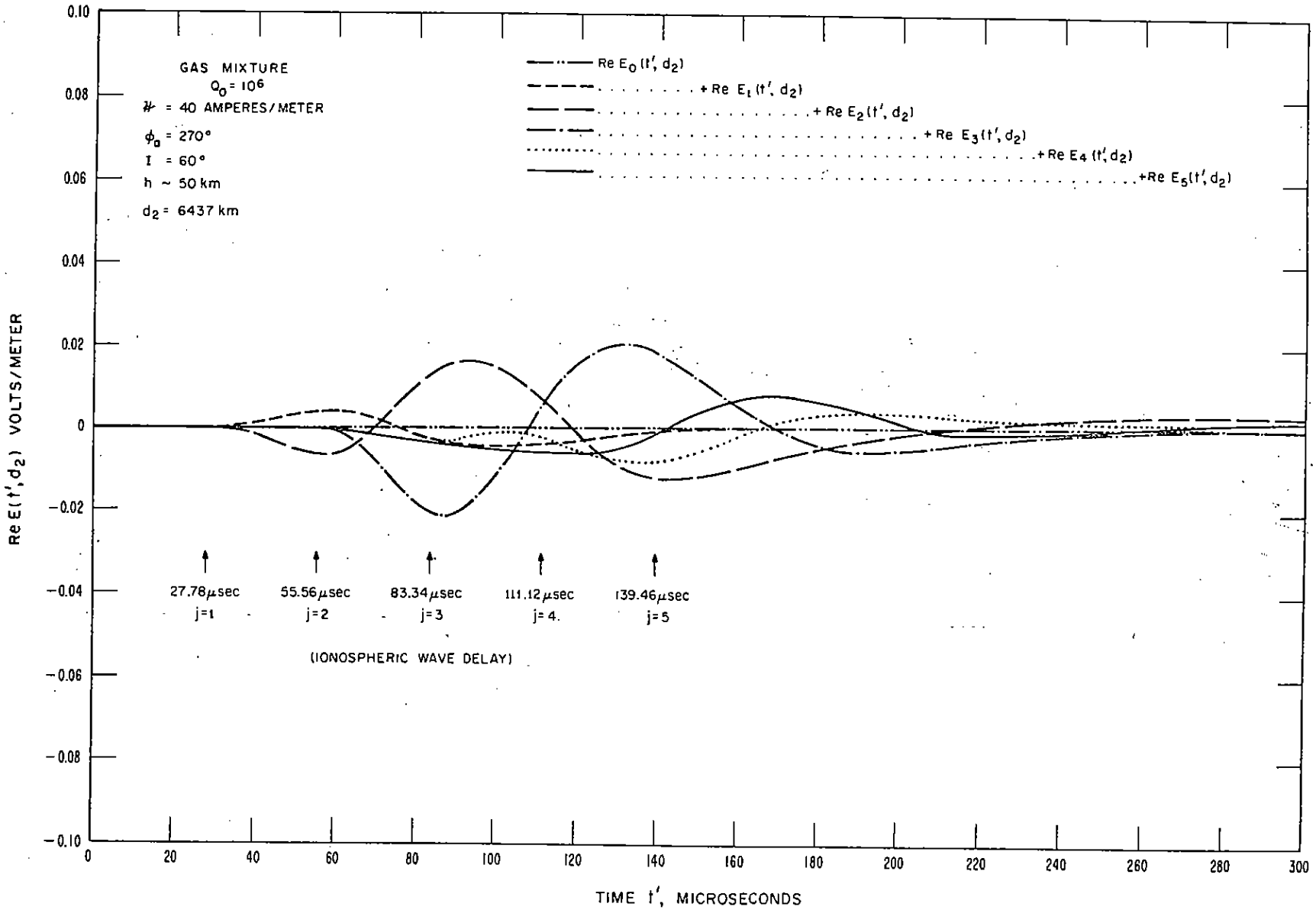

Figure 49. Illustrating theoretical reconstruction of the pulse from a nuclear burst at distance, d = 6437 km, as a sum of pulses in the time domain, where each component pulse corresponds to a term of the geometric series, j = 0, 1, 2, 3 ···. The ionosphere has been disturbed theoretically by the

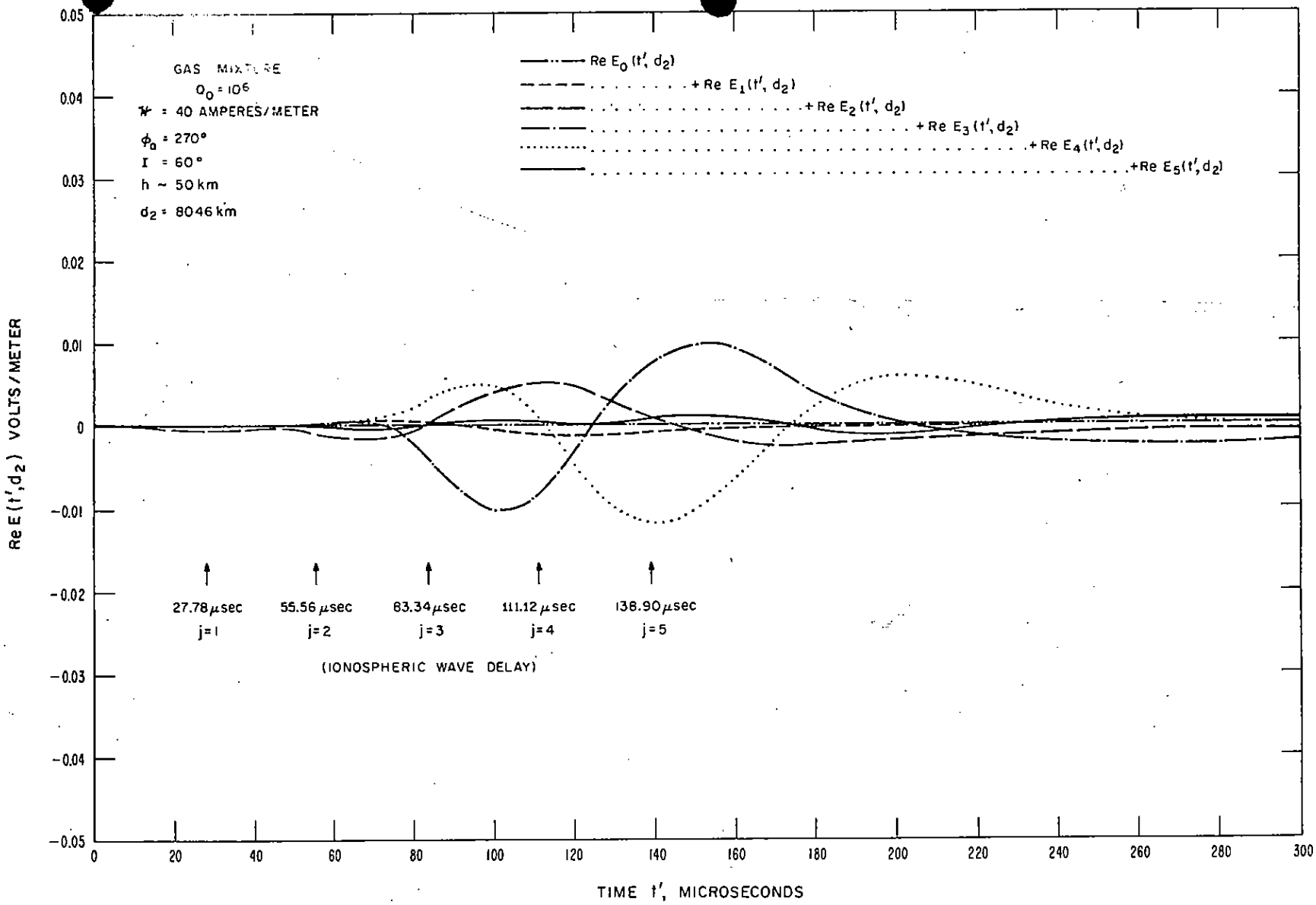

Figure 50. Illustrating theoretical reconstruction of the pulse from a nuclear burst at distance, d = 8046 km, as a sum of pulses in the time domain, where each component pulse corresponds to a term of the geometric series, j = 0, 1, 2, 3 · · · . The ionosphere has been disturbed theoretically by the nuclear debris production rate $Q_0 = 10^6$ ion pairs per cubic centimeter per second per atmosphere.

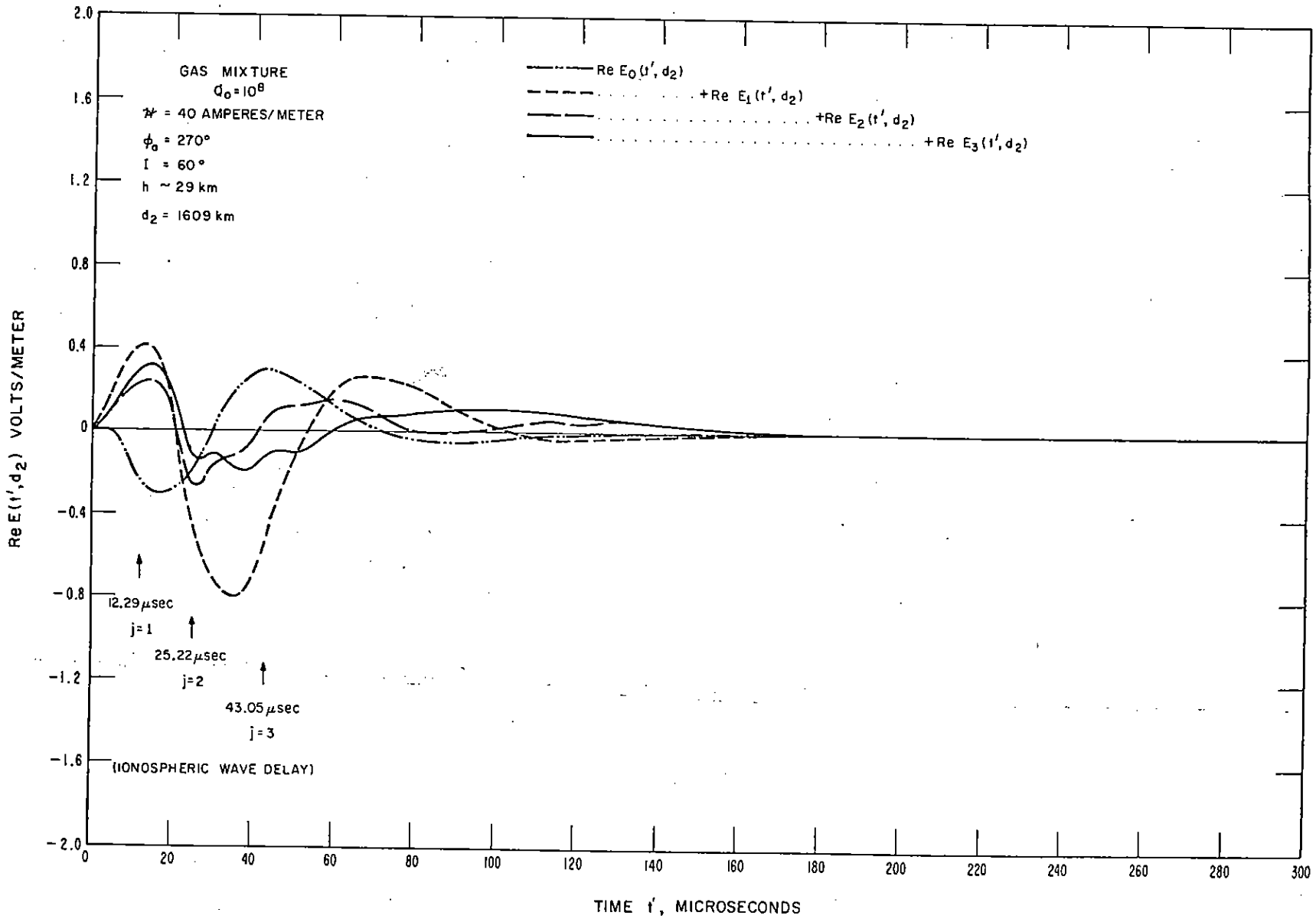

Figure 51. Illustrating theoretical reconstruction of the pulse from a nuclear burst at distance, d = 1609 km, as a sum of pulses in the time domain, where each component pulse corresponds to a term of the geometric series, j = 0, 1, 2, 3 · · · . The ionosphere has been disturbed theoretically by the nuclear debris production rate $Q_0 = 10^8$ ion pairs per cubic centimeter per second per atmosphere.

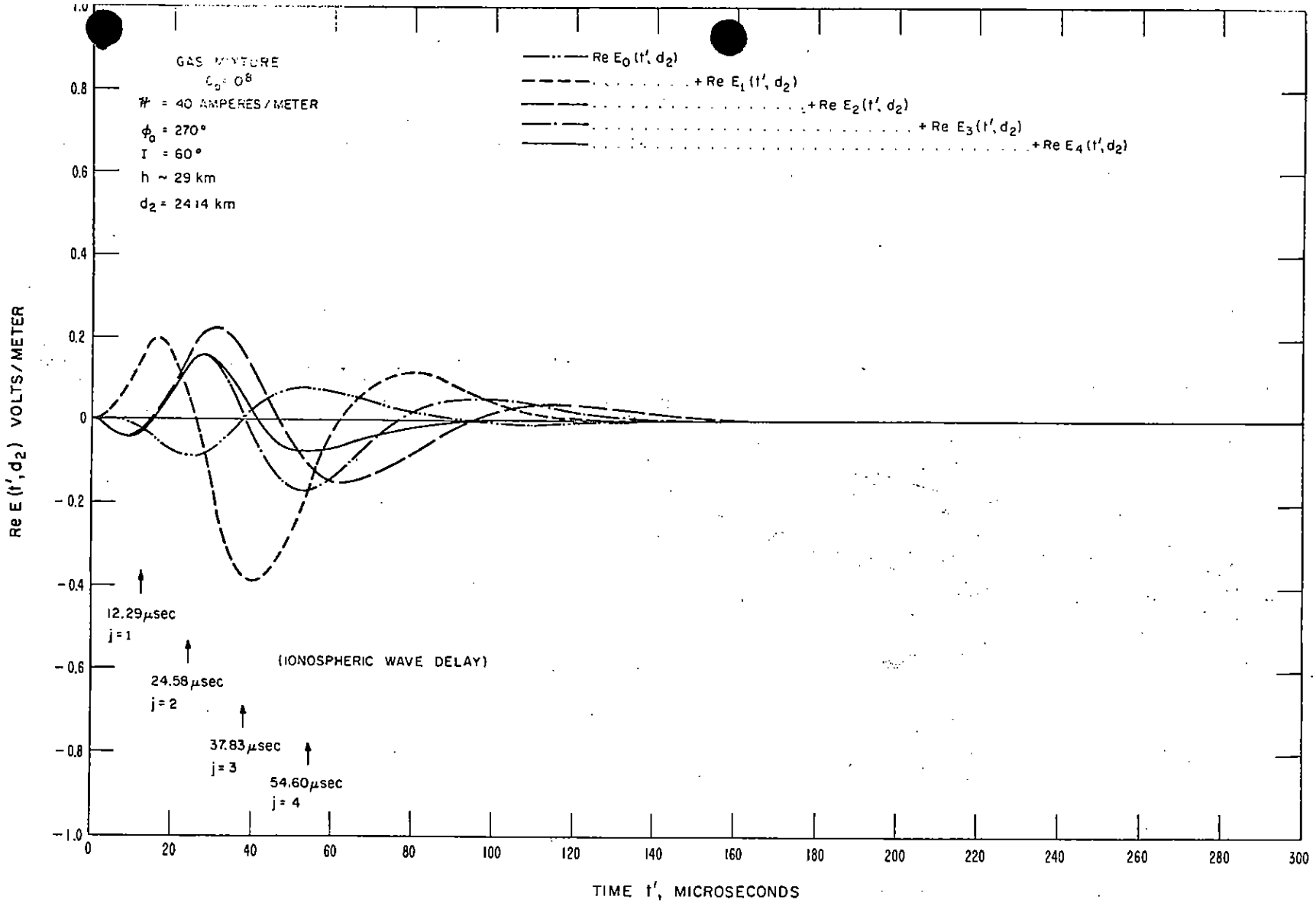

Figure 52. Illustrating theoretical reconstruction of the pulse from a nuclear burst at distance, d = 2414 km, as a sum of pulses in the time domain, where each component pulse corresponds to a term of the geometric series, j = 0, 1, 2, 3 · · ·. The ionosphere has been disturbed theoretically by the nuclear debris production rate $Q_0 = 10^8$ ion pairs per cubic centimeter per second per atmosphere.

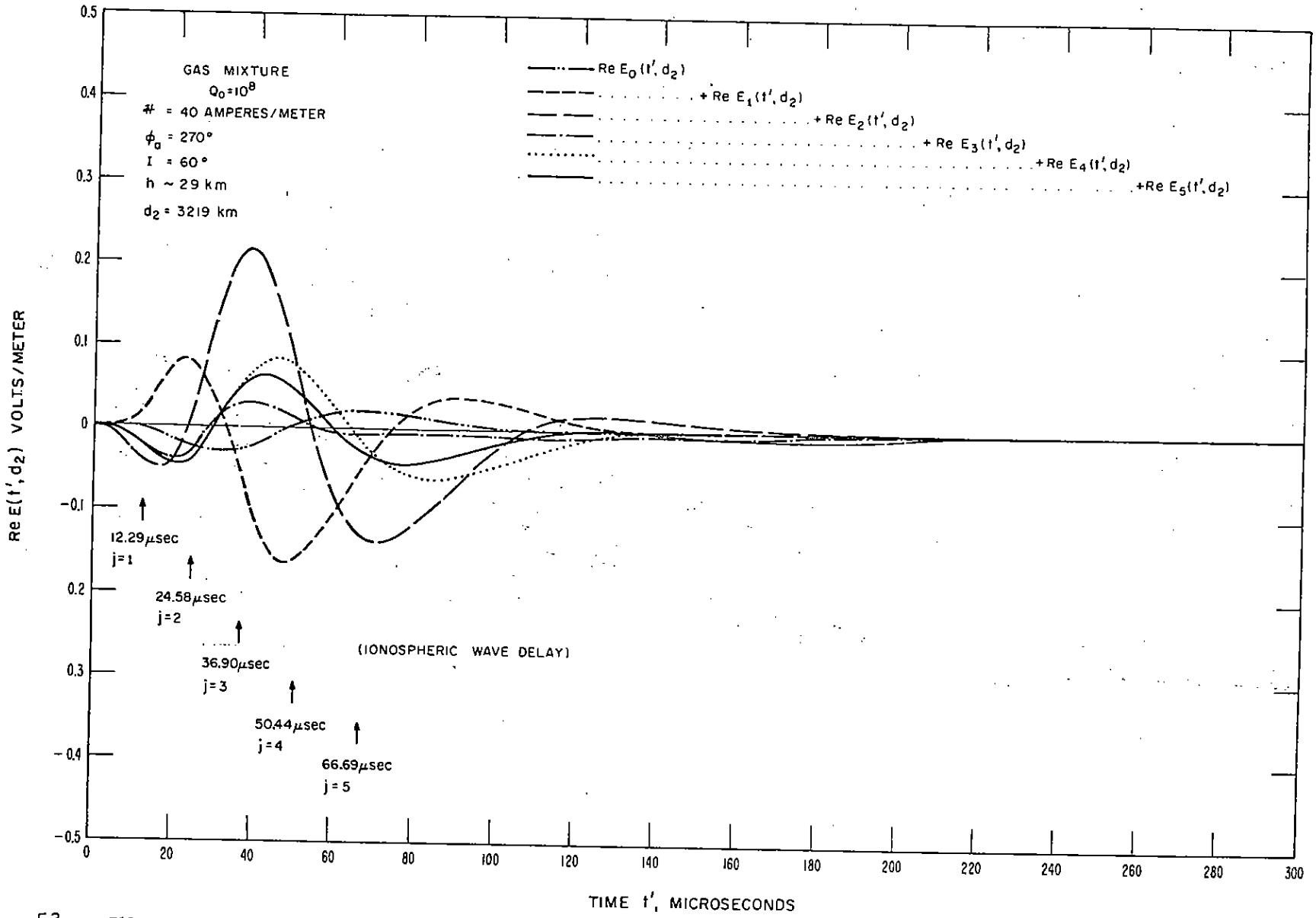

Figure 53. Illustrating theoretical reconstruction of the pulse from a nuclear burst at distance, d = 3219 km, as a sum of pulses in the time domain, where each component pulse corresponds to a term of the geometric series, j = 0, 1, 2, 3 . . . . The ionosphere has been disturbed th[illegible]tically by the nuclear debris production rate $Q_0 = 10^8$ ion pairs per cubic centimeter per [illegible] per atmosphere.

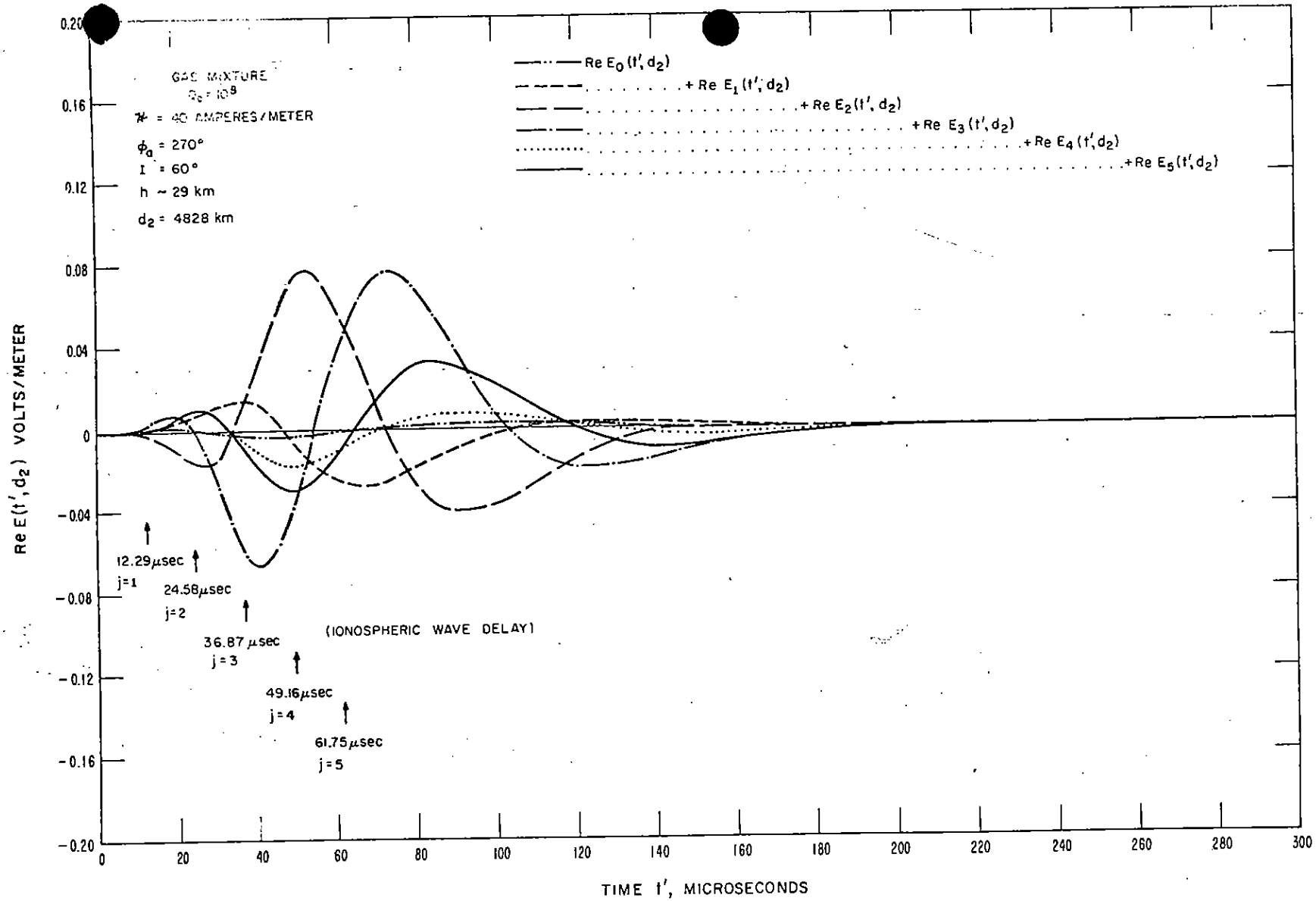

Figure 54. Illustrating theoretical reconstruction of the pulse from a nuclear burst at distance, d = 4828 km, as a sum of pulses in the time domain, where each component pulse corresponds to a term of the geometric series, j = 0, 1, 2, 3 · · · . The ionosphere has been disturbed theoretically by the nuclear debris production rate $Q_0 = 10^8$ ion pairs per cubic centimeter per second per atmosphere.

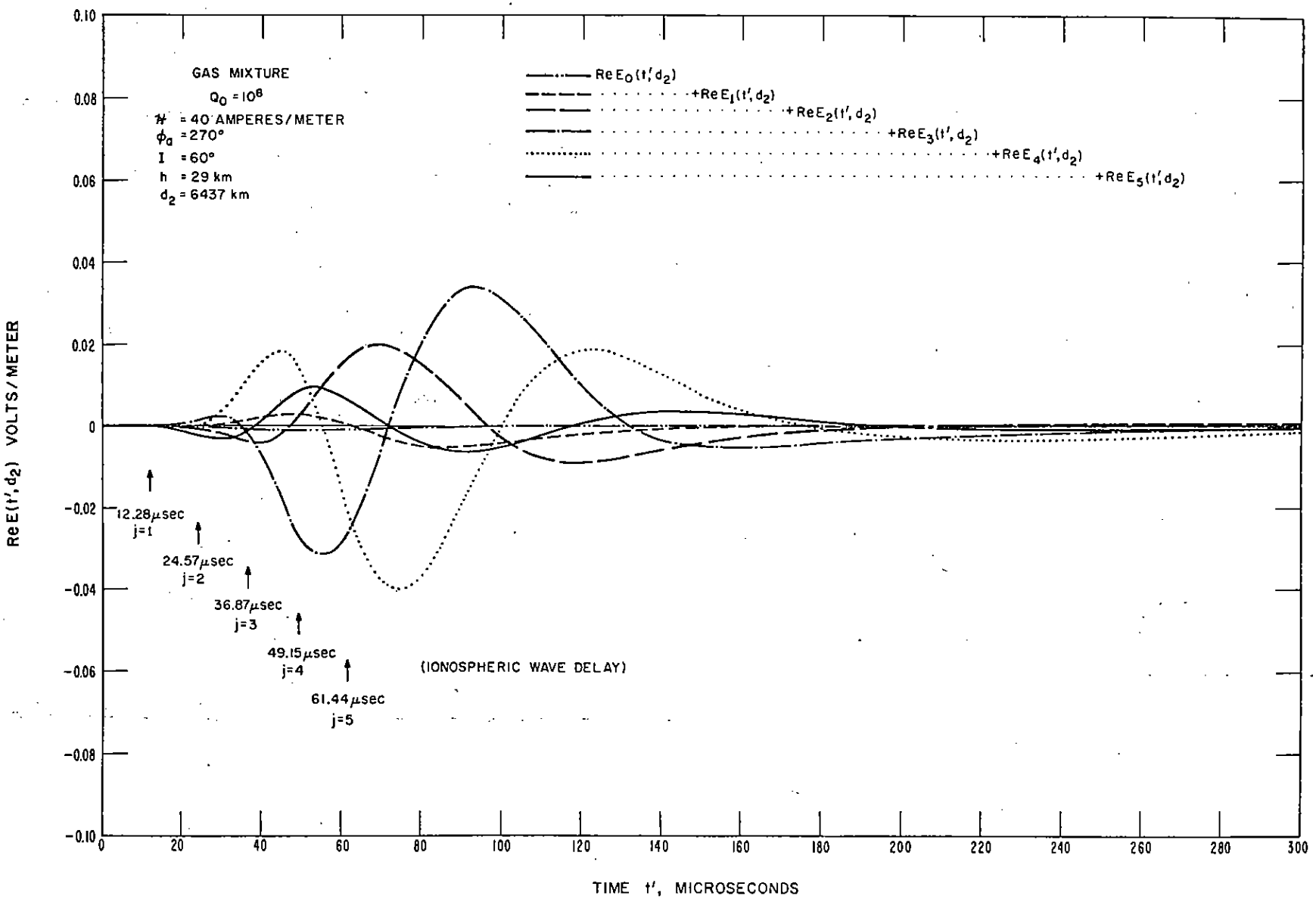

Figure 55. Illustrating theoretical reconstruction of the pulse from a nuclear burst at distance, d = 6437 km, as a sum of pulses in the time domain, where each component pulse corresponds to a term of the geometric series, j = 0, 1, 2, 3 · · ·. The ionosphere has been disturbed theoretically by the nuclear debris production rate $Q_0 = 10^8$ ion pairs per cubic centimeter per second per atmosphere.

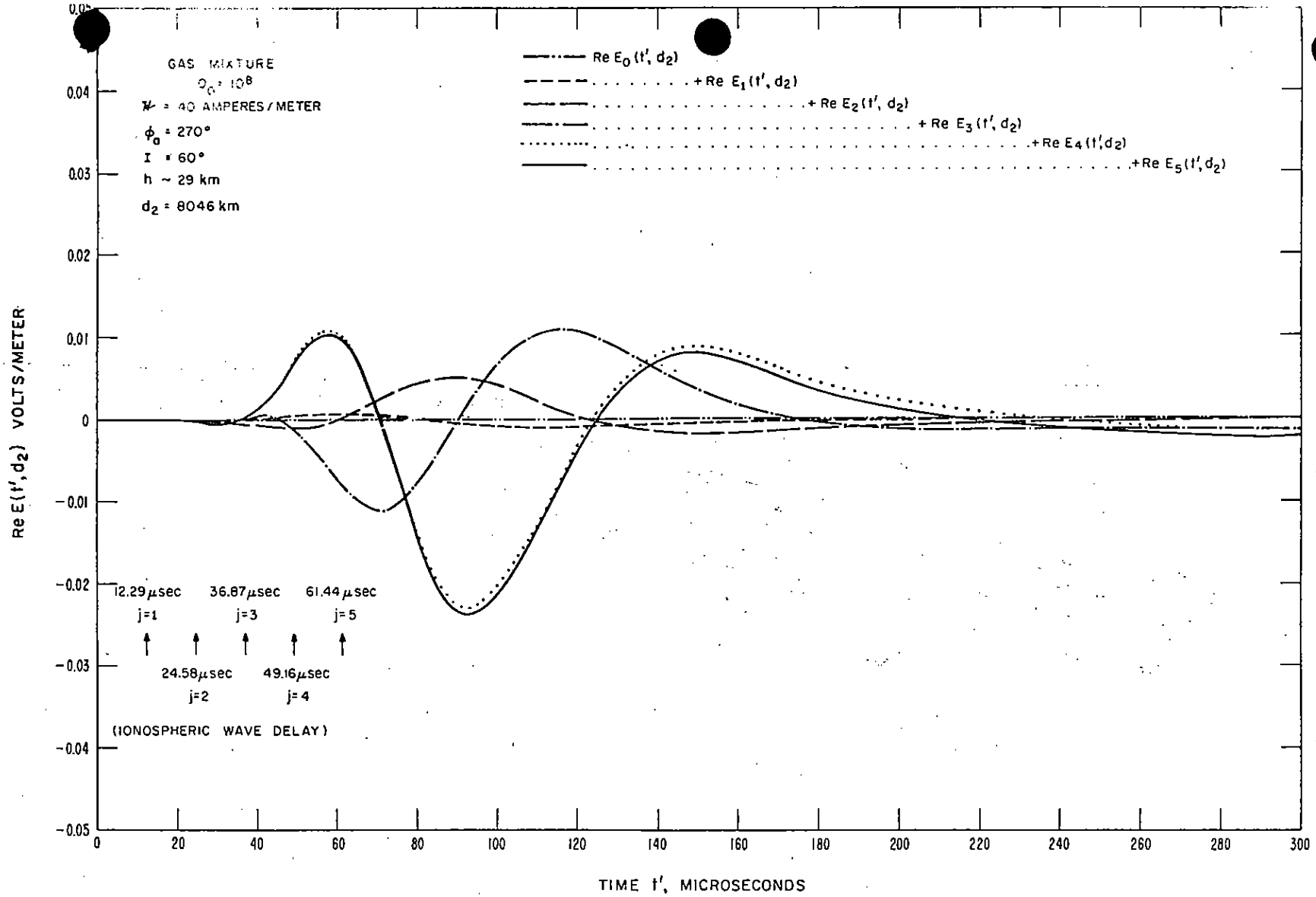

Figure 56. Illustrating theoretical reconstruction of the pulse from a nuclear burst at distance, d = 8046 km, as a sum of pulses in the time domain, where each component pulse corresponds to a term of the geometric series, j = 0, 1, 2, 3 ···. The ionosphere has been disturbed theoretically by the nuclear debris production rate $Q_0 = 10^8$ ion pairs per cubic centimeter per second per atmosphere.

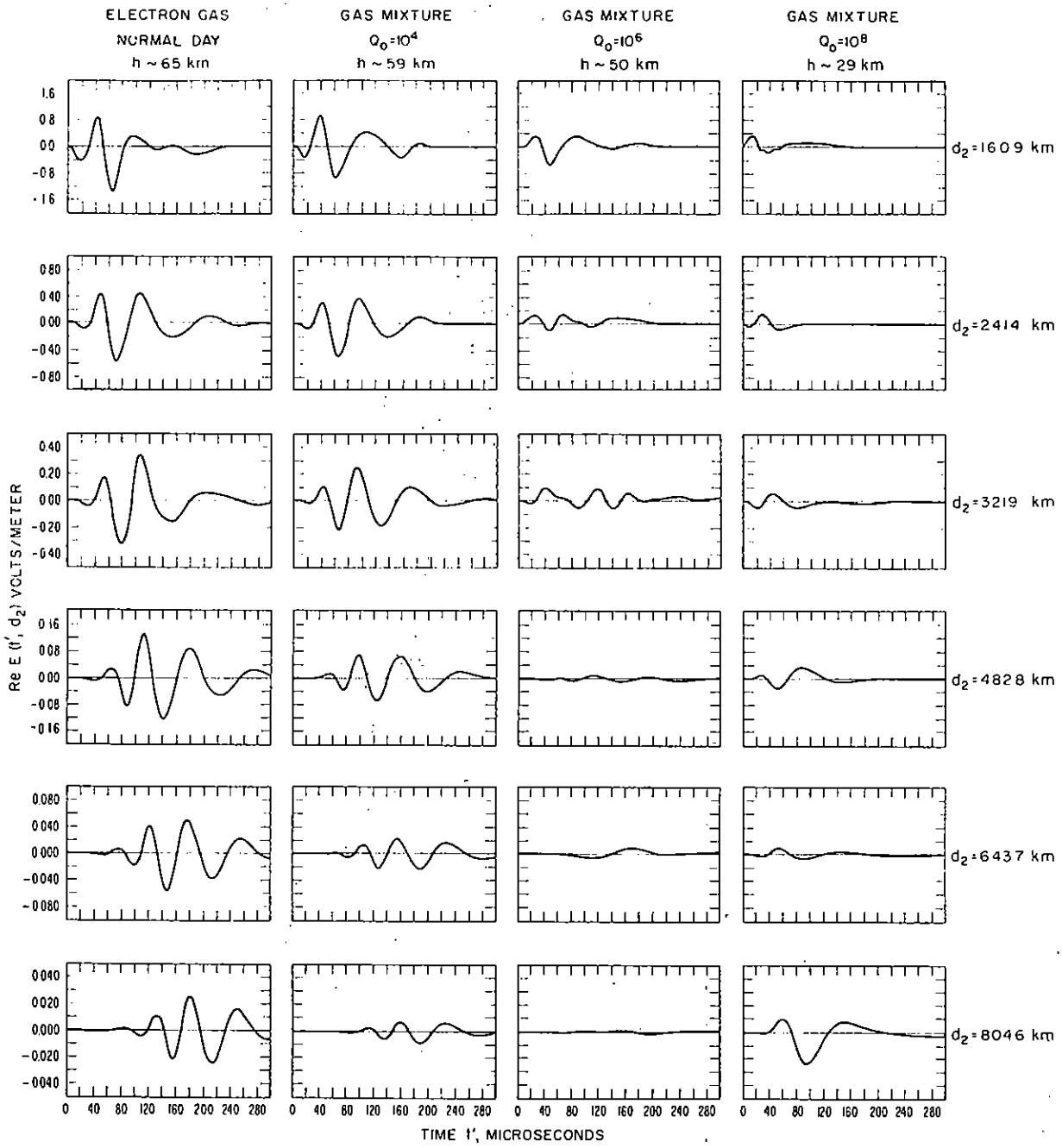

Figure 57. Pulse propagated theoretically from a nuclear burst to various distances between 1609 and 8046 km, illustrating a comparison between normal day conditions and various disturbed ionosphere production rates, $Q_0 = 10^4$, 10^6, 10^8 ion pairs per cubic centimeter per second per atmosphere.

GPO 832-587